PB96-187810

HYDROLOGIC MODELING OF BOREAL FOREST ECOSYSTEMS

WASHINGTON UNIV., SEATTLE

APR 95

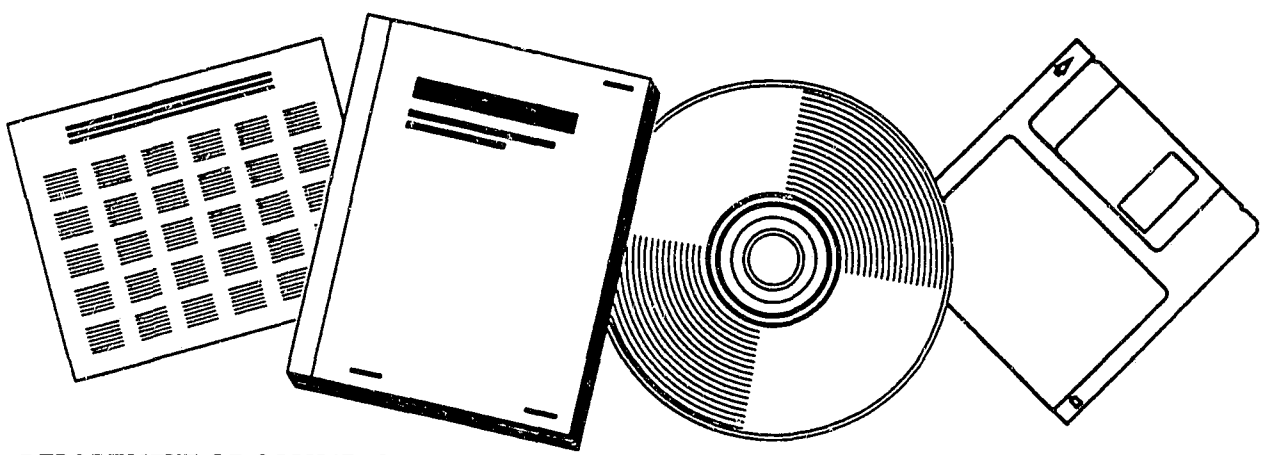

U.S. DEPARTMENT OF COMMERCE
National Technical Information Service

Department of Civil Engineering
University of Washington
Seattle, Washington 98195

HYDROLOGIC MODELING OF BOREAL FOREST ECOSYSTEMS

by

INGJERD HADDELAND
DENNIS P. LETTENMAIER

Water Resources Series
Technical Report No. 143

April 1995

REPORT DOCUMENTATION PAGE

Form Approved
OMB No. 0704-0188

1. PB96-187810

2. REPORT DATE: Apr 95

3. REPORT TYPE AND DATES COVERED: Final

4. TITLE AND SUBTITLE
Hydrologic Modeling of Boreal Forest Ecosystems

5. FUNDING NUMBERS
G NAG 5-2294

6. AUTHOR(S)
Ingjerd Haddeland and Dennis P. Lettenmaier

7. PERFORMING ORGANIZATION NAME(S) AND ADDRESS(ES)
Department of Civil Engineering
University of Washington
Seattle, WA 98195

8. PERFORMING ORGANIZATION REPORT NUMBER
Water Resources Series
Technical Report No. 143

9. SPONSORING/MONITORING AGENCY NAME(S) AND ADDRESS(ES)
NASA

10. SPONSORING/MONITORING AGENCY REPORT NUMBER

11. SUPPLEMENTARY NOTES

12a. DISTRIBUTION/AVAILABILITY STATEMENT

12b. DISTRIBUTION CODE

13. ABSTRACT *(Maximum 200 words)*

14. SUBJECT TERMS

15. NUMBER OF PAGES

16. PRICE CODE

17. SECURITY CLASSIFICATION OF REPORT	18. SECURITY CLASSIFICATION OF THIS PAGE	19. SECURITY CLASSIFICATION OF ABSTRACT	20. LIMITATION OF ABSTRACT
Unclassified	Unclassified	Unclassified	UL

ABSTRACT

A key aspect of the response of vegetation to climate is the interaction of plant use of energy and water. This study focused on the hydrologic response, including vegetation water use, of two test regions within the Boreal-Ecosystem-Atmosphere Study (BOREAS) region in the Canadian boreal forest, one north of Prince Albert, Saskatchewan, and the other near Thompson, Manitoba. Fluxes of moisture and heat were studied using a spatially distributed hydrology soil-vegetation-model (DHSVM). Previous uses of DHSVM have been in mountainous regions, therefore the model's performance was first tested in a point mode for selected vegetation types. In addition, a preliminary run of the fully distributed model was made.

Some aspects of DHSVM's formulation of aerodynamic resistance were found to be unrealistic, and two changes are suggested. First, the vertical wind profile within forests was changed to a form that merges an exponential profile and a logarithmic profile above the understory; previously the profiles were merged within the understory. Second, the original assumption of linear dependence of wind speed on fraction of overstory cover was removed in favor of using the canopy attenuation coefficient and roughness characteristics to account for forest density. These changes eliminated the previous inconsistency that lead to lower values of the aerodynamic resistance for understory within forest than in open areas. Results of point a point application of DHSVM at the two BOREAS study areas showed that the interaction of energy and moisture supply strongly affected evapotranspiration and runoff. Predicted annual total evapotranspiration averaged for a Black Spruce (Pica Mariana) and a Fen site in the northern area was 255 mm (61 percent of precipitation). While the precipitation in the southern area was smaller (91 percent of the northern area), predicted evapotranspiration was higher; 324 mm (85 percent of precipitation). This was caused by higher temperatures, higher leaf area index, a longer snow free period and hence more evenly distributed moisture supply

The role of moss in the hydrologic cycle was analyzed through field observations and modeling. The field results showed that a significant amount (around half) of the precipitation that reached the forest floor at a site where moss was the dominant ground cover, was lost through evapotranspiration. Model analyses showed that the presence or absence of the moss carpet influences the resulting heat fluxes, as does the distribution of roots in the moss and underlying mineral soil.

A preliminary fully distributed run of DHSVM for the southern BOREAS modeling subarea showed that the model predicted the amount of seasonal runoff correctly, but the observed shape of the hydrograph was not reproduced. Predicted peak flows were much higher than observed, while baseflow was much too low. Spatial resolution of precipitation data was shown to influence resulting heat fluxes significantly, both spatially and temporally. Latent heat fluxes, both in the spatial analysis and in the moss analysis, were to high compared to measured values. Whether these results are caused by incorrect parameter estimates, or deficiencies in the model structure, is the topic of ongoing research.

ACKNOWLEDGMENTS

The research described in this report is based on the Masters thesis of the first author, which was supported in part by the University of Washington's Valle Scholarship and Scandinavian Exchange Program, and by NASA Grant NAG 5-2294 to the University of Washington. The work reported herein is a contribution of the University of Washington to the Boreal Ecosystem Atmosphere Study (BOREAS). BOREAS is a collaboration of U.S. and Canadian universities and government agencies, the lead agency for which in the U.S. is NASA. The assistance of BOREAS staff at NASA/GSFC, as well as other BOREAS investigators who supplied some of the data used in this report, and to friends and fellow students for help and encouragement is greatly appreciated. The comments of Dr. Susan Bolton (College of Forest Resources, University of Washington) who served on the first author's MS committee are appreciated as well.

TABLE OF CONTENTS

Page intentionally left blank

LIST OF FIGURES

LIST OF TABLES

CHAPTER 1: INTRODUCTION.

1.1 BACKGROUND.

Global warming is a complex environmental issue of major concern and importance. Since the onset of the industrial revolution in the 1800s, the activities of the human population have added increasing quantities of CO_2 and other greenhouse gases to the atmosphere, and the atmospheric concentration of CO_2 is now about 30 percent higher than the pre-1800 level of about 280 ppm [Houghton et al., 1990]. Long term analyses of global average temperature seem to show an increasing trend, which may be accounted for by these atmospheric pollutants [Cox and Moore, 1993; Gates, 1993].

Future global warming caused by increased atmospheric concentration of CO_2 and other radiatively important trace gases has been predicted by most General Circulation Models (GCM) of the atmosphere [Houghton et al., 1990], and also by the more simple upwelling-diffusion and pure diffusion models [Wigley and Raper, 1987]. Even though most scientists agree that there is a high probability of major global warming during the next century, they also acknowledge uncertainties in our understanding of the climate system and its behavior [Gates, 1993]. This reduces the confidence in predictions of the magnitude of the changes and how quickly they might take place. The reliability of GCM predictions is greatest at the global scale and least at the regional scale [Neilson and Marks, 1994].

Several important deficiencies limit the ability of climate models to understand and predict the effects of changes in atmospheric chemistry on climate. Among these are difficulties in modeling the effects of clouds at large scales, poor treatment of land-ocean interactions, and difficulties in representing the land surface. With respect to the latter, our ability to simulate feedbacks between the biosphere and the atmosphere (see Figure 1.1) is especially limited [King and Neilson, 1992]. It is important to quantify these feedbacks, at both short and long time scales, in order to improve our predictions of future environmental changes of the biomes, including possible redistribution of vegetation [Neilson and Marks, 1994]. At what rate might vegetation changes occur, and what intermediate changes might occur? Forests could be

displaced gradually or abruptly, they could be replaced by plants better suited for a new climate or suddenly die because of increased incidents of fires or drought.

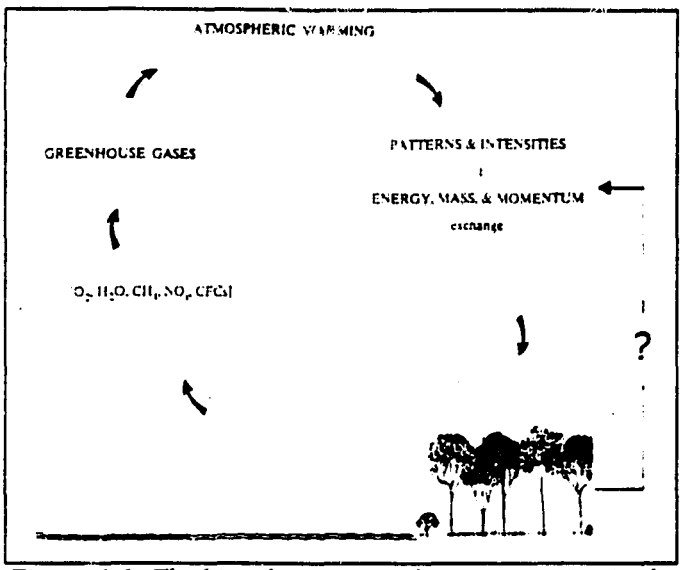

Figure 1.1: The biosphere-atmosphere interaction in the climatic system. Source: Graetz [1991].

1.2 POTENTIAL EFFECTS OF CLIMATE CHANGE AT HIGH LATITUDES.

Many studies indicate that the climatic effects of increased atmospheric concentrations of greenhouse gases would be greatest at high latitudes (45°N-65°N) [Monserud et al., 1993, cf Manabe et al., 1980, Jäger, 1988]. At these latitudes, there is some consensus that temperature as well as fall and winter precipitation would increase. While mean annual increases in global temperature are predicted to be in the range 3°C ± 1.5°C over the next hundred years by many GCMs [Houghton et al., 1990], northern continental areas could experience an increase in temperature twice as high [AES Environment Canada, 1994].

Vegetation.

Fossils and pollen from forests dominated by Jack Pine are buried in the peat bogs of coastal North Carolina [Watts, 1980]. Today, the southernmost occurrence of this species is in Massachusetts, 900 km to the north. Paleobotanists believe that the distribution of vegetation in

North America has changed gradually as glacial conditions have given way to our present climate [Davis, 1981].

Vegetation models indicate future changes in the major biomes would be associated with climate change [e.g. Emanuel et al., 1985; Pastor and Post, 1988]. A major part of the terrestrial biomass is in forests, which makes it important to understand the response of these biomes to increased temperature and atmospheric trace gas concentrations, especially CO_2. The boreal forest, which is circumpolar in extent and covers a broad band up to 1000 km across the Eurasian and North American continents [Larsen, 1980] (Figure 1.2), represents the part of the world which has experienced the largest changes in surface air temperature during the instrumental record of the past century [D'Arrigo et al., 1987]. These observed changes in temperature are associated with GCM predictions that the largest greenhouse warming for doubled CO_2 should occur towards the poles. The boreal forest has a total area of over 14.7×10^6 km^2, or 11 percent, of the earth's terrestrial surface [Bonan and Shugart, 1989], which makes it one of the most widespread global forest formations (it accounts for 23 percent of forested area and 14 percent of total forest biomass [Gates, 1993]). This region is of particular concern because the soils of the boreal forest hold between 16 and 24 percent of the global soil carbon [Gates, 1993]. Increasing temperature might result in the release of considerable CO_2 from the soils, and thus intensify the greenhouse effect.

In Canada, the boreal forest stretches from Newfoundland to the Alaska border and accounts for more than half of all the Canadian forest lands [Larsen, 1980]. Although the forests are primarily conifers, broad-leaved species occur as well, such as aspen, birch, and tamarack [Rowe, 1977].

Hydrology.

The hydrologic implications of global warming include increased evapotranspiration and increased precipitation on a global scale. This follows from the fact that higher temperatures increase the water holding capacity of the air, and hence it is expected that on a global basis, evaporation would increase. Higher air temperatures are the result of increased net radiation, and the latent and sensible heat fluxes would have to increase to maintain energy balance. On a

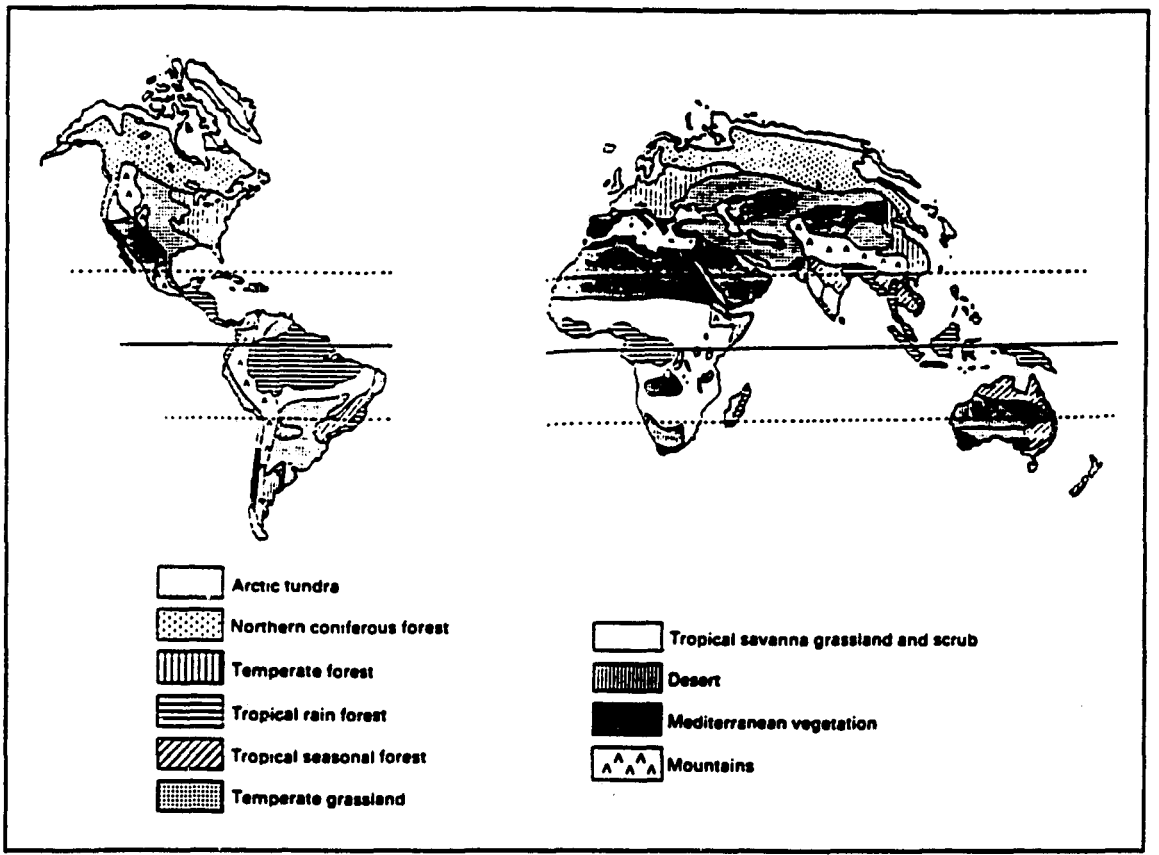

Figure 1.2: Distribution of the major terrestrial biomes of the world. (Northern coniferous forest = Boreal forest.) Source: Cox and Moore [1993].

global basis, average precipitation must balance average evaporation, so one would expect more precipitation. On the other hand, the increased cloudiness caused by more moisture in the air affects net radiation which results in an atmospheric limitation on evapotranspiration. Changes in temperature, precipitation and evapotranspiration caused by climate change will result in changes in soil moisture and runoff as well. At the moment, there is some uncertainty about the role of vegetation in relation to runoff following climate change [Dooge, 1992], and no definite conclusion can be made whether runoff will increase or decrease. The dependency of ecosystem processes on the water-balance may be altered by the direct and indirect responses of water-use efficiency to atmospheric CO_2-concentrations [Wyman, 1991]. For example, the stomatal resistance of the plants increases as the carbon dioxide content of the atmosphere is increased [Rogers et al., 1983]. On the other hand, increased temperature increases plant

productivity, and the final result is an approximate doubling of the water use efficiency for most types of plants [Idso, 1989].

1.3 BOREAS (Boreal Ecosystem-Atmosphere Study).

BOREAS (Boreal Ecosystem-Atmosphere Study) is an intensive field study being conducted at two locations in the Canadian boreal forest (see Figure 1.3), under the sponsorship of U.S. and Canadian government agencies. The overall goal of BOREAS is to "improve our understanding of the interactions between the boreal forest biome and the atmosphere in order to clarify their roles in global change" [BOREAS Experiment Plan, 1994]. Most of the BOREAS field activities took place during the winter and summer of 1994.

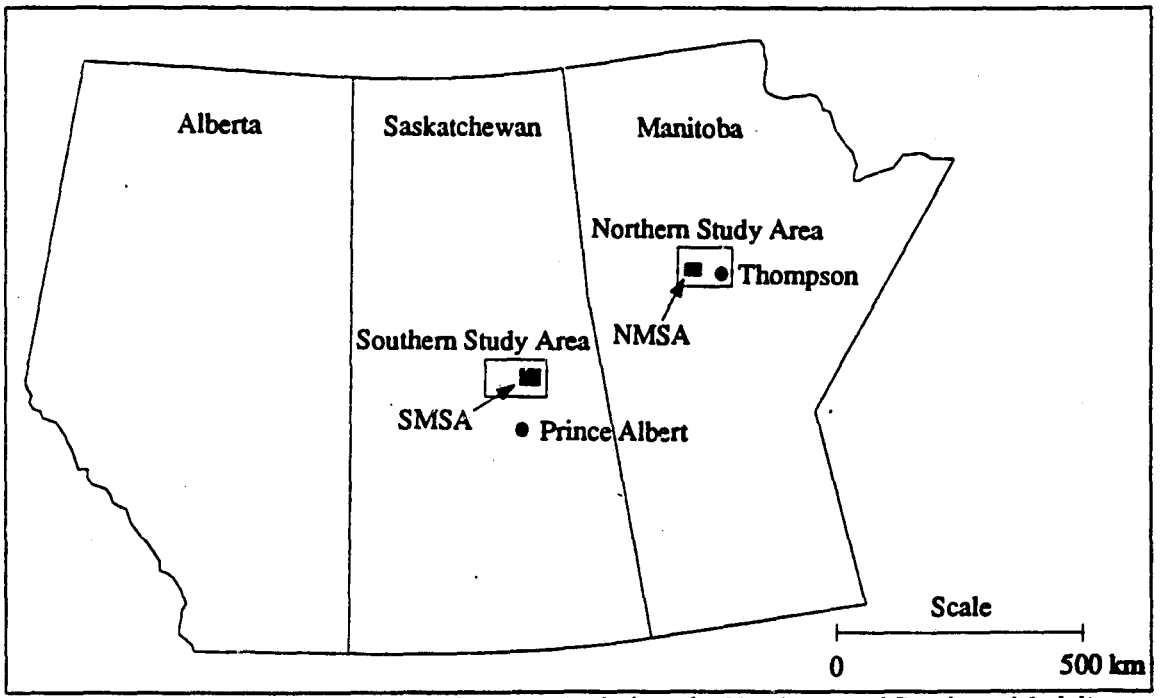

Figure 1.3: Location of BOREAS study areas, including the Northern and Southern Modeling Subareas (NMSA and SMSA). Redrawn from BOREAS Experiment Plan [1994].

BOREAS focuses on contrasting boreal forest conditions: The cold, short growing season of the north near Thompson, Manitoba, and the somewhat warmer, drier conditions of the southern extreme near Prince Albert, Saskatchewan. Within the northern and the southern study areas,

two modeling subareas are defined (Figure 1.3); the Northern Modeling Subarea (NMSA) and the Southern Modeling Subarea (SMSA). Much of the research being conducted in BOREAS focuses on the use of energy, water and trace gases by plants during the most intensive growth period. Most global change scenarios predict warming and drying in the mid-continent, and these two study areas allow the observation of processes associated with controlling factors (i.e. temperature and moisture) which are most likely to undergo change in case of climate change [BOREAS Experiment Plan, 1994]. An important objective of BOREAS is to develop improved computer simulation models of the important processes controlling the exchanges of energy, heat, water, CO_2 and the trace gases between the boreal forest and the atmosphere. These models would allow prediction of changes that might take place in the boreal forest beyond the relatively short BOREAS observation period. The project is coordinated with remote sensing and meteorological studies, which will be used to scale up and apply the process models at regional and global scales. These models can be used by scientists to anticipate the effects of global climate change on the biome [BOREAS Science Team, 1995]. The knowledge gained by the project should help researchers to better track future changes in the boreal forest biome.

1.4 OBJECTIVES OF THIS STUDY.

This thesis studies the relation between water use and vegetation in two climatic regimes within the boreal forest. Moisture availability during the growing season exerts an important control on the vegetation's functioning. By better understanding the cycling of water at the land surface in boreal regions, we should be able to improve our understanding of the possible consequences of future climate changes.

The principal objective of this thesis is to analyze and contrast moisture and heat fluxes of major vegetation types at two locations near the southern and northern extremes of the boreal region: The study focuses on differences in the energy and water budgets caused by climatic characteristics, and also on spatial differences within one of the BOREAS areas (SMSA). Spatial variability of precipitation leads to spatial variability of heat and moisture fluxes.

Therefore a second objective of this thesis is to evaluate the impact the spatial resolution of precipitation measurements has on the ability to represent the hydrology of a vegetated area.

One of the important characteristics of the boreal forest is the moss that covers a large part of the ground. The role of moss in surface energy and moisture exchange within the boreal forest is investigated through a combination of field observations and modeling. This moss carpet is thought to regulate soil moisture and temperature levels, and a third objective of this study is to investigate the role of moss in the hydrologic cycle.

Page intentionally left blank

CHAPTER 2: LITERATURE REVIEW.

2.1 BOREAL ECOSYSTEMS.

Climate.

The boreal climate is dominated by the influence of the high latitude and continental air masses, which produce large annual ranges of temperature. On average, summer temperatures reach 10°C, while winter temperatures may drop below -40°C. Despite long days, the subsoil can remain frozen well into the summer. Annual precipitation ranges from over 1000 mm on Norway's west coast to less than 200 mm in eastern Siberia and northwestern Canada [Critchfield, 1983]. In North America, the boreal forests normally experience dry winters, and more than half of the annual precipitation falls in the summer [Bonan and Shugart, 1989].

In the boreal region, the radiation balance is negative for a large part of the year, as shown in Figure 2.1. However, the net radiation gained in the summer more than balances the winter deficit, and no parts of the boreal region have a negative radiation balance at the surface for the entire year [Pruitt, 1978, cf Dolgin, 1970, Orvig, 1970]. In temperate and tropical regions convection and conduction are the important mechanisms of heat flow in the atmosphere, but further north on the northern hemisphere radiant energy exchange becomes increasingly important [Pruitt, 1978]. A cold atmosphere is usually associated with small vapor pressure gradients, resulting in small latent heat fluxes. At the same time, the temperature gradient between the vegetated surface and the cold, surrounding air is large, which tends to give high values of sensible heat. Both these factors favor a large Bowen ratio [Rouse, 1993].

Vegetation.

The boreal forest is characterized by low species diversity [Tivy, 1993]. The dominant trees in the boreal forest are conifers, particularly spruce. Toward the northern boundary of the boreal forest, growth is slower and trees become stunted and more widely spaced. Large shrubs are normally scattered and sparse in numbers. The ground layer of vegetation is dominated by low shrubs, which are underlain by mosses and lichens.

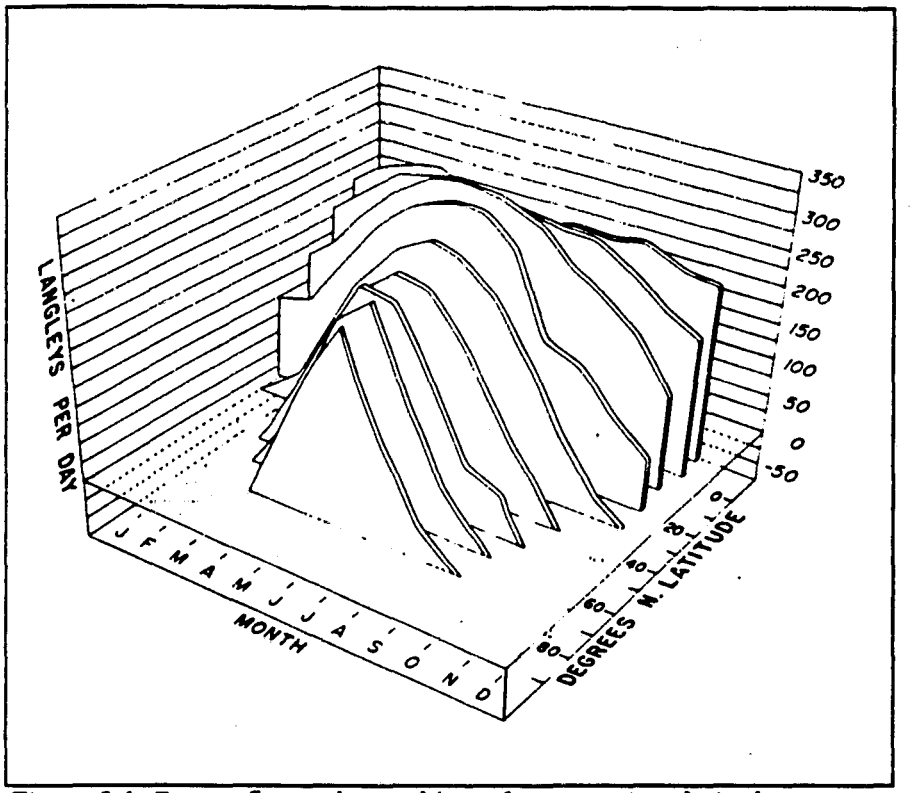

Figure 2.1: Energy flux at the earth's surface at various latitudes throughout the year. Source: Pruitt [1978].

Boreal plants are adapted to the temperature and light conditions in northern regions, and they attain maximum photosynthetic rates at lower temperatures than are characteristic of plants of more southern regions [Larsen, 1980]. Conifers have significant rates of photosynthesis at near-freezing temperatures, hence they are able to photosynthesize over a much longer time period than deciduous trees [Vowinckel et al., 1975].

During the growing season the boreal conifers are normally not limited by photosynthetically active radiation (PAR). Vowinckel et al. [1975], for instance, found no seasonal variations in photosynthesis in Black Spruce (Picea Mariana) over June, July and August, in contrast to the temperate deciduous forest's spring burst and midsummer lull in activity [Larsen, 1980].

The productivity of boreal forests is less than that of temperate forests, since they have less energy available. The amount of organic matter in the northern coniferous forest is of the order 22-60 tons/ha, which is considerably less than the 370-410 tons/ha that is found in temperate

broad-leaved forests. A decrease in average growth rates is also found along the latitudinal gradient northward through the boreal forest [Larsen, 1980].

In moist, shaded woods, moss is the dominant ground cover, and a thick moss ground cover composed primarily of feathermosses (Hylocomium Splendens, Pleurozium Schreberi) or Sphagnum species (Sphagnum Subsecundum, Sphagnum Nemoreum) is common throughout the boreal forests of North America [Bonan and Shugart, 1989]. Mosses are thought to regulate soil moisture and temperature levels [Skre and Oechel, 1981, cf Viereck, 1975, Weetman, 1968], and are thus of major importance in the hydrologic cycle.

Limits of the growth of boreal forests.

Forest communities exist in a dynamic equilibrium with climatic conditions, and the northern tree line of the boreal forest has moved several times over the last 15,000 years [Chabot and Mooney, 1985]. These movements have been associated with gradual temperature changes and extensive fires. The geographic distribution of tree species and the northern and southern limits to the boreal forests are correlated with climatic parameters [Larsen 1980; Bonan and Sirois, 1992, cf Hopkins, 1959, Bryson, 1966, Skre 1979, Walter 1979], but the causes of these relationships have not been established [Bonan and Sirois, 1992]. Such an understanding is needed to predict the effects of a possible warming on the future distribution of vegetation [Emanuel et al., 1985; Pastor and Post, 1988].

Although there is no consensus to what the most limiting factor of the growth and areal distribution of the boreal forest in Canada is, the most widespread opinion seems to be that temperature plays a major role. The northern limit of the boreal forest has been associated with the summer position of the front that separates continental Arctic and maritime Pacific air masses (July isotherm of 13°C), while the southern limit is associated with the winter position of the Arctic front (July isotherm of 18°C) [Oechel and Lawrence, 1985; Bonan and Sirois, 1992, cf Bryson, 1966], see Figure 2.2.

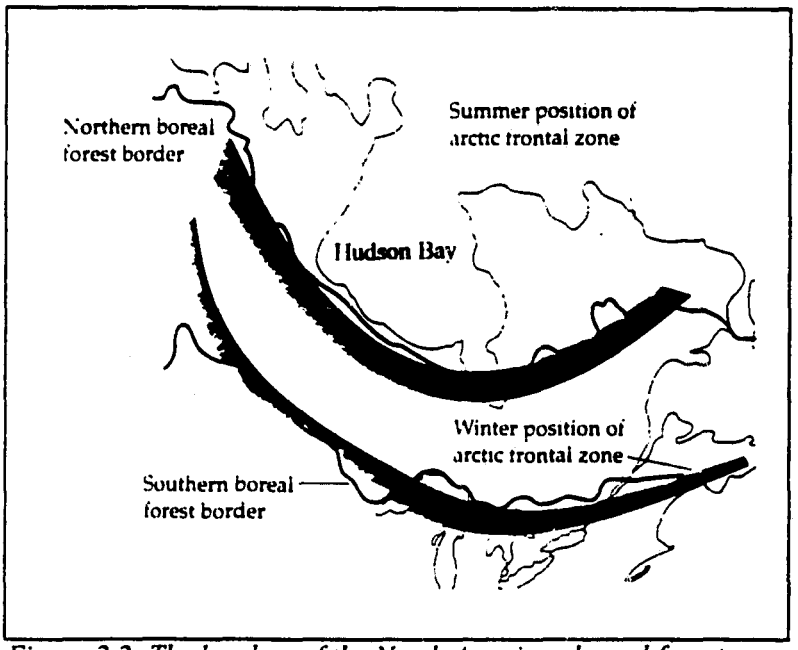

Figure 2.2: The borders of the North American boreal forest biome and the position of the continental Arctic front in summer and winter. Source: Gates [1993].

Black and Bliss [1980] studied Black Spruce at the tree line in The Northwest Territories, and found that this species is limited by temperature at the stage of seedling germination. Others indicate that plant processes may be more limited by extreme climatic fluctuations rather than by average weather patterns. Woodward [1987], for instance, suggested that winter frost tolerance rather than summer temperature controls tree growth, and Skre [Bonan and Sirois, 1992, cf Skre, 1979] concluded that minimum temperature for growth respiration is an important factor determining the distribution of plants in the boreal region. Sakai and Weiser [1973] and George et al. [1974] found that the approximate threshold for many temperate evergreens and deciduous species is -40° to -45°C, while many boreal conifers and hardwoods were found to survive even the lowest experimental temperatures (typically -70° to -80°C).

The presence or absence of permafrost is another important ecological factor in boreal ecosystems, which restricts the extension of the forest into areas that are now tundra [Larsen, 1980]. Broadly, there are two permafrost zones in Canada: continuous and discontinuous, and tree line is an approximate boundary between the two zones [French and Slaymaker, 1993a].

Moisture stress has been related to limitation of growth in boreal forests. Hare [1950] suggested that 300 mm of annual average precipitation defines the limits of forest growth. Others argue that water stress is a limiting factor only on thin canopied southern exposures [Oechel and Lawrence, 1985], and the study by Stephenson [1990] suggests that drought does not determine forest type. Oechel and Lawrence [1985], Hare and Ritchie [1972] and Larsen [1980] also mention that total radiation received and the amount absorbed and lost, limit biomass production. Yearly net radiation is over 28 MW/(m^2 year) at the southern extreme of the Canadian boreal forest, but decreases to about 10 MW/(m^2 year) at the edge of the tundra. In the north, the canopy is less developed than in the south, which increases the snow season albedo and decreases the interception and capture of solar radiation [Pruitt, 1978; Oechel and Lawrence, 1985, cf Hay, 1969]. Larsen [1980] suggested that the location of the Arctic and the Pacific fronts are significant only because they determine the characteristics of the energy budget during the growing season.

The effect of energy supply is not independent of water supply. A plant needs water to utilize energy for growth, otherwise the energy acts only to heat and stress the plant. Supply of water, without energy, results in the water percolating through the soil or running off unused [Stephenson, 1990]. The effects of climate on plants, therefore, are dependent on the interactions of energy and water, not just their absolute amounts. Stephenson's [1990] analysis showed that the distribution of North American plant formations has a higher correlation with the water balance (moisture deficit and evapotranspiration) than with temperature and precipitation, which he suggested is caused by the ability of the water balance to distinguish between climates similar in mean annual energy and water supplies but different in the seasonal timing of the two.

Soil fertility has received attention as possibly controlling the distribution of coniferous and deciduous forests; conifers tend to occur in less fertile soils [Monk, 1966; Chabot and Hicks, 1982]. Sirois [1992] suggested that the northern limit of Black Spruce reflects an inability to reproduce on the thick lichen mat rather than an inability to grow in a cold climate. A thick lichen mat can hinder tree growth through its effect on soil temperature and nutrient availability [Brown and Mikola, 1974]. Soil fertility is often a consequence of the amount and timing of energy and water supply [Meentemeyer, 1978; Arkley, 1967]. Stephenson [1990] suggests that

the large-scale distribution of forest types probably is more controlled by the availability of energy and water than soil fertility.

The southern limits of the boreal forest may be caused by increased radiation. However, Bonan and Sirois' [1992] study suggests that for Black Spruce the direct effects of excessive heat on tree growth is not a causal factor, and that Black Spruce can grow far south of current southern limit. Many other boreal conifers grow well in gardens south of their natural ranges [Woodward, 1987]. In regions where soil moisture does not limit growth, the southern limits to boreal tree species might reflect an interaction of air temperature, incident PAR and/or nutrients [Bonan and Sirois, 1992]. The increased radiation also benefits the hardwoods' superior photosynthetic rate, and they might outcompete conifers [Stephenson, 1990].

Decreased reproductive potential with warmer air temperatures might also be a factor in defining the southern boundary of the boreal forest, because pollen abundance for many species decreases with temperatures warmer than an optimum. Chilling requirements for budburst might also limit the southern extension of cold tree species [Bonan and Sirois, 1992]. The factors influencing the growth of the boreal forest are summarized in Figure 2.3.

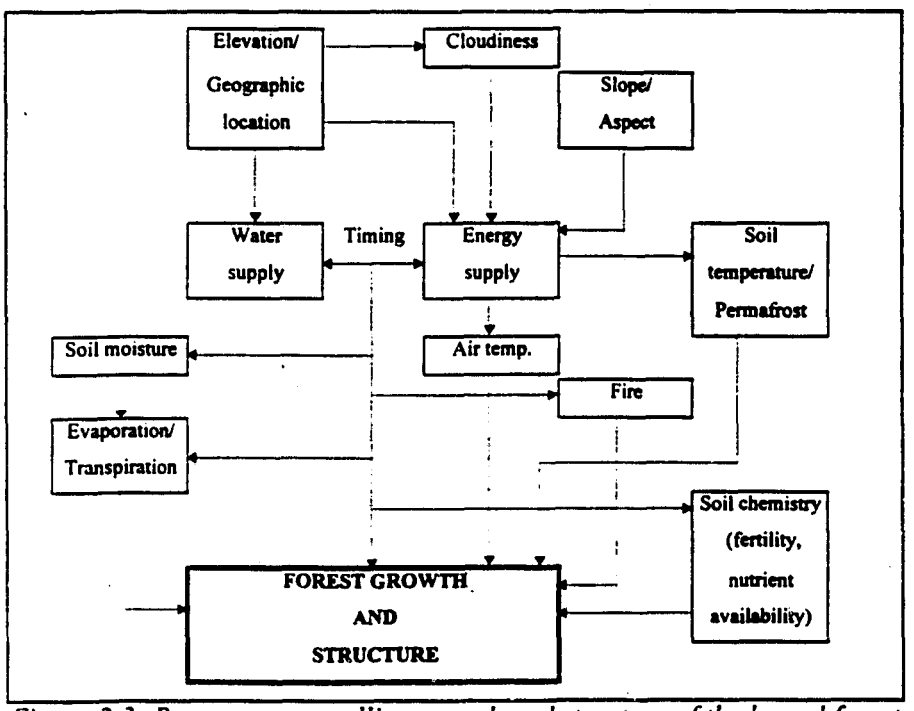

Figure 2.3: Processes controlling growth and structure of the boreal forest.

2.2 RESPONSE OF VEGETATION TO DIFFERENT CLIMATIC CONDITIONS.

Background.

Changes in the physical climate system of the boreal forest will influence biophysical processes (Figure 2.4, arrow (A)). The biophysical system affects the atmosphere through changes in energy, heat and water exchange (B). A future rise in temperature would result in reduced continental and oceanic snow and ice. This would cause the average global albedo to decrease, and the land and oceanic surfaces to absorb more solar radiation. The earth's sensitivity to such radiative forcings is moderated by the presence of trees in northern latitudes. The northern forests mask the high reflectance of snow, leading to warmer winter temperatures than if trees were not present. The boreal forest absorbs energy within the canopy, resulting in higher air temperatures in the summer as well. If the boreal forest for some reason disappeared, the summers and winters would be cooler. In contrast, a warmer climate might cause the boreal forest to migrate northwards, and hence causing decreased albedo and future warming in those areas. The result of the interaction of climate warming and migration of the boreal forest is not fully understood. However, Rowntree [1988] reviewed the sensitivity of albedo, vegetation and climate as predicted by GCMs, and found that for albedo increases the major effects on global climate were decreased land evaporation and decreased precipitation over land.

Whether future vegetation changes will result in more or less storage of carbon remains to be resolved. Increased primary production caused by increased temperature would result in higher storage of carbon, while increased nutrient cycling rates would release CO_2 and CH_4 from the soil carbon pool back to the atmosphere (arrow (C) in Figure 2.4). What we do know is that sudden changes in climate would result in larger release of carbon than gradual changes, since in the latter case the plants would have time to acclimate to new environmental conditions. Estimates of global carbon storage using GCMs, assuming equilibrium conditions under double-CO_2 climate scenarios, suggest that the terrestrial biosphere could store ~0% to 30% more carbon above ground than it currently does [King and Neilson, 1992, cf Smith et al., 1991, Prentice and Fung, 1990, Prentice, 1990]. In contrast, King and Neilson [1992] focused on the dynamic redistribution of vegetation, and found that the terrestrial vegetation would release stored carbon, and thus act as a positive feedback to climate change. Studies by D'Arrigo et al. [1987], suggest that some boreal forest species in North America might be growing faster as a

result of rising levels of CO_2 in the atmosphere, and are thus acting as a sink for the world's excess carbon. Finally, Billings et al. [1982, 1983] suggest that future climate changes might release some of the soil organic carbon stored on land, and renew the northward extension of the vegetation zones. Whether the boreal forest is a sink or a source of carbon and CH_4 on a long-term basis is one of the long-term effects BOREAS is addressing, and the extensive field measurements should give some answers as to how the boreal forest responds to different levels of temperature and CO_2 in the atmosphere.

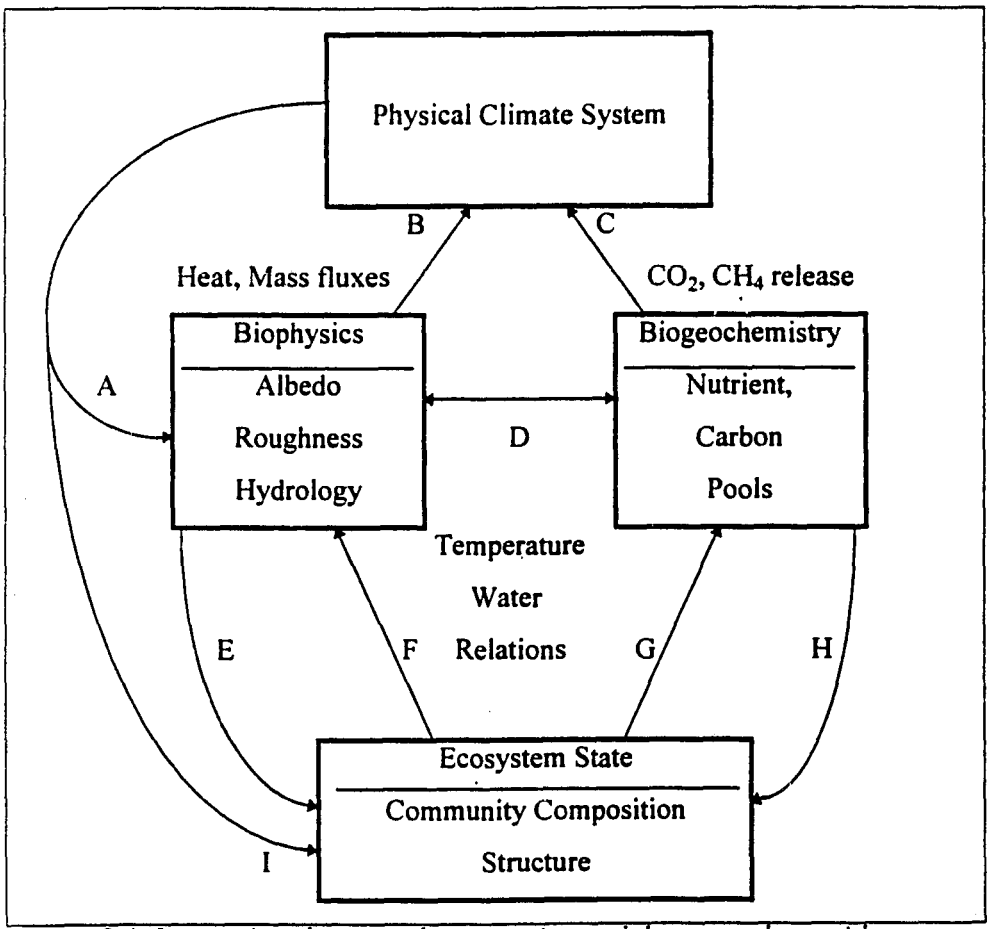

Figure 2.4: Interactions between the vegetation and the atmosphere with respect to global change. Redrawn from BOREAS Experiment Plan [1994].

The uptake or release of CO_2 and CH_4, together with changes in water and nutrient availability, influence community composition and structure (arrows E and H in Figure 2.4), which finally will result in changes in surface biophysical characteristics and biogeochemical process rates (F and G). Two of the most obvious factors influencing the character and distribution of

ecosystems are the amount and variability of temperature, and the amount of rainfall (see Figure 2.3). Davis [1981] has suggested that many tree species may not be able to disperse rapidly enough to track areas of suitable climate, and in that way the climate system can influence the ecosystem state directly (I).

Predictions of boreal forest response to climate change.

Monserud et al. [1993] used a global vegetation model and GCM climate scenarios to predict global changes in vegetation patterns from climate change (CO_2 doubling). They found that the vegetation in the boreal areas would undergo great changes and that all the boreal vegetation classes probably would shrink. If the productivity of the boreal ecosystem is limited over large areas by temperature rather than moisture, a possible climatic warming should increase the productivity of these ecosystems, and the demand for water would increase. Kauppi and Posch [1985] modeled the forest growth in Finland, given an increase in temperature. In the range of 0.1°C to 5°C, the maximum increase of growth would occur in southern-central and maritime ecosystems ($\bar{T}$ = 4.5°C), while the highest relative increase would occur in northern ($\bar{T}$ =-1.0°C) regions.

Rizzo and Wiken [1992] used output from a GCM to predict the future distribution of ecosystems in Canada. Their work showed that major changes in Canadian ecosystems would occur in a doubled CO_2 climate. In particular, the boreal region would decrease substantially (see Figure 2.5). Cool, temperate systems would expand into boreal zones. The dry, continental boreal province (including SMSA) would virtually disappear, and would be replaced by grassland. The area including NMSA, now on the border between 'dry continental boreal' and 'subarctic', was predicted to change to 'cool temperate'.

Using data from the Goddard Institute for Space Studies (GISS) and Geophysical Fluid Dynamics Laboratory (GFDL) GCMs, French and Slaymaker [1993b] predicted the shifts in the position of the northern and southern boundaries of the boreal forest in Canada, based on growing degree-days. They found that the possible shift in the northern boundary would range from 100 to 700 km, while the shift in the southern boundary would be much greater; 250 to 900 km. Sargent [1988] used a model based on climatic parameters controlling plant survival,

to model the response of the Canadian boreal forest to climate change. His results indicate that with a doubled CO_2 climate scenario, the boreal forest would shift northwards by about 5 degrees and would be largely reduced in area (Figure 2.6).

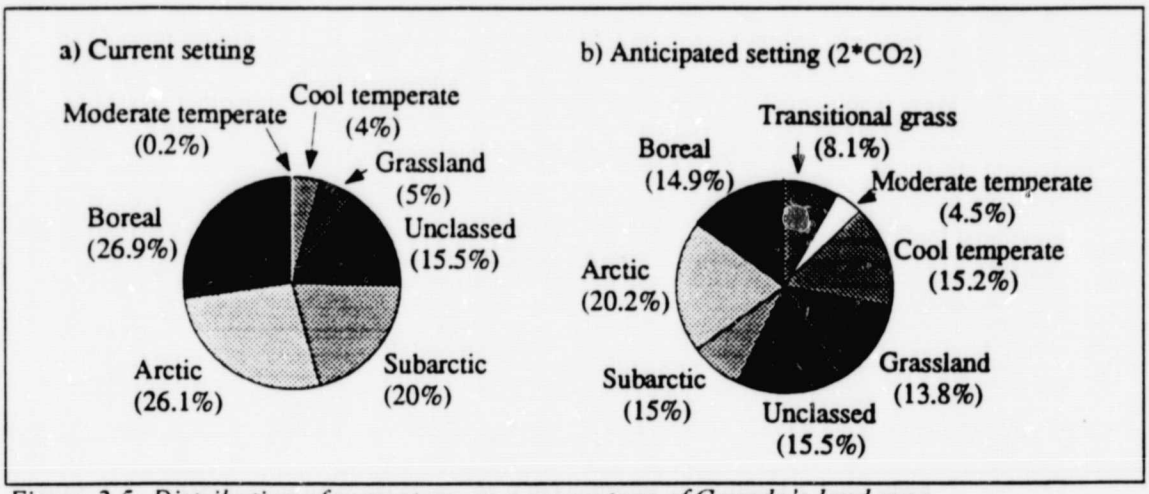

Figure 2.5: Distribution of ecosystems as a percentage of Canada's land area. Data from Rizzo and Wiken [1992].

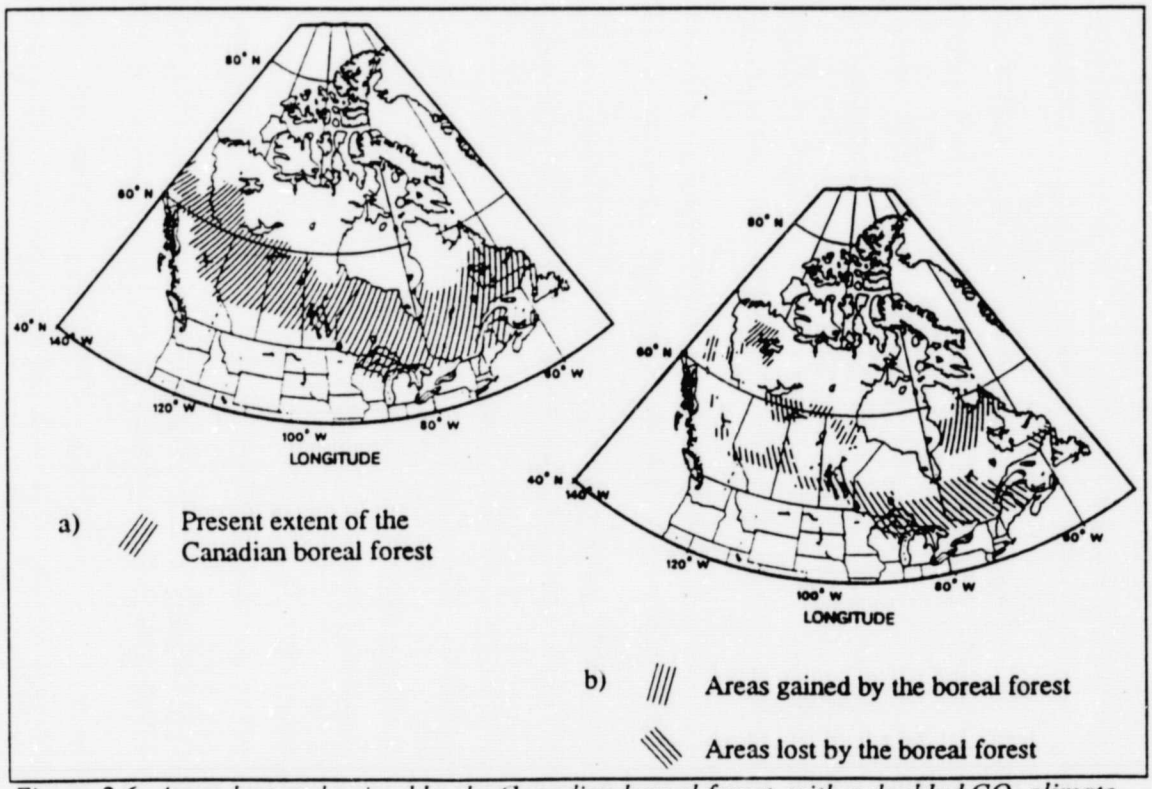

Figure 2.6: Areas lost and gained by the Canadian boreal forest, with a doubled CO_2 climate scenario. Source: Sargent [1988].

All these results must be evaluated in light of the model assumptions, and the fact that we do not yet fully understand how the climate affects ecological processes. The field experiments and analyses conducted under BOREAS are expected to increase our understanding of the physical impacts of climate change, and this knowledge should eventually help to improve model predictions. This thesis emphasizes the hydrology of boreal forest ecosystems under current climatic conditions. Soil moisture, evapotranspiration and runoff are dependent on vegetation type, temperature and topography, and have a high spatial and temporal variability. Since forest growth and structure depend both on energy and water supply, knowledge of present vegetation response to both the amount and the timing of these variables should help our understanding of vegetation response to a possible future climate change. Some of this knowledge can be obtained by using hydrologic models that give predictions of the partitioning of water among the various pathways of the hydrologic cycle.

Page intentionally left blank

CHAPTER 3: MODEL DESCRIPTION.

3.1 LOCATION AND DESCRIPTION OF STUDY AREAS.

The modeling work reported in this thesis was done in connection with BOREAS, which focuses on a northern modeling subarea (NMSA) near Thompson, Manitoba, and a southern modeling subarea (SMSA) near Prince Albert, Saskatchewan (see Figure 1.3). Table 3.1 gives descriptive summary characteristics of the study areas.

Table 3.1: Descriptive data of the northern (NMSA) and southern (SMSA) modeling subareas.

	NMSA	SMSA
Area	30×40 km	40×50 km
Latitude/Longitude, northwest corner	56.06N, 98.72W	54.09N, 105.18W
Mean elevation	261 m	520 m
Mean annual temperature[1]	-3.9°C	0.1°C
Mean annual precipitation[1]	544 mm	398 mm

During parts of 1994 several flux towers were operated in each of the modeling subareas (Figure 3.1) for the purpose of measuring fluxes of energy, moisture and trace gases. The Tower Flux (TF) sites were located in the center of homogeneous areas of about 1 km^2 of the vegetation cover they were selected to represent. The two regions are described briefly below.

Northern Modeling Subarea.

The NMSA is 40 km in the east-west direction by 30 km in the north-south direction, and the terrain is flat and broadly rolling. The mean elevation is 261 m, ranging from 81 m to 337 m, and is a little higher in the northern part than in the southern part of the area. The vegetation is dominated by Black Spruce which occurs in stands of varying density. Because the NMSA is relatively flat and has abundant wetland areas, the drainage of much of the site is poor. Several

[1] Mean annual temperature and precipitation are for Thompson Airport (NMSA) and Prince Albert Airport (SMSA).

significant streams and a few lakes exist within the area. The soils mostly consist of clay [BOREAS Experiment Plan, 1994].

Southern Modeling Subarea.

The SMSA is 50 km (east-west) × 40 km (north-south) and is fairly flat, with elevations ranging from 432 in the southeastern part to 656 m in the northwestern part, with a mean elevation of 520 m. The dominant vegetation is coniferous forest, mainly consisting of Black Spruce, as in the NMSA. Deciduous trees are mostly found in mixed stands with conifers. The area includes some lakes, the largest of which is White Gull Lake in the western part of the area. The soils are mainly sand and loam [BOREAS Experiment Plan, 1994].

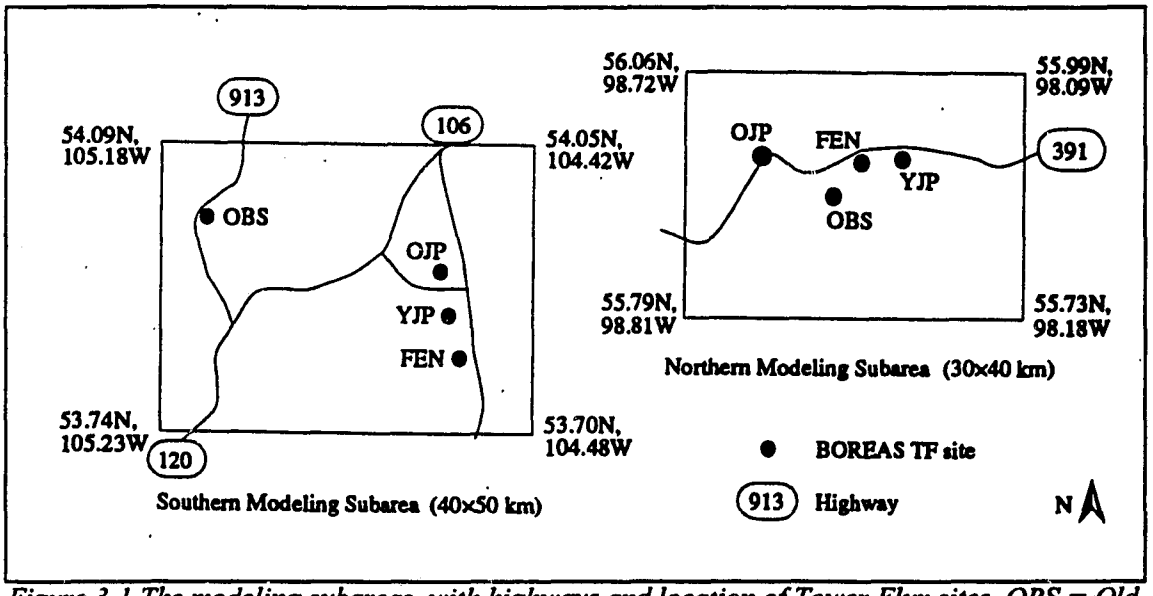

Figure 3.1 The modeling subareas, with highways and location of Tower Flux sites. OBS = Old Black Spruce, OJP = Old Jack Pine, YJP = Young Jack Pine, and FEN = Fen. Redrawn from BOREAS Experiment Plan [1994].

3.2 DISTRIBUTED HYDROLOGY-SOIL-VEGETATION MODEL.

Model basis.

The distributed hydrology-soil-vegetation model (DHSVM) [Wigmosta et al., 1994] was used as the basis for the modeling part of this study. The model assumes that the vegetation consists

of an overstory and an understory. Radiation and wind speed are attenuated through overstory and understory, based on cover density and leaf area index (LAI). The model estimates evapotranspiration using a Penman-Monteith approach. Snow accumulation and melt are simulated using an energy balance model, and moisture movement through the rooting zones is calculated using Darcy's law. Downslope redistribution of soil moisture is modeled on a pixel-by pixel basis. Figure 3.2 illustrates the model representation of a drainage basin.

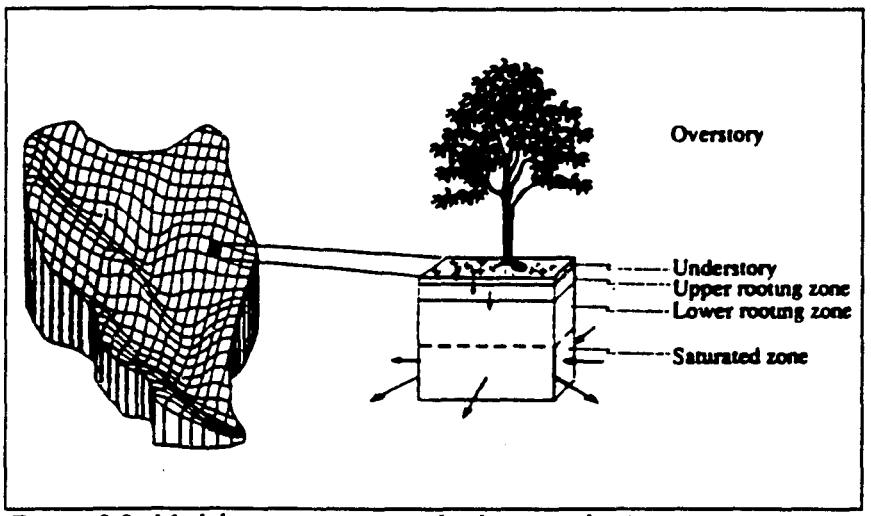

Figure 3.2: Model representation of a drainage basin.
Source: Wigmosta et al. [1994].

The model is physically based, and accounts explicitly for the spatial distribution of land-surface processes. It can be used as a distributed model or as a point model, and can be run at hourly to daily time steps. When used as a distributed model, the terrain is characterized by use of a digital elevation model (DEM). Previously, the model has been used in mountainous terrain with good results [e.g. Wigmosta et al., 1994; Arola, 1993]. However, it has not been applied previously in the relatively flat terrain and continental climate that characterize the NMSA and SMSA.

The forcing variables which are required at each time step, are wind speed, air temperature, dew point temperature, precipitation, cloud cover and shortwave radiation. Longwave radiation can either be given as an input parameter or estimated within the model. In addition, initial conditions for soil moisture, interception storage, snow water equivalent, and depth to water table must be specified. Each pixel is assigned vegetation and soil parameters, e.g. LAI, stand

height, porosity, field capacity and saturated hydraulic conductivity. All of these, with the exception of LAI, are fixed; LAI may be allowed to vary seasonally.

This thesis focuses on the heat and moisture fluxes in the boreal forest. The formulations of latent and sensible heat fluxes are given in Eqs. 3.1 and 3.2:

$$Q_e = \lambda E \tag{3.1}$$

$$Q_s = \rho_a c_p (T_a - T_s) / r_a \tag{3.2}$$

where Q_e: Latent heat flux

λ: Latent heat of evaporation

E: Evapotranspiration

Q_s: Sensible heat flux

ρ_a: Air density

c_p: Specific heat of air

T_a: Temperature, air

T_s: Temperature, vegetation, snow or soil surface

r_a: Aerodynamic resistance

Evapotranspiration is calculated from the Penman-Monteith equation:

$$E = \frac{\Delta R_n + \rho_a c_p (e_s - e) / r_a}{\lambda[\Delta + \gamma (1 + r_c / r_a)]} dt \tag{3.3}$$

where Δ: Slope of saturated vapor pressure-temperature curve

R_n: Net radiation

e_s: Saturation vapor pressure

e: Vapor pressure

r_a: Aerodynamic resistance

γ: Psychrometic constant

r_c: Canopy resistance

dt: Time step

Evaporation of intercepted water (maximum 0.1 mm*LAI) is assumed to occur at the potential rate, which can be found by setting the canopy resistance, r_c, in Eq. 3.3, to zero. If the evaporation is less than the potential, transpiration is calculated from:

$$E = (E_p - E_i)\frac{\Delta + \gamma}{\Delta + \gamma(1 + r_c / r_a)} \tag{3.4}$$

where E_p: Potential evaporation

E_i: Evaporation from intercepted water

Aerodynamic resistances are calculated separately for overstory, understory, ground surface and snow surface, and are taken in series (see also Section 4.1). The calculation of canopy resistance is adapted from Dickinson et al. [1991], who based their formulation on minimum stomatal resistance, soil or air temperature (DHSVM uses air temperature), vapor pressure deficit, photosynthetically active radiation (PAR) and LAI. Canopy resistance is calculated separately for understory and overstory, where the leaves are assumed to contribute in parallel:

$$r_c = \frac{< r_s >}{LAI} \tag{3.5}$$

where r_c: Canopy resistance

r_s: Stomatal resistance

LAI: Projected leaf area index

and the angle brackets denote an inverse average. Stomatal resistance depends on vegetation type and environmental factors, and is taken as a product of four limiting factors each with a minimum value of one:

$$r_s = r_{s\min} f_1(T) f_2(vpd) f_3(PAR) f_4(\theta) \tag{3.6}$$

where r_{smin}: Minimum stomatal resistance

T: Temperature

vpd: Vapor pressure deficit

PAR: Photosynthetically active radiation

θ: Soil moisture

Adjustments made to the model.

For boreal regions, it is known that the subsoil can be much colder than the air well into the summer [Critchfield, 1983], and is limiting for water uptake and growth [Bonan and Shugart, 1989; French and Slaymaker, 1993a]. Air temperature normally does not limit photosynthesis during the growing season [Oechel and Lawrence, 1985; Vowinckel et al., 1975]. DHSVM was

modified to incorporate soil temperature as one of the factors controlling canopy resistance. Stathers and Spittlehouse [1990, cf Örlander et al., 1990] present water uptake by roots as a function of soil temperature for Norway Spruce (Picea Abies) and Scots Pine (Pinus Sylvestris) seedlings growing in Sweden. The climate of the Swedish and Canadian boreal forests are somewhat similar, and results from field experiments in Alberta and Alaska suggest the same pattern is valid also for mature Black Spruce and Jack Pine (Pinus Banksiana) [Tryon and Chapin III, 1983; Strong and La Roi, 1983]. A curve was fit to the data given by Stathers and Spittlehouse [1990], and the following equations were used to estimate canopy resistance:

$$1/f_{bs} = 0.176 + 0.0770T_s - 0.0018T_s^2 \quad (3.7)$$

$$1/f_{jp} = 0.0705T_s - 0.0013T_s^2 \quad (3.8)$$

where $1/f_{bs}$: Correction factor used for Black Spruce

$1/f_{jp}$: Correction factor used for Jack Pine

T_s: Soil temperature

The same correction factor as for Jack Pine was used for all other vegetation types, because of lack of data.

Lake evaporation is not incorporated explicitly in DHSVM, so for the lakes a simple approach was taken: Evaporation from the lakes was assumed to occur at the potential rate, and no lateral flow was allowed within the lake. In case rainfall (or incoming lateral flow) causes the water level to rise above the given height of the DEM, the excess water is assumed to go to surface runoff. The surface runoff is routed to the outlet of the basin using distance to the outlet and pixel-dependent velocity. The velocity is computed based on slope and upstream drainage area, and hence travel time to the outlet of the watershed (or to the edge of the area if not working with an entire watershed) can be computed. This routing scheme was developed by Pascal Storck of the Department of Civil Engineering at the University of Washington, based on work by Jorge Ferreira (Department of Civil Engineering, University of Washington) and Maidment et al. [1995].

Moss covers much of the ground in the boreal area. It was not incorporated by Wigmosta et al. [1994], since moss was essentially absent in the watershed they modeled. The soil information given for SMSA (see Section 3.3) indicates two different layers of mineral soil for some of the area, in addition to a humus layer at the surface. Many boreal tree species (for example Black Spruce) have a root structure with shallow lateral roots in addition to taproots. Because of the

root structure and the soil information, a third root zone (i.e. a moss layer) was added to the model, to allow better representation of the distribution of roots in the soil column.

3.3 DATA ACQUISITION.

Meteorological data.

Point Model.

Air temperature, dew point temperature, wet bulb temperature, cloud cover and wind speed are recorded at an hourly time step at Thompson Airport (212 masl) and Prince Albert Airport (428 masl), near the northern and southern sites (see Figure 1.3). Accumulated precipitation is measured every six hours. Data for 1989 were prepared by Joseph Coughlan, NASA Ames Research Center, who also estimated shortwave and longwave radiation for this period.

Distributed model.

For the distributed model runs (described in detail in Section 5.2), 1989 data for Prince Albert Airport, and data from December 1993 to mid August 1994 from two automated meteorological stations operated by Saskatchewan Research Council (SRC) for the BOREAS project were used. In the southern study area, SRC operates stations at the Old Jack Pine (OJP) and Old Aspen (Populus Tremoluides) (OA) sites (Figure 3.3). Data from OJP were used when available, since this station is located within the SMSA, otherwise data from the OA station were used. In addition, some meteorological data from the Atmospheric Environment Service Canada (AES) station at Nipawin, about 80 km southeast of the OJP site, were used when data were missing at both OJP and OA. At the SRC-and AES-stations, measurements of incoming short- and longwave radiation, temperature, relative humidity and wind speed are recorded every 15 minutes. Dewpoint temperature was estimated from relative humidity and air temperature, using the following equation which is accurate to within 0.3°C in temperature ranges from -40° to 50°C [Linsley et al., 1982]:

$$T - T_d = (14.55 + 0.114T)X + [(2.5 + 0.007T)X]^3 + (15.9 + 0.117T)X^{14} \qquad (3.9)$$

where T: Air temperature

T_d: Dew point temperature

X: 1-f/100

f: Relative humidity

For the summer of 1994, a precipitation radar was located south of the SMSA (Figure 3.3). The radar's maximum effective range was 220 km, and it used a wave length of 5 cm (C-band), which gives high quality measurements within a radius of 80 km [Eley, personal communication]. The radar data were mapped on a 2×2 km pixel basis, with the radar location as the reference point. The raw precipitation images were prepared by Joe Eley and Terry Krauss, Canada Atmospheric Environment Service, Saskatoon.

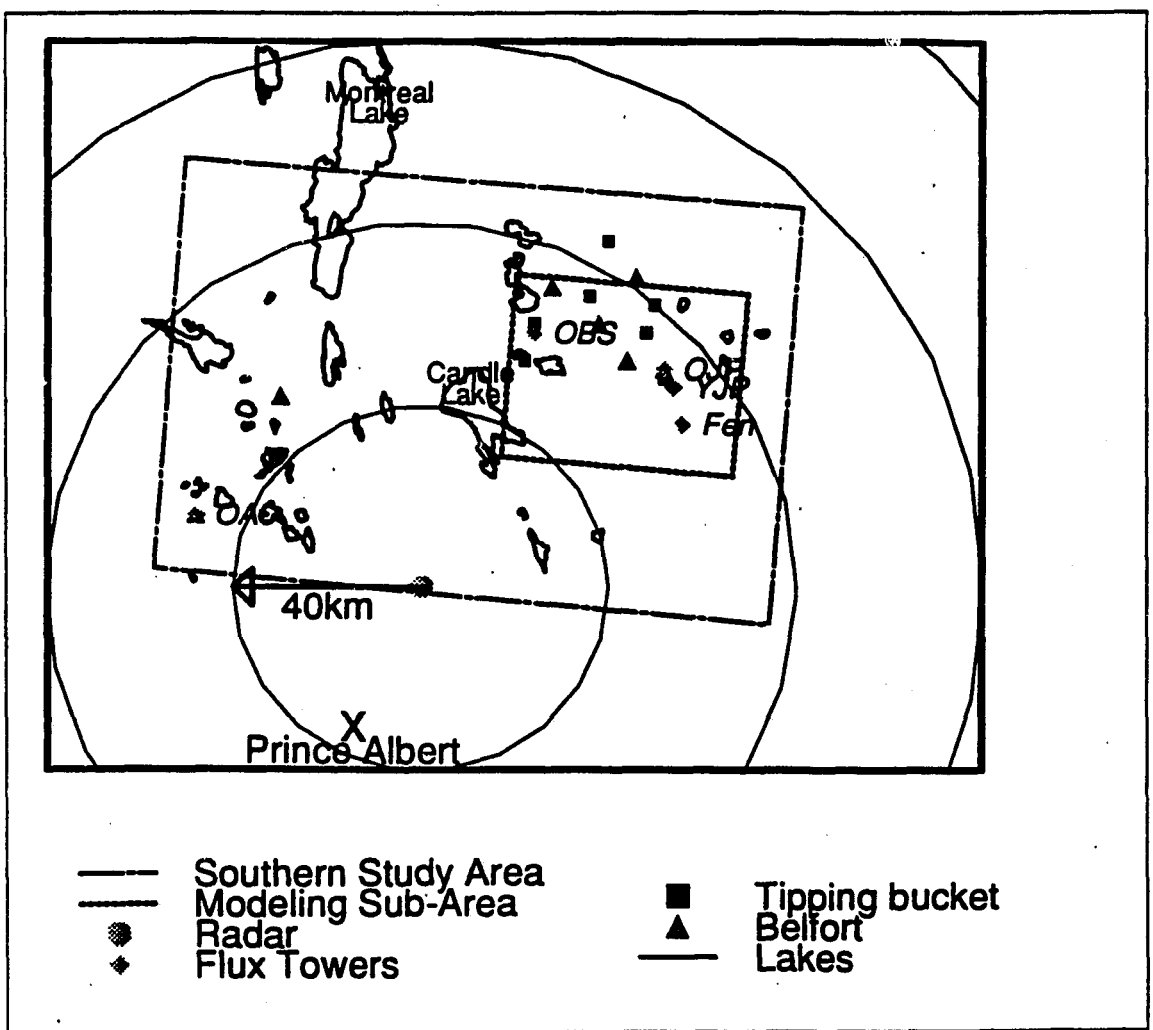

Figure 3.3: Location of radar, rain gauges and tower flux sites in the southern study area.

Solar radiation was calculated for each grid cell using the Image Processing Workbench (IPW) [Frew, 1990; Longley et al., 1993], following the method of Arola [1993], which is based on Dubayah et al. [1990]. The resulting files give direct beam and diffuse radiation for each grid cell for each time step. These values are for clear sky-conditions, and must be corrected for cloud cover. Cloud cover was not measured at the SRC-stations; instead calculated clear sky solar radiation values, at the pixel corresponding to the location of the SRC-station at OJP, were corrected according to measurements of incident solar radiation at this site. The same correction factor was assumed over the entire area, and was hence used as a substitute for cloud cover.

Digital elevation model (DEM).

A digital elevation model for the southern modeling subarea area was prepared by Xuewen Wang of the Department of Geography at the University of Toronto. The original topographical data he used were in vector format, digitized from 1:50,000 maps. The DEM was made by use of TOPOG software [Vertessy et al., 1993], and has a spatial resolution of 100×100 m. The DEM is shown in Figure 3.4. Table 3.2 gives the areal coverage of the DEM.

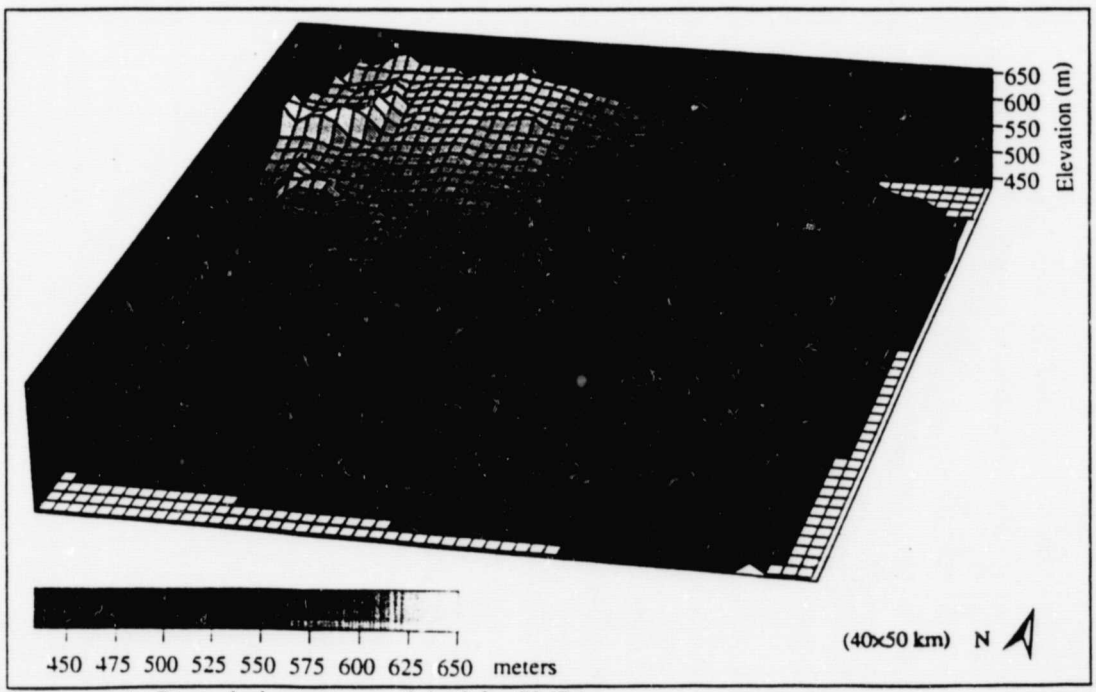

Figure 3.4: Digital elevation model of the SMSA.

Table 3.2: Boundaries of the DEM.

	UTM, NAD 27 (zone 13)	Latitude, Longitude
Northwest corner	5993700N, 488200E	54.09N, 105.18W
Northeast corner	5989400N, 538200E	54.05N, 104.42W
Southeast corner	5949500N, 534700E	53.70N, 104.48W
Southwest corner	5953800N, 484800E	53.74N, 105.23W

Vegetation data.

Vegetation data for the SMSA were classified by BOREAS Science Staff (Forest Hall and Dave Knapp) of the NASA Goddard Space Flight Center (NASA/GSFC), using Landsat TM data for July 25, 1990. The source of these data was the Canadian Centre for Remote Sensing. BOREAS Science Staff at NASA/GSFC gridded the data to a pixel size of 30 meters from the original resolution of 28.5 meters, using the BORIS coordinate system [BOREAS Experiment Plan, 1994].

A conversion program prepared by BOREAS Science Staff was used to transform the northwest corner of the vegetation image to UTM-coordinates. IPW was used to reproject the entire image to a UTM map projection, and rescale it to 10 m pixels. The image was then resampled to 100 m pixels, and each pixel was assigned the dominant vegetation-cover within the 100 m pixel area. Figure 3.5 shows the vegetation image, and Table 3.3 gives the spatial coverage of each vegetation type. For presentation purposes, the vegetation classes in Table 3.3 are aggregated into fewer classes in Figure 3.5.

A triangle in the southeastern corner of the SMSA, of area $4337*10^4$ m^2 (2.16% of the entire SMSA), was missing in the vegetation image. Most of the SMSA is covered by Black Spruce, and in cooperation with BOREAS Science Staff, this area was assigned to the class "Conifer wet".

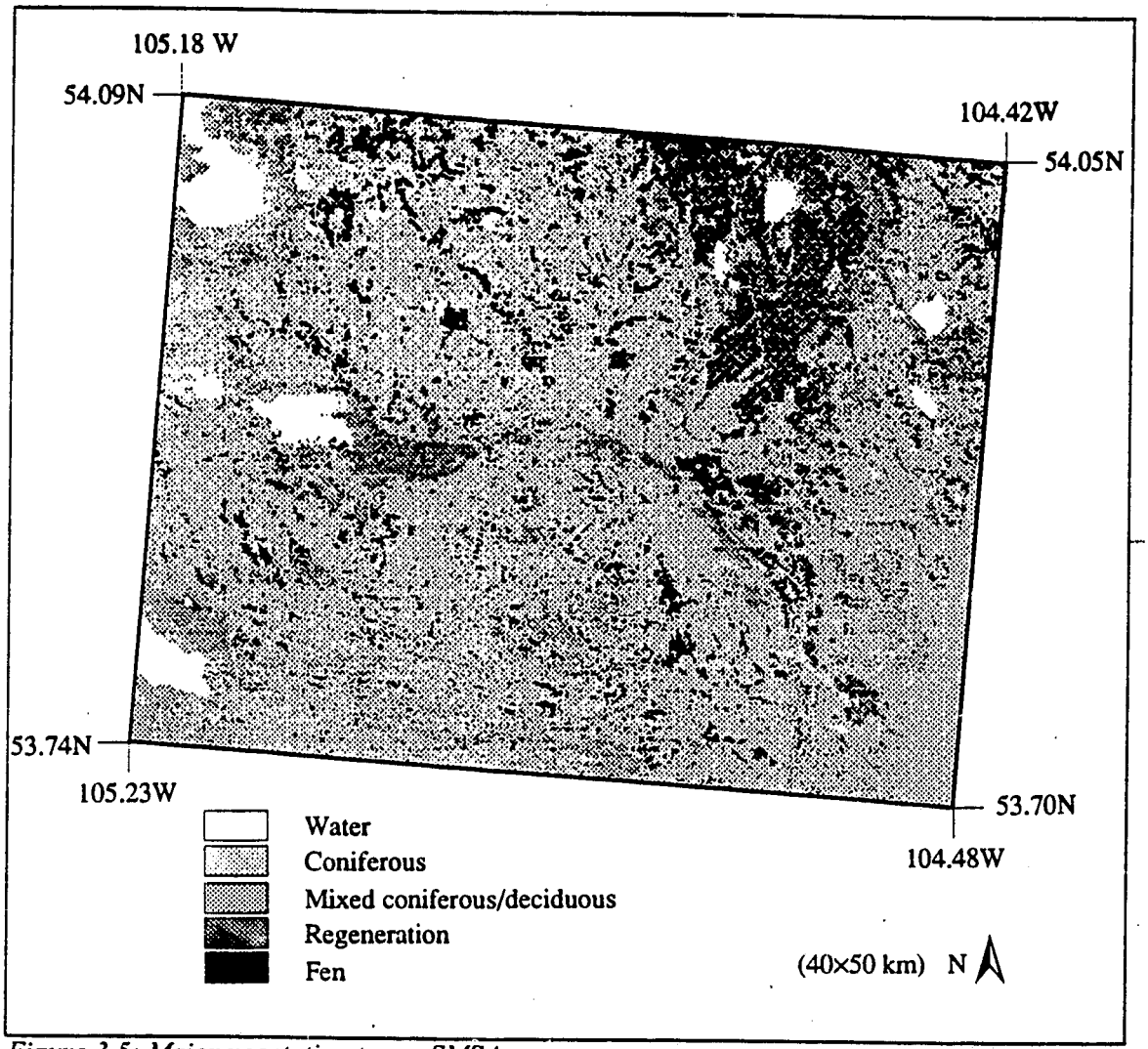

Figure 3.5: Major vegetation types, SMSA.

Table 3.3: Vegetation types, SMSA.

Vegetation type	Area ($*10^4$ m^2)	Percent coverage	Class in Figure 3.5
Conifer Wet	130657	65.07	Coniferous
Conifer Dry	3336	1.66	Coniferous
Mixed (Coniferous and Deciduous)	24707	12.31	Mixed con./dec.
Deciduous	2931	1.46	Mixed con./dec.
Regeneration (Young)	4381	2.18	Regeneration
Regeneration (Older)	14550	7.25	Regeneration
Regeneration (Medium)	2543	1.27	Regeneration
Fen	8197	4.08	Fen
Burn	142	0.07	Coniferous
Disturbed	1826	0.91	Coniferous
Water	7517	3.74	Water

Soil data.

Soil data were obtained from BOREAS Science Staff, who had gridded the data to a cell size of 1000 meters, using 1:1 million scale data originally produced in vector form by the Land Resource Centre of Agriculture Canada. This image was provided in the BORIS coordinate system, and was reprojected and rescaled by use of IPW to 100 m pixels in UTM-coordinates, following a similar procedure to that used to process the vegetation image. Table 3.4 describes the soils which are shown in Figure 3.6. In this figure, "Fine sandy loam/Sandy loam" are merged into "Sandy loam", and "Loamy sand" and "Loamy sand/Sand" are both presented as "Loamy sand/Sand".

Because of different spatial resolutions and origins, 'water' (e.g. lakes) did not show up at the exact same pixels in the vegetation and soil image. The vegetation image originally had the finest resolution, and was therefore made dominant, that is, the areas that were identified as water in the vegetation image were imposed as water in the soil image as well.

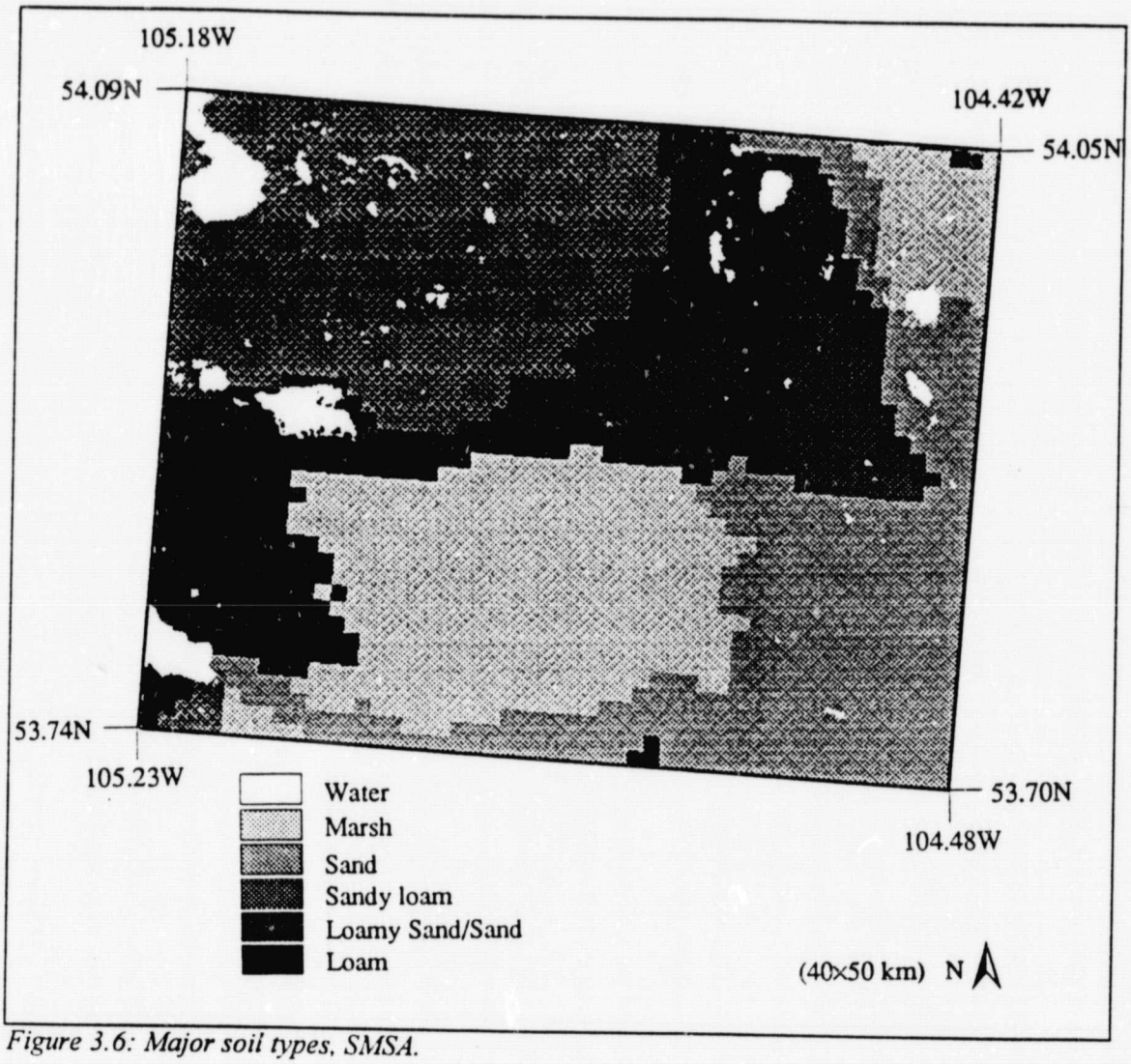

Figure 3.6: Major soil types, SMSA.

Comments on projections and accuracy of data.

The DEM was in UTM-coordinates, and it was therefore decided to use this map-projection for the modeling, since the DEM provides the fundamental structure for DHSVM. The vegetation and soil data both were in BORIS coordinates, which are based on an Albers projection. To prepare the solar radiation images, the DEM had to be in global (latitude-longitude) coordinates. The DEM was therefore reprojected for this purpose, the solar files were made, and reprojected from global coordinates to UTM-coordinates. The BORIS coordinate conversion program is specified to be accurate within 200 m; therefore the location of the northwest corner of the vegetation and soil files has possible error of up to 200 m. When a

reprojection is done, some additional distortions will occur, which means that the images may have some discrepancies.

Table 3.4: Soil types, SMSA.

Attributes	Soil class							Water
Surface texture of mineral soil	Fine sandy loam	NA[2]	Sand	Loamy sand	Loamy sand	Sandy loam	Loam	
Parent material (>40%)	Sandy loam	NA	Sand	Loamy sand	Sand	Sandy loam	Loam	
Subdominant parent material	NA	Sandy loam	NA	NA	NA	NA	NA	
Available water	100 mm	High water table	50 mm	50 mm	50 mm	100 mm	100 mm	
Drainage class	Well	Very poor	Rapid	Well	Rapid	Well	Well	
Depth to water table	> 3m	0-2 m	> 3m	> 3m	> 3m	> 3m	> 3m	
Thickness of humus	11-20 cm	NA	< 5 cm	< 5 cm	< 5 cm	11-20 cm	11-20 cm	
Area ($*10^3$ m^2)	984	45866	43688	301	33388	47470	21573	7517
Percent coverage	0.49	22.85	21.76	0.15	16.63	23.64	10.74	3.74

[2] NA = Non applicable. The second soil class consists mainly of water. In Figure 3.6 it has been named 'marsh', but this information was not obtained from the soil images.

CHAPTER 4: POINT ANALYSES.

4.1 WIND ANALYSIS.

Background.

Energy exchange is a fundamental concept underlying biophysical ecology. The transport of heat can occur through convection, conduction, radiative exchange, and latent heat transfer. An understanding of the principles and sensitivity of these processes is important in improving model predictions of the physical environment. Preliminary testing of DHSVM in the BOREAS study areas indicated inconsistencies between predictions of latent and sensible heat in forested areas compared to those predicted for unforested areas. Therefore, DHSVM's modeling of wind profiles in forested and open areas was investigated, especially the sensitivity of the resulting aerodynamic resistances to the model assumptions. Air flow within and above forest and other vegetation plays a significant role in the surface energy budget, as the transport of heat and water vapor occurs mainly because of air movement. Eqs. 3.1 - 3.4 (Section 3.2) show mathematically how latent heat, sensible heat and evapotranspiration are calculated in DHSVM.

Latent and sensible heat fluxes depend upon, among other variables, the aerodynamic resistance, r_a, which is determined by the degree of turbulence in the air. Aerodynamic resistance is the resistance to transport of heat and water vapor between the surface of the vegetation, the ground or snow surface and the air above it (for practical purposes, the "air above it" is taken to be at the height where wind measurements are taken; also known as the reference height). The turbulence is dependent on the wind speed and the surface roughness. The higher the wind speed or roughness, the more turbulence, which results in more mixing (lower resistance), hence more transport of heat, as well as moisture and momentum. The aerodynamic resistance can be calculated from the wind velocity and the roughness characteristics, z_0 and d_0, of the surface, where z_0 is the roughness length and d_0 is the zero plane displacement height. Above the canopy, or if no overstory is present, the wind profile in DHSVM is taken to be logarithmic [see Monin and Yaglom, 1971]:

$$u(z) = u(z_x)\frac{\ln[(z - d_{0i})/z_{0i}]}{\ln[(z_x - d_{0i})/z_{0i}]} \qquad (4.1)$$

where u: Wind speed

z: Height above ground level

z_x: Reference height

d_{0i}: Zero plane displacement height (taken as $0.63h_i$ (Monteith [1973]))

z_{0i}: Roughness length (taken as $0.13h_i$, following Monteith [1973])

h_i: Height of vegetation

The subscript *i* stands for *o*, overstory, *u*, understory, *s*, snow or *g*, ground surface.

The zero plane displacement height, d_0, is an equivalent height for the absorption of momentum (a 'centre of pressure') [Monteith and Unsworth, 1990]. The roughness length, z_0, is a measure of the aerodynamic roughness of the surface, and depends on the shape, height and spacing of the roughness elements. The logarithmic wind profile between $z_0 + d_0$ and the reference height, z_x, is assumed to transport the same amount of mass as the actual wind profile.

To estimate the wind within the canopy, DHSVM uses a formulation suggested by Campbell [1977], which he reported to work fairly well when the vegetation is spatially uniform:

$$u(z) = u(h_o)e^{c_n(z/h_o - 1)} \tag{4.2}$$

where c_n: Canopy attenuation coefficient

Figure 4.1 illustrates the wind speed profiles resulting from Eqs. 4.1 and 4.2. Wind speed is assumed to merge into a new logarithmic profile near the ground or snow surface. Consequently, with a complete overstory, the vertical wind profile is modeled using three layers.

During the initial work with DHSVM, some problems with the calculation of aerodynamic resistances were detected. For instance, the aerodynamic resistance for the understory with complete overstory was found to be lower than the resistance when no overstory was present, even though the wind speed close to the ground was predicted to be lower. To locate the source of the problem, the sensitivity of the empirical parameters included in the formulas for aerodynamic resistance (roughness length, zero plane displacement height, canopy attenuation coefficient and fraction of overstory cover) were investigated. For these analyses a canopy height of 10 m and an understory height of 0.2 m was used, which is similar to the Old Black

Spruce site in the NMSA. Heat transfer from the vegetation to the atmosphere depends on reference height, and the reference height needs to be above the canopy. For this analysis, a reference height of 12 m was used.

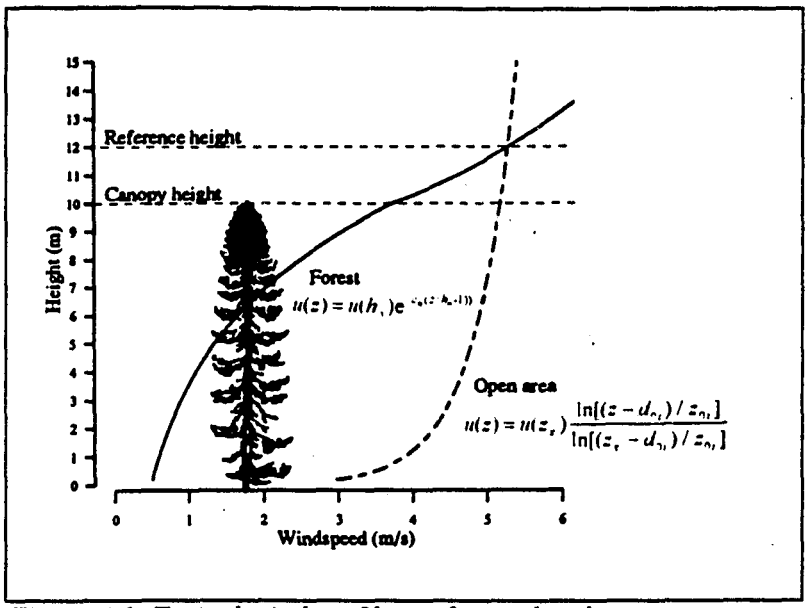

Figure 4.1: Typical wind profiles in forested and open areas, as assumed in DHSVM.

Calculation of aerodynamic resistances, according to DHSVM.

DHSVM calculates separate aerodynamic resistances for the overstory, understory, and ground surface or snow surface, based on the assumption of a three layer wind profile. Resistances to turbulent transport are taken in series, and the aerodynamic resistance at the ground surface is:

$$r_a = r_{\log} + r_{\exp} + r_{over} \tag{4.3}$$

where r_a: Total aerodynamic resistance

r_{log}: Aerodynamic resistance associated with lower logarithmic wind profile

r_{exp}: Aerodynamic resistance associated with exponential wind profile

r_{over}: Aerodynamic resistance associated with upper logarithmic profile

In the following, r_a is used as notation for total aerodynamic resistance, either for overstory, understory, ground or snow surface, and can be composed of one, two or all three terms in Eq. 4.3.

Above the canopy.

Above the canopy, a logarithmic wind profile is used (Eq. 4.1). The resulting aerodynamic resistance for understory, with no overstory, is illustrated in Figure 4.2a (r_{over_u}), and for overstory (r_{over_o}) in Figures 4.2b-4.2d. The resistances are calculated using the following widely used equation [Monteith, 1976]:

$$r_a = r_{over\_u} = \frac{\ln[(z_x - d_{0i}) / z_{0i}]^2}{u(z_x)k^2} \tag{4.4}$$

where r_{over_u}: Aerodynamic resistance from reference height to canopy source height ($d_{0i} + z_{0i}$)

k: von Karman's constant (0.41)

Complete overstory cover.

With a complete overstory, the resistance from the understory to the reference height is assumed to be the sum of the resistance above and within the canopy (see Figure 4.2b), which gives:

$$r_a = r_{exp} + r_{over\_o} \tag{4.5}$$

where $$r_{exp} = \frac{1}{u(z_x)k^2} \ln\left(\frac{z_x - d_{0o}}{z_{0o}}\right) \frac{h_o e^{(-c_n)}}{c_n(h_o - d_{0o})} \left(e^{(-c_n(d_{0o}+z_{0o})\frac{1}{h_o})} - e^{(-c_n(d_{0o}+z_{0o})\frac{1}{h_o})}\right) \tag{4.6}$$

r_{exp}: Aerodynamic resistance, exponential part of wind profile

and r_{over_o} is calculated as in Eq. 4.4. The wind profile is assumed to merge into a new logarithmic profile near the ground surface (Figure 4.2d), and the aerodynamic resistance for the ground surface is given by:

$$r_a = r_{log} + r_{exp} + r_{over\_o} \tag{4.7}$$

where $$r_{log} = \frac{1}{u(z_m)k^2} \ln\left(\frac{z_m}{z_{0g}}\right)^2 \tag{4.8}$$

z_m: Height at which the wind profile is assumed to go from exponential to logarithmic.

and r_{exp} and r_{over_o} are given in Eqs. 4.4 and 4.6.

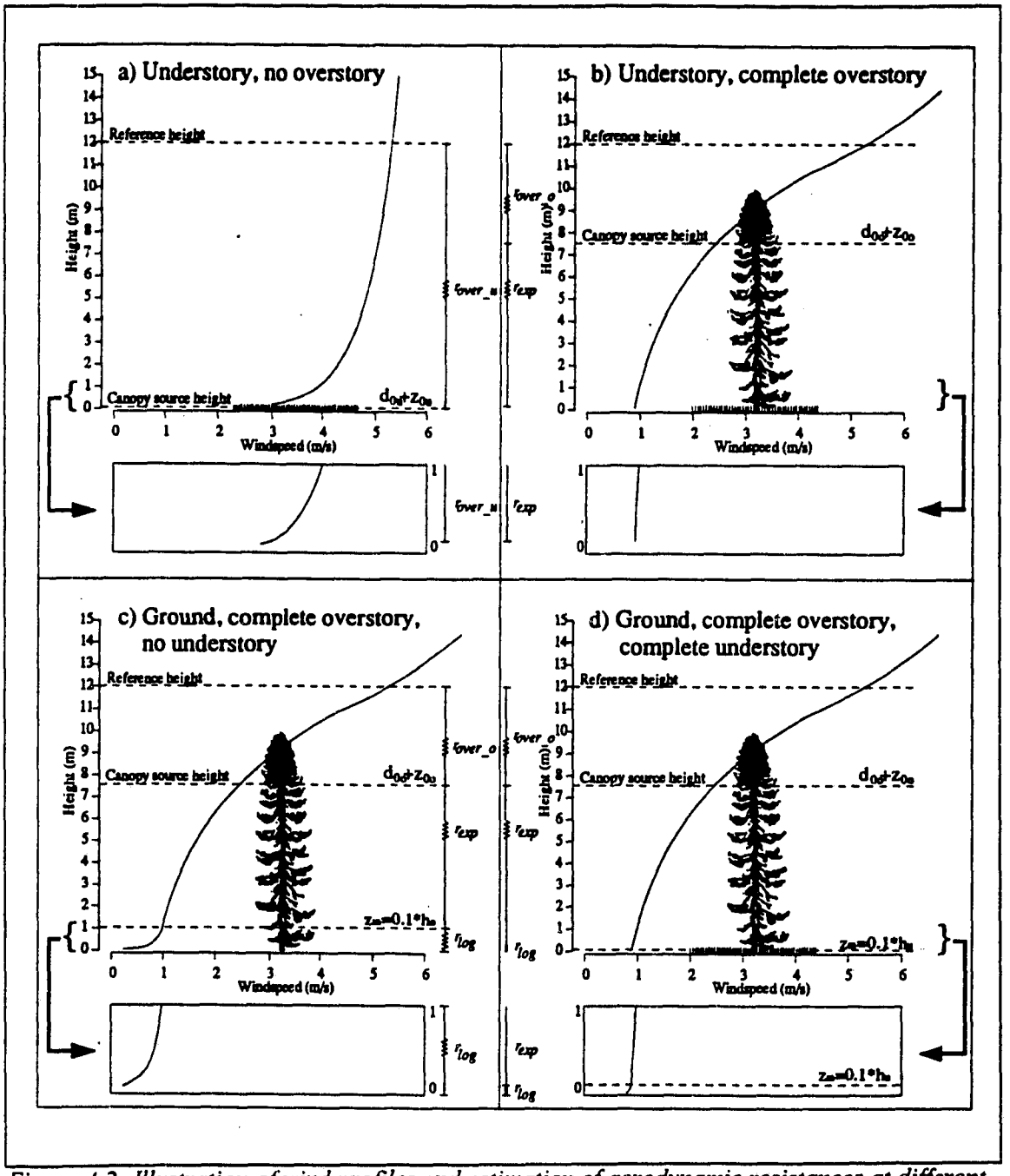

Figure 4.2: Illustration of wind profiles and estimation of aerodynamic resistances at different levels in DHSVM. The figure shows the part of the wind profile which is used in a) Eq. 4.4, b) Eq. 4.5, c) Eq. 4.7, with $z_m=0.1h_o$, and d) Eq. 4.7, with $z_m=0.1h_u$. The upper logarithmic wind profile is used to calculate r_{over_i}, r_{exp} makes use of the exponential wind profile, while the lower logarithmic wind profile is used to estimate r_{log}

When there is snow on the ground, the understory is assumed to be covered. The aerodynamic resistance for snow, or for the ground if no understory is present, is calculated using Eq. 4.7 (Figure 4.2c), except that the logarithmic profile is assumed to start at $0.1h_o$ and not at $0.1h_u$ as for ground resistance when understory is present. The assumption that the logarithmic profile starts at $0.1h_o$ when no understory is present, and at $0.1h_u$ when understory is present, is a generalization made by Wigmosta et al. [1994], based on Campbell's [1977] representation of wind profiles in forest canopies.

Incomplete overstory cover.

The degree of turbulence is clearly affected by canopy density, but the relative relationship between canopy density and the resulting aerodynamic resistances is not obvious, nor is there a commonly accepted way to represent the relationship numerically. Various approaches have been used to account for the effect of forest density on the near-surface wind profile. Shuttleworth and Wallace [1985] assumed the resistances to vary linearly with overstory density. Campbell [1977] suggests that the canopy attenuation coefficient (c_n in Eqs. 4.2 and 4.6) should range from close to zero for very sparse canopies to around four for dense canopies. DHSVM adapted the assumption of Shuttleworth and Wallace [1985], which they reported had limited effect on evaporative fluxes in their studies.

Analysis of DHSVM calculation.

Fraction of overstory cover, and canopy attenuation coefficient.

Figure 4.3 shows the aerodynamic conductances (inverse of resistance) that result for different vegetation types, by using a canopy attenuation coefficient of 3 and a wind velocity at the reference height of 5 m/s. In the figure, conductances are shown instead of resistances, because of its linear dependence on forest cover. The overstory conductance (Figure 4.3a, F= 100%) is higher than the understory conductance (Figure 4.3b, F = 0%) for open areas. This is in accordance with Shuttleworth [1993], who stated: "The resistance for overstory is much less than that for understory where no cover is present". What is surprising in Figure 4.3, is that the conductance for the understory *increases* with fraction of overstory cover, in contrast to the

expected *decrease* in conductance as the tree density increases. For snow and bare ground, the expected decrease in conductance occurs. The conductance is expected to decrease because the wind speed under the canopy will decrease as the forest becomes denser (see also Figure 4.1).

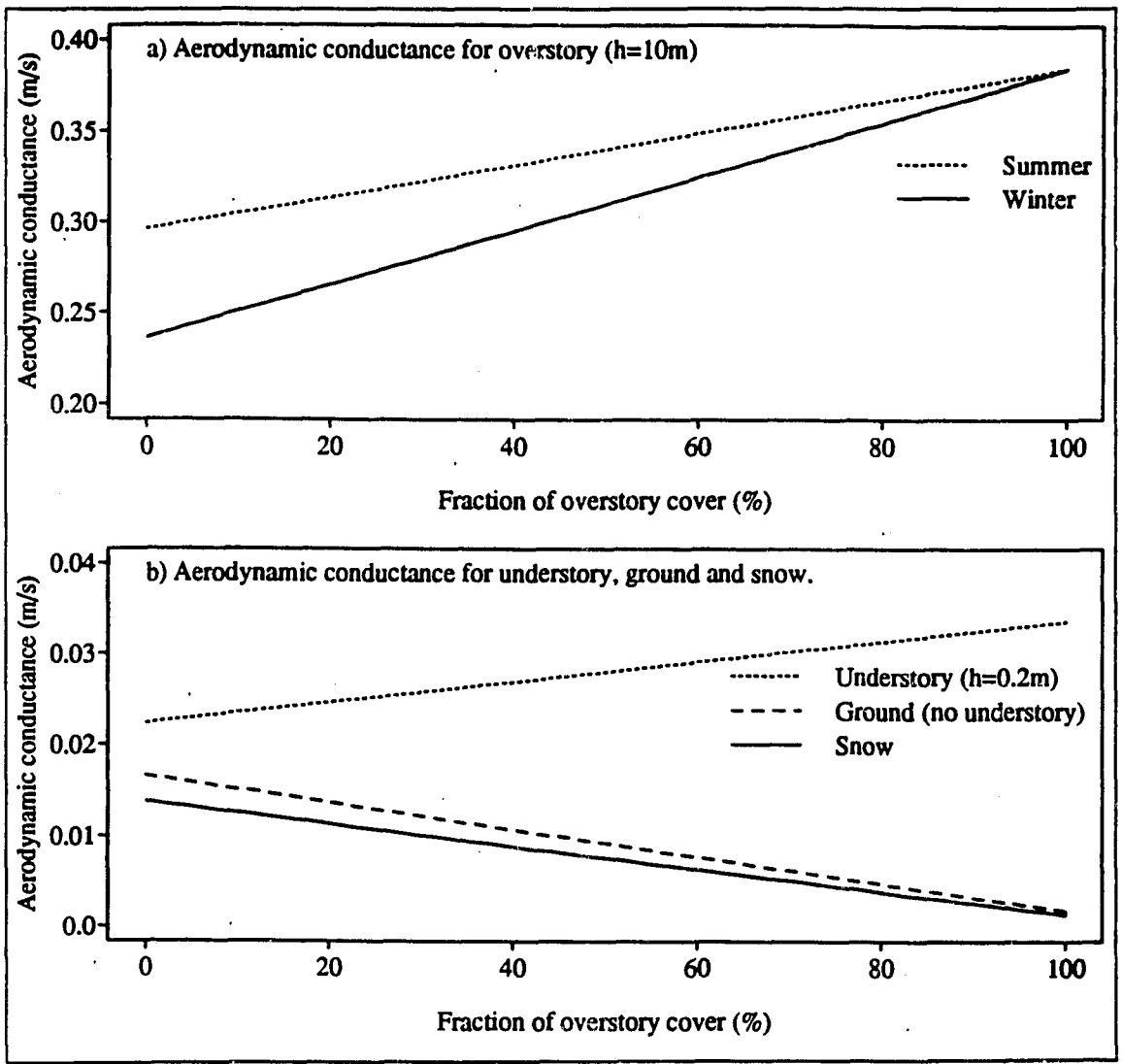

Figure 4.3: Aerodynamic conductance for different vegetation types and fraction of overstory cover (c_n =3, $u(z_x)$ = 5 m/s). In a) Eq. 4.4 is used, in b) Eqs. 4.5 (understory) and 4.7 (ground (z_{0g} = 1 cm) and snow (z_{0s} = 0.5 cm)) are used.

Figure 4.4, which illustrates the consequence of using different attenuation coefficients, shows the effect in another way: With canopy attenuation coefficients of 2 and 3, the aerodynamic conductance is actually higher with complete overstory cover than in a clearing (F = 0, Figure

4.4a). By increasing the attenuation coefficient to 4 (a dense forest according to Campbell [1977]), the result is a little more realistic, - now the conductance decreases as the forest density increases, but it is still very close to the result for open areas. The aerodynamic conductance for snow, and ground surface (no understory) is always lower within the forest than outside (Figure 4.3b), and is not very sensitive to choice of attenuation coefficient (Figure 4.4b). Only the conductance for snow is shown in Figure 4.4, because the only difference between the conductance for snow and bare ground is the roughness length; 0.5 cm and 1 cm for snow and ground surface, respectively.

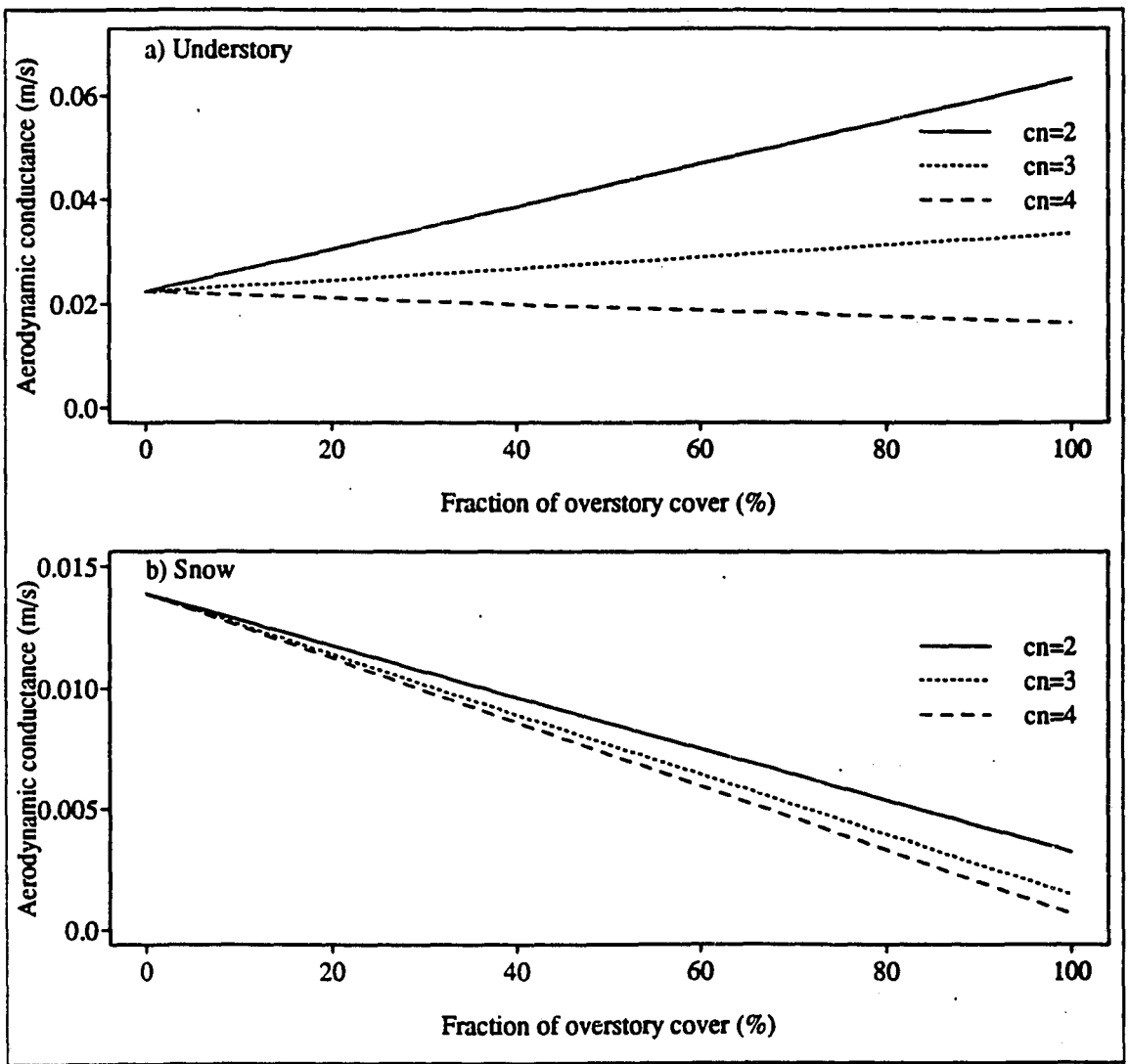

Figure 4.4: Aerodynamic conductance for different attenuation coefficients and fraction of overstory cover ($u(z_x)$ = 5 m/s).

Eqs. 4.5 and 4.7 show that understory resistance is dependent on the two upper wind layers, while the resistance for snow and the ground surface is dependent on all three wind layers. The resistance caused by the lowest wind layer is dominant in the calculations of aerodynamic resistances for snow and ground surface (Figure 4.5a). This explains both why the conductance decreases as the wind speed decreases (increasing forest density), and why the conductance is less sensitive to choice of canopy attenuation coefficient for ground surface than for understory. Figure 4.5b shows that increasing c_n to 4 results in an understory resistance (with complete overstory) that is higher than the resistance when no overstory is present, which explains why the conductance decreases as the forest density increase (Figure 4.4a, cn = 4).

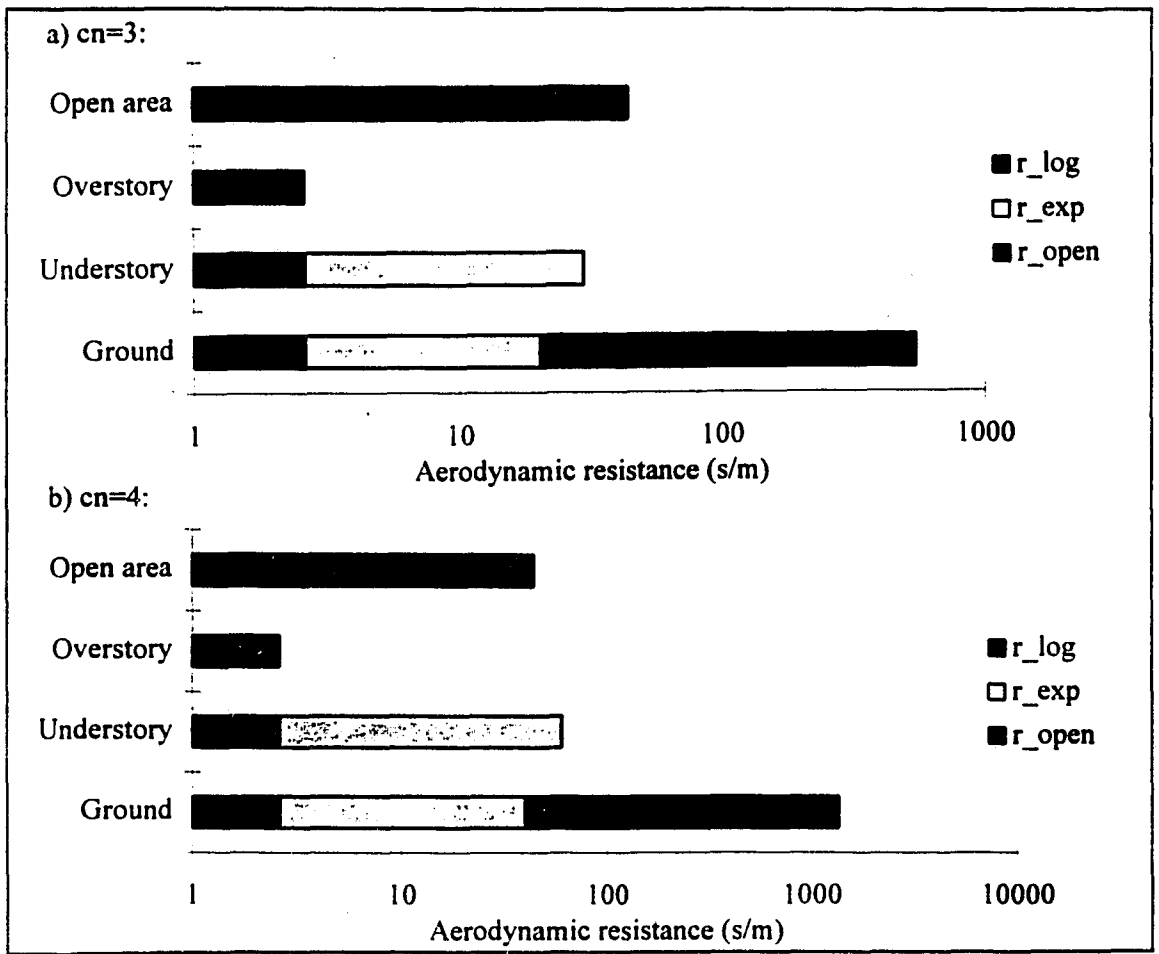

Figure 4.5: Aerodynamic resistance for different types of vegetation cover and attenuation coefficients.

Suggested changes to DHSVM formulation.

Clearly, the formulation proposed by Wigmosta et al. [1994] is unrealistic, at least with the suggested parameters. It does not make sense that the conductance increases as the wind decreases. One approach would be to change the formulation for the exponential profile to increase the resistance. Another approach is to assume that the logarithmic profile starts above the understory, rather than at a height of $0.1h_u$, which is assumed now. The assumption of a three layer wind profile used in DHSVM is taken from Campbell [1977], who says that the logarithmic profile extends from the ground surface to 5 to 10 percent of the canopy height. Wigmosta et al. [1994] use an upper limit of the logarithmic profile as equal to one tenth of the understory height or one tenth of overstory height if no understory is present, or if there is snow on the ground. The formulation proposed by Campbell is only for one story; the generalization of Campbell's formulation used in DHSVM was proposed by Wigmosta et al. [1994]. For this study, it was decided to assume that the logarithmic wind profile starts at $0.1h_o$ whether understory is present or not, which adds one new term to Equation 4.5:

$$r_a = r_{\log} + r_{\exp} + r_{over\_o} \tag{4.9}$$

where $$r_{\log} = \frac{1}{u(z_m)k^2} \ln\left(\frac{z_m - d_{0u}}{z_{0u}}\right)^2 \tag{4.10}$$

Figure 4.6 shows that adding the resistance associated with the lower logarithmic profile decreases the understory conductance, and results in decreasing understory conductance with overstory cover, F.

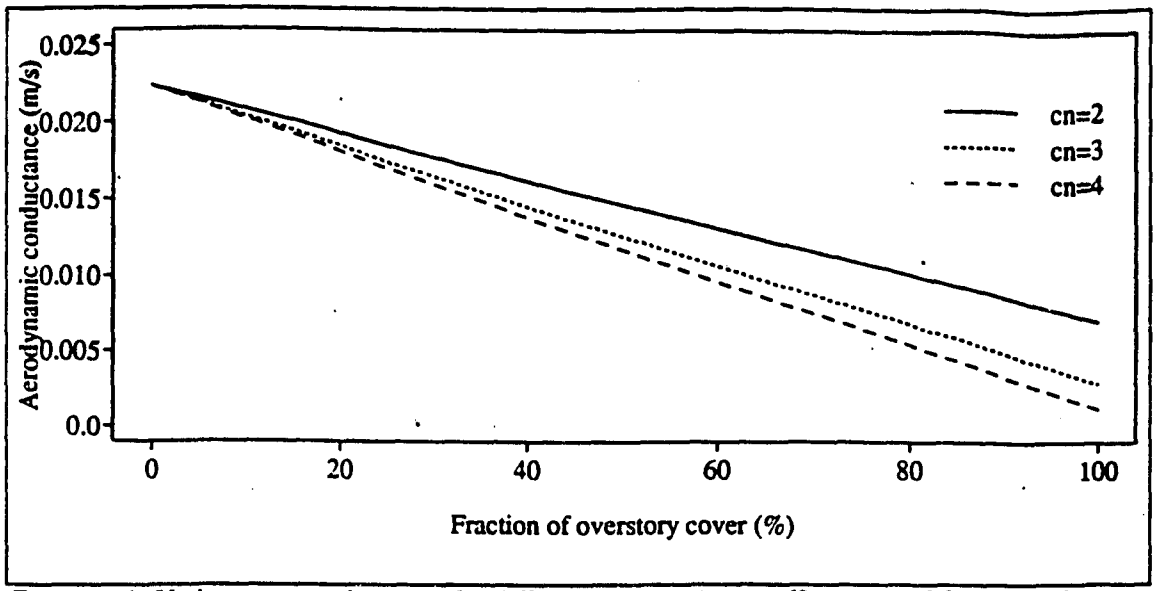

Figure 4.6: Understory conductance for different attenuation coefficients and fraction of overstory cover ($u(z_x)$ = 5 m/s), new approach.

Resistance caused by lower logarithmic profile.

Campbell [1977] suggested that the exponential wind profile should extend down to 5 to 10 percent of the canopy height. With the new approach of calculating aerodynamic resistance, the exponential wind profile is assumed to merge into a logarithmic wind profile at 10 percent of the overstory height ($z_m = 0.1h_o$), and the resistance of this lower logarithmic profile is added to the resistance caused by the exponential profile within the canopy and the logarithmic profile above the canopy. Figure 4.7 shows the sensitivity of the aerodynamic conductance to z_m and h_u.

As Figure 4.7 shows, the understory conductance is not very sensitive to choice of z_m if the understory height is small. When h_u increases, however, the sensitivity to z_m increases, - the aerodynamic conductance becomes an exponential function of h_u/h_o. When h_u approaches z_m, the resistance caused by the lower logarithmic profile decreases substantially, and the resulting conductance approaches that calculated in the original formulation for understory conductance in DHSVM, where the lower logarithmic profile did not influence the total understory conductance. This demonstrates that if the understory is tall, the choice of z_m is critical. In

coniferous forests, which dominate the boreal region, the understory vegetation is low, and taking z_m equal to 10 percent of the overstory height should not cause problems.

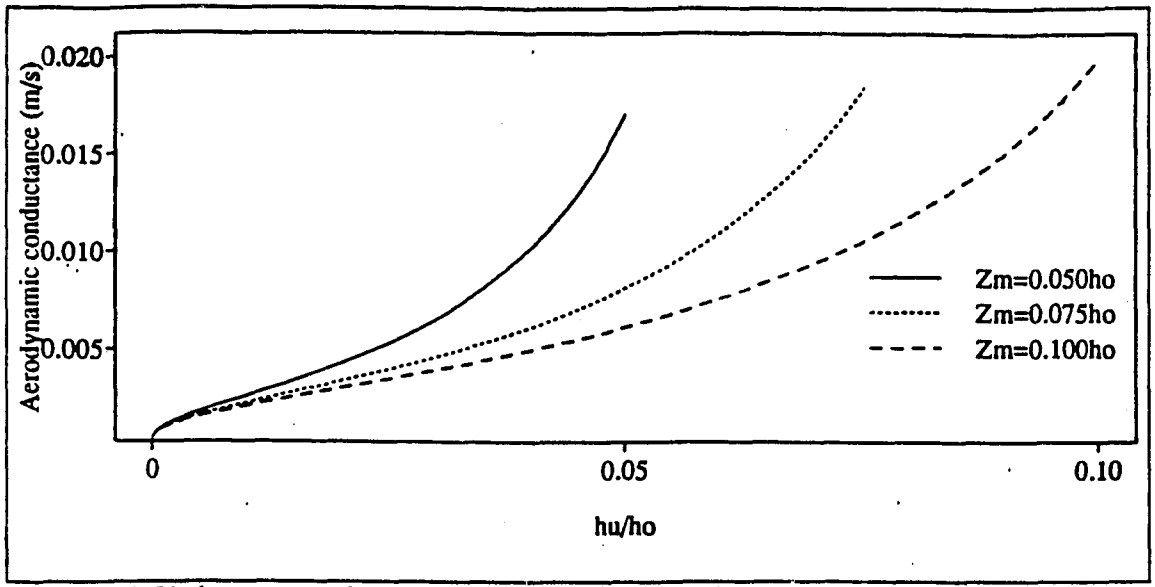

Figure 4.7: Understory conductance as a function of h_u and z_m (c_n = 3, F = 1, $u(z_v)$ = 5 m/s), by use of Eq. 4.9.

Roughness characteristics.

The roughness length (z_0) and the zero plane displacement height (d_0) are commonly assumed to be a constant fraction of overstory height. DHSVM uses $z_0 = 0.13h$ and $d_0 = 0.63h$, following Monteith [1973]. Grace [1983] says the roughness length can be assumed to be 0.1h for most crops, but for sparser or denser vegetation this cannot be assumed. Jones [1992] suggests $z_0 = 0.075h$ and $d_0 = 0.78h$ for forests. Jones' values decreases the wind speed both above and within the canopy, compared to the DHSVM's assumption. Field [Lindroth, 1993] and numerical model results reported by Shaw and Pereira [1982] show that the roughness length and zero plane displacement height depend quite strongly on the height and density of the vegetation, in addition to the wind speed [Monteith and Unsworth, 1990]. Figure 4.8 shows how the aerodynamic conductance changes with d_{0o} and z_{0o} (d_{0u} and z_{0u} kept constant). The roughness lengths and displacement heights in Figure 4.8 are within ranges for coniferous forest given by Monteith [1976]. The figure shows that the conductance is quite sensitive for all values of z_0, and is increasingly sensitive to d_0 with increasing z_0. The absolute difference for

understory conductance is not alarming (understory conductance is dominated by the first term in equation 4.9, which does not include z_0 and d_0 for overstory). However, the choice of displacement height and roughness length for the overstory has quite a large influence on the resulting overstory conductance.

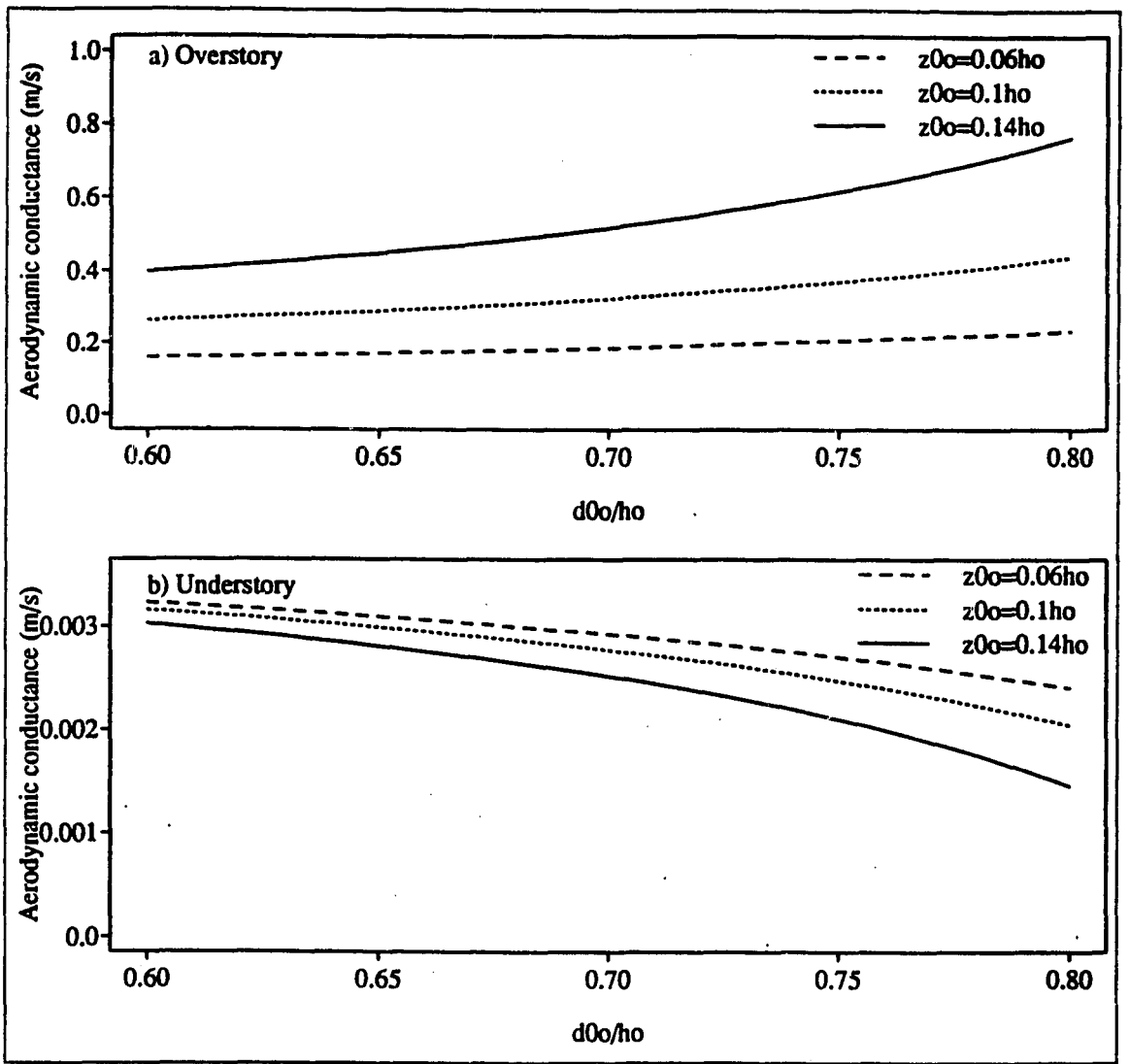

Figure 4.8: Overstory and understory conductance, as a function of overstory displacement height, d_{0o} (= xh_o), and overstory roughness length, z_{0o} (= y*h_o) (c_n = 3, F = 1, $u(z_x)$ = 5 m/s, d_{0u} and z_{0u} kept constant)*

In Figure 4.8, the overstory conductance increases with increasing d_0, and also with increasing z_0, while the opposite is true for understory conductance. The resistance caused by the logarithmic profile above the canopy decreases because of increased d_0 and z_0, but the

resistance caused by the exponential profile decreases more than the overstory resistance decreases, which results in the decreasing understory conductance.

Interpolation scheme.

The assumption of linear dependence of aerodynamic resistance on forest density is adapted from Shuttleworth and Wallace [1985], who studied sparse crops, with a typical height of 0.3 m. The wind profile for areas covered by overstory is adapted from Campbell [1977], whose source is Businger [1975]. Businger also compared theoretical and measured wind profiles (Figure 4.9). Neither Campbell nor Businger attempted to estimate wind profiles for partial vegetation cover, instead they used the canopy attenuation coefficient to account for the vegetation density. The evaporative fluxes resulting from using an interpolation scheme may not be significantly different for sparse crops [Shuttleworth and Wallace, 1985], but when dealing with forest canopies, the assumption that wind speed is a linear function of vegetation cover can not be justified, since the roughness added to the surface by even a sparse canopy will decrease the wind speed under the canopy substantially. Instead, cn, d_0, and z_0 can be used to account for the vegetation density. Of course, it would be best to fit the wind profile to measured values.

Practical influences of changes.

The point version of DHSVM was run for the OBS site in the BOREAS northern study area with the old and the new formulation for calculation of aerodynamic resistance. 1989-data from Thompson Airport, as described in Section 3.3, were used. An overstory fraction of 50 percent was assumed, and the root zones were kept at field capacity to minimize moisture stress. A roughness length of 0.13h, zero plane displacement height of 0.63h, and canopy attenuation coefficient of 3 were used for both approaches. This run was done for illustration purposes only, and the original formulation for canopy resistance was used; meaning canopy resistance was dependent on air temperature and not soil temperature. The resulting overstory and understory transpiration, latent and sensible heat are shown in Figure 4.10. As the figure shows, the transpiration both for overstory and understory started later in the spring with the new

approach, because the snow disappeared later (see Figure 4.10c), and the model assumes there is no vegetative activity as long as there is snow on the ground. Without interpolation of wind speed between complete and no overstory cover, the aerodynamic resistances, and hence the potential evapotranspiration, decrease.

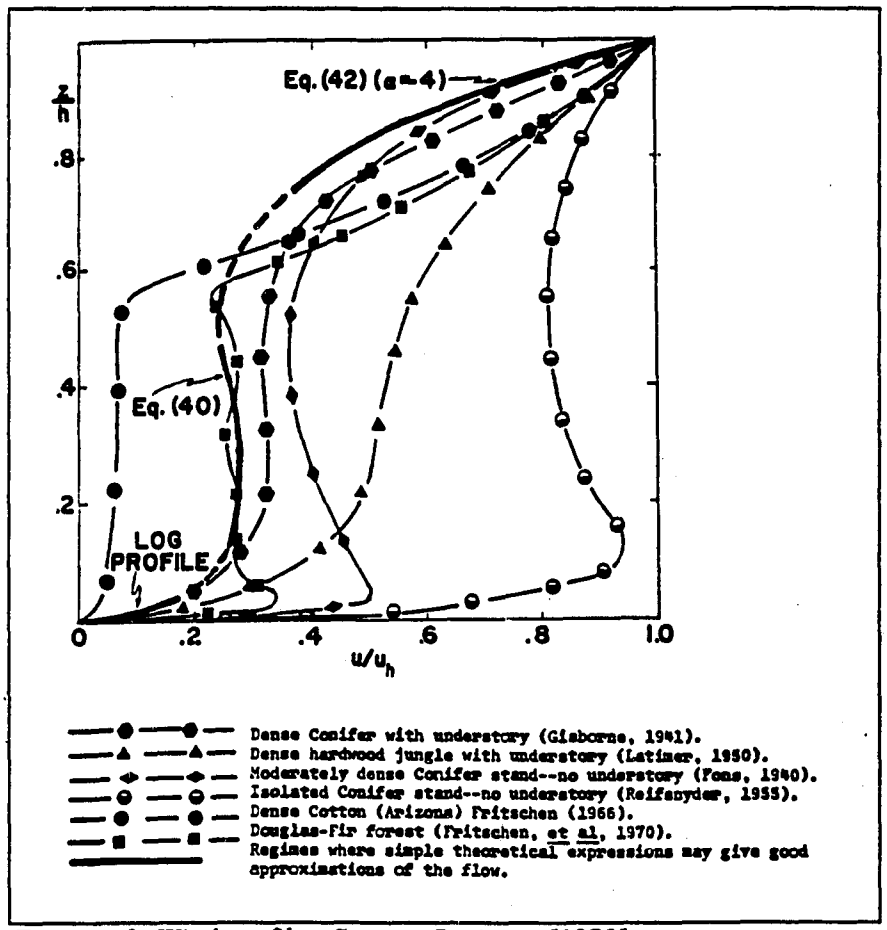

Figure 4.9: Wind profiles. Source: Businger [1975].

During the mid summer, the overstory transpiration is a little higher with the old approach (Figure 4.10a), but the difference is hardly noticeable. The understory transpiration is quite different, though (Figure 4.10b), and the transpiration is highest using the new approach. Overstory resistance increases and understory resistance decreases using the new approach, and the difference is most significant for the understory (the relative difference is 1.13 $u(z_x)$and 0.11 $u(z_x)$ for overstory and understory, respectively). While decreased aerodynamic resistance

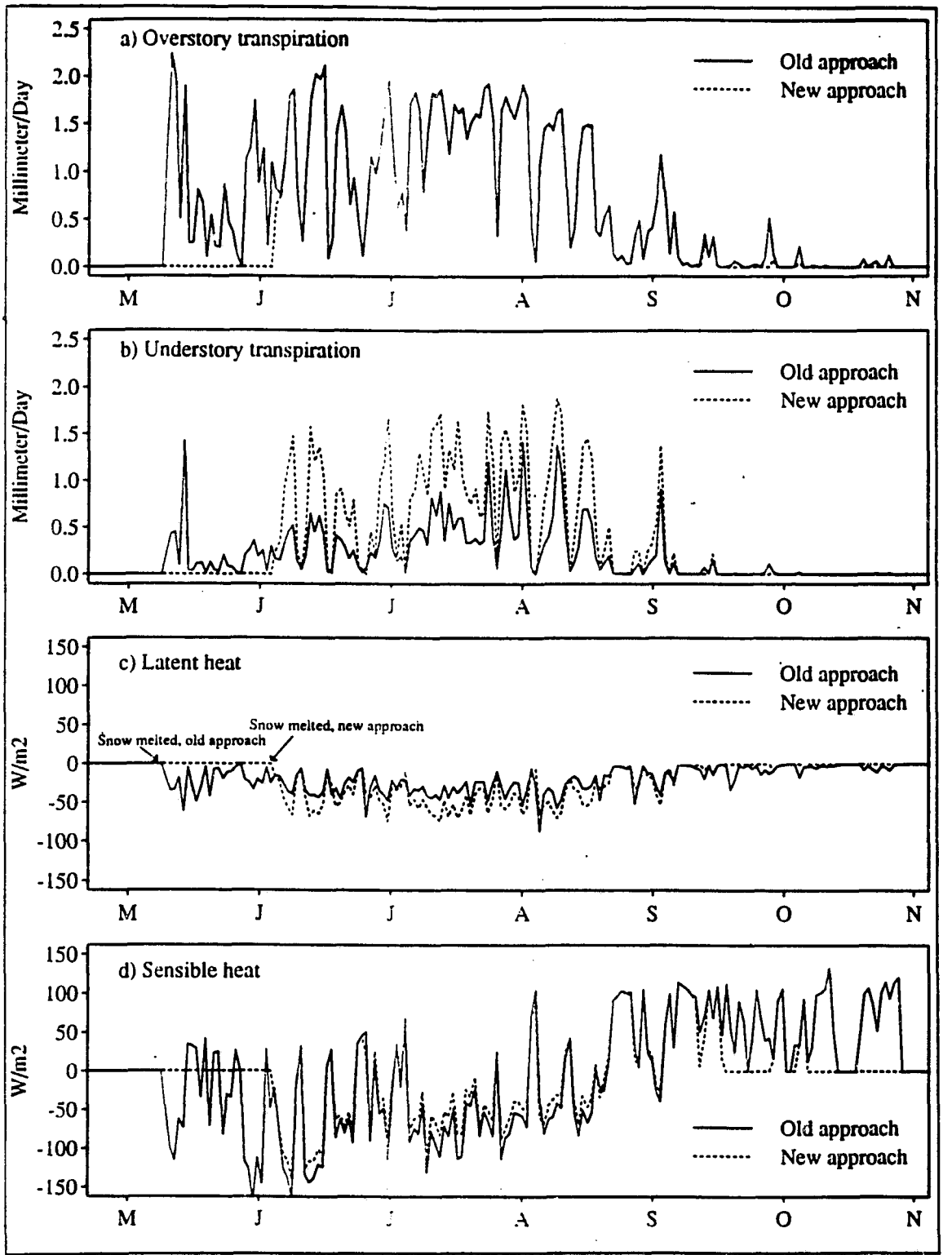

Figure 4.10: Effects of changes in the estimation of aerodynamic resistances on predicted energy and moisture fluxes at northern OBS. The figure shows daily total overstory and understory transpiration, and daily average heat fluxes.

causes the potential evapotranspiration to decrease, it causes the actual transpiration to increase, which is shown mathematically in Eq. 3.4. Physically, Grace [1983] explained this by the effect wind speed has on surface temperatures. When the energy absorption is high (e.g. warm summer days), an increase in wind speed (i.e. a decrease in aerodynamic resistance) causes a decline in surface temperature and thus, the transpiration rate is reduced. At low rates of energy absorption (e.g. R_{net}=10 W/m^2), the leaf is cooler than the air, and an increase in wind speed increases the transpiration rate.

Total daily evapotranspiration increases with the new approach, which is reflected in increased latent heat flux (Figure 4.10c). The decrease in understory resistance is more significant than the increase in overstory resistance, which results in decreased sensible heat flux (Figure 4.10d). One might question the late snow melt observed using the new approach (Figure 4.10c). For the purpose of comparison, the analysis was done with the same roughness characteristics and canopy attenuation coefficient in both the old and the new approach. With 50 percent overstory cover, it might be better to use a canopy attenuation coefficient of 2, which would make the snow disappear earlier.

Discussion and conclusion.

The analyses done in this section show that the aerodynamic resistances, and hence the resulting heat and moisture fluxes, are sensitive to the assumptions made about roughness characteristics and shape of wind profile. Analyses of DHSVM's formulation of wind profiles and calculation of aerodynamic resistances showed that, with the suggested parameters, some of the assumptions made in DHSVM are unrealistic. Two changes which will make the formulation more realistic are suggested. First, DHSVM's calculation of understory resistance with complete overstory cover, which originally was dependent on the two upper wind layers of the wind profile (see Figure 4.2b), was changed to be made dependent on all three layers of the wind profile, similar to what is shown in Figure 4.2c. Second, the assumption of linear dependence of wind upon fraction of overstory cover is removed; instead the roughness characteristics, d_0 and z_0, and canopy attenuation coefficient, c_n, should be used to account for forest density.

The exponential and logarithmic equations used in DHSVM to represent the wind profile within and above the canopy are theoretical, but can be fitted quite well to observed values [Businger, 1975]. Measured values are necessary, though, to be able to represent the wind profile as correctly as possible. A good fit will indicate what canopy attenuation coefficient and roughness characteristics to use; these parameters influence the aerodynamic resistance and hence evapotranspiration significantly. In addition to the two layers within the canopy which DHSVM uses, Businger used a third layer between the lower logarithmic and the exponential layer (Figure 4.9). As the figure shows, this layer does not have a major impact on the wind profile. However, the wind speed where the wind profile is assumed to merge into the lower logarithmic profile is somewhat higher than if the exponential profile was assumed to extend down to the lower logarithmic profile. Higher wind speed causes more turbulence, and as a consequence the aerodynamic resistance should be lower.

The analyses are done with the reference height at 2 meters above the canopy. If the distance between the vegetation and the reference height changes, the aerodynamic resistances would increase, which would influence the evaporation and transpiration. Which reference height to use has been widely discussed [e.g. de Bruin and Moore, 1985; Zoumakis, 1993, 1994], in practice it is a question of where the wind speed measurements are taken.

4.2 VEGETATION RESPONSE UNDER DIFFERENT CLIMATIC CONDITIONS.

Background.

DHSVM was run in point mode to analyze and contrast moisture characteristics and energy fluxes of vegetation in different climates within the boreal region. That is, the model was run for Black Spruce and Fen in both of the modeling subareas (NOBS, SOBS, NFEN and SFEN). The point modeling was done as a part of a preliminary modeling project within BOREAS, the intent of which was to compare the performance of different biophysical and hydrologic models with the same initial values and boundary conditions and identical climate data. Because DHSVM has previously not been applied to boreal areas, another objective of the point modeling was to perform sensitivity analyses to better understand how the model responds to the boreal climate and vegetation characteristics.

Approach.

Meteorological data.

Meteorological data for Thompson Airport and Prince Albert Airport for 1989 were provided to the BOREAS modeling group by J. Coughlan (see Section 3.3), who estimated shortwave radiation by the method of Heitor et al. [1991], and longwave radiation with a site-specific regression of longwave radiation on temperature and humidity measured at the SRC-stations in the NMSA and SMSA in 1994 [Coughlan, personal communication]. Wind speed and temperature measurements both at Thompson Airport and Prince Albert Airport are taken at about 2 meters above ground level. For the purpose of calculating aerodynamic resistances (see Section 4.1), wind speed data above the canopy are needed, and the wind speed was therefore extrapolated to 2 m above the canopy, by use of a logarithmic wind profile and roughness characteristics of bare soil or snow. This height was used as the reference height for calculation of aerodynamic resistances.

Table 4.1 gives total precipitation and mean temperature for the NMSA and the SMSA in 1989, and Figure 4.11 illustrates the temperature and precipitation distribution over the year. By comparing Table 3.1 and Table 4.1, it can be seen that the precipitation in 1989 was 77 percent of the mean in the NMSA, while it was 96 percent of the mean in the SMSA. The annual average temperature for the north was close to the long-term mean (-3.9°C), while the south was a little warmer than average (long-term annual mean: 0.1°C).

Table 4.1: Precipitation and temperature, 1989.

	NMSA	SMSA
Mean temperature	-3.8°C	1.0°C
Total precipitation	417.4 mm	381.6 mm

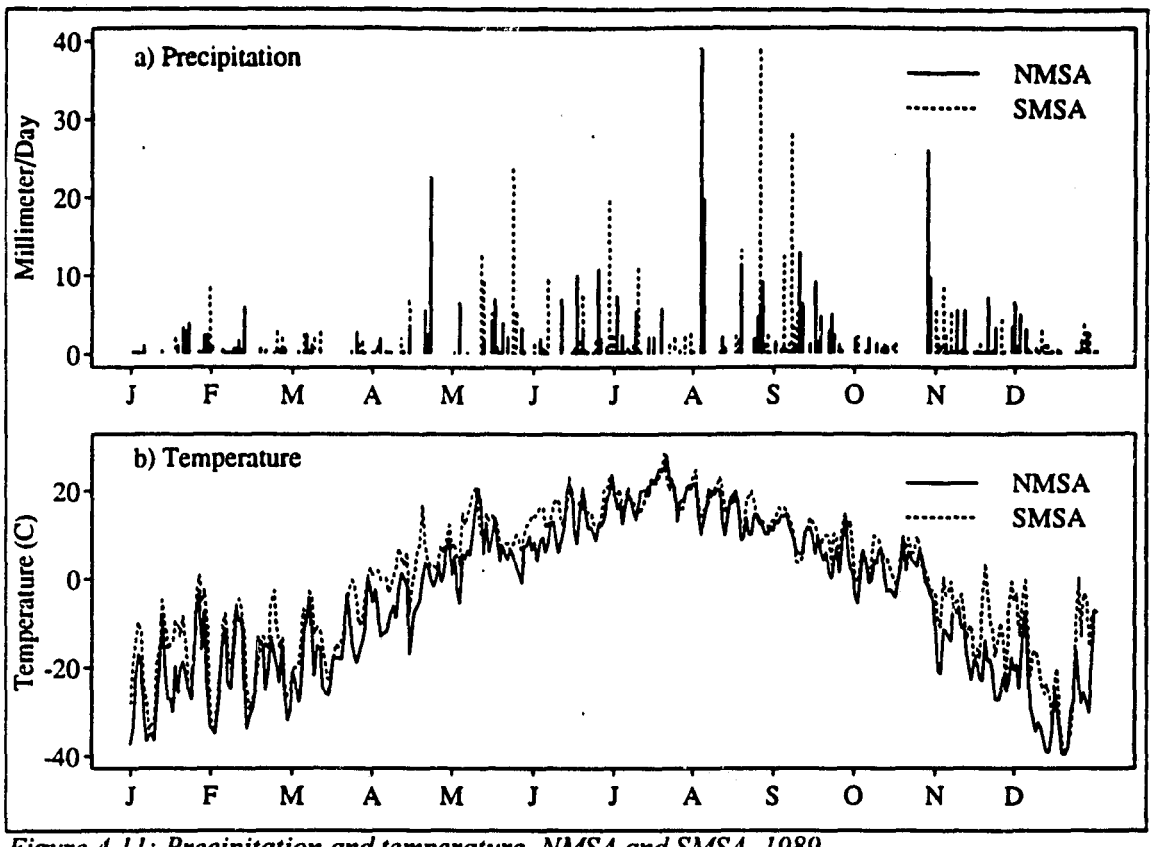

Figure 4.11: Precipitation and temperature, NMSA and SMSA, 1989.

Vegetation and soil parameters.

The biophysical parameters estimated by the BOREAS modeling group are given in Table 4.2, and these parameters were used as a starting point for the analyses. DHSVM requires some parameters not provided; these parameters are listed with their selected values in Table 4.3.

Table 4.2: Biophysical variables given by the modeling subgroup.

	NMSA		SMSA	
	Black Spruce	Fen	Black Spruce	Fen
Canopy height (m)	10	1	12	1
LAI (projected)	2.5	4.5	5	6
Maximum stomatal conductance (m/hr)	13.5	22.5	13.5	22.5
Understory	Moss	Fen	Moss	Fen
Emissivity	1	1	1	1
Albedo, vegetation	0.1	0.15	0.1	0.15
Soil class				
root zone 1	Peat	Fen	Peat	Fen
root zone 2	Clay-sand-loam		Clay-sand-loam	
Rooting depth (m)	0.5	0.5	0.5	0.5
Damping depth (m)	1	1	1	1
Saturated hydraulic conductivity (m/hr)				
root zone 1	0.072	0.072	0.072	0.072
root zone 2	0.023	0.072	0.023	0.072
Porosity				
root zone 1	0.8	0.8	0.8	0.8
root zone 2	0.4	0.8	0.4	0.8
Field capacity				
root zone 1	0.35	0.35	0.35	0.35
root zone 2	0.24	0.35	0.24	0.35
Wilting point				
root zone 1	0.13	0.13	0.13	0.13
root zone 2	0.14	0.13	0.14	0.13
Bubbling pressure (m)	0.12	0.12	0.12	0.12
Pore size distribution				
root zone 1	0.25	0.25	0.25	0.25
root zone 2	0.14	0.25	0.14	0.25
Roughness length (fraction of vegetation height)	0.1	0.1	0.1	0.1

Table 4.3: Parameters.

	NMSA		SMSA	
	Black Spruce	Fen	Black Spruce	Fen
Minimum stomatal conductance (m/hr)[1]	0.72	0.72	0.72	0.72
Height, understory (m)	0.2	-	0.2	-
LAI, understory	3	-	3	-
Max. stomatal conductance, understory (m/hr)	1.14	-	1.14	-
Min. stomatal conductance, understory (m/hr)	0.72	-	0.72	-
Depth, root zone 1	0.25	0.25	0.25	0.25
Depth, root zone 2	0.25	0.25	0.25	0.25
Canopy attenuation coefficient	2	-	2	-
Extinction coefficient, overstory	0.5	0.5	0.5	0.5
Fraction of roots in root zone 1	0.9	1.0	0.9	1.0

[1]Minimum stomatal conductance from Wigmosta et al. [1994, cf Dickinson et al., 1986].

The NMSA and the SMSA have an average slope of 3.2 percent and 2.1 percent respectively, which indicates that both areas are fairly flat, and that the NMSA is slightly steeper than the SMSA. For this study, both NOBS and SOBS were assigned a slope of 0.5 percent, to allow for some baseflow. Fens are typically located in flat areas, so the Fens were therefore not assigned any slope. As stated in Section 3.2, soil temperature was used as one of the parameters regulating transpiration. DHSVM computes soil surface temperature based on the surface energy balance, using a sinusoidal representation of the temperature at damping depth (here: 1m) as the lower boundary condition (see Figure 4.12). For this study, the soil temperature in the upper root zone was estimated by adding 1/3 of the temperature at damping depth to 2/3 of the temperature at the soil surface. The temperature in the lower root zone was obtained in a similar way, but with opposite weighing factors. The temperature at damping depth was used as a control of when the soils were frozen, and no baseflow was allowed when this temperature was below 0°C.

The model was initiated on September 1, with soils at saturation, and was run for one year until equilibrium was reached in the root zones (threshold: 0.1 mm). At that point the final run, which lasted from September through December 16 months later, was started. 1989 data were

used for the entire period, and the analyses were done on a calendar year basis to be consistent with other models run by the BOREAS modeling group.

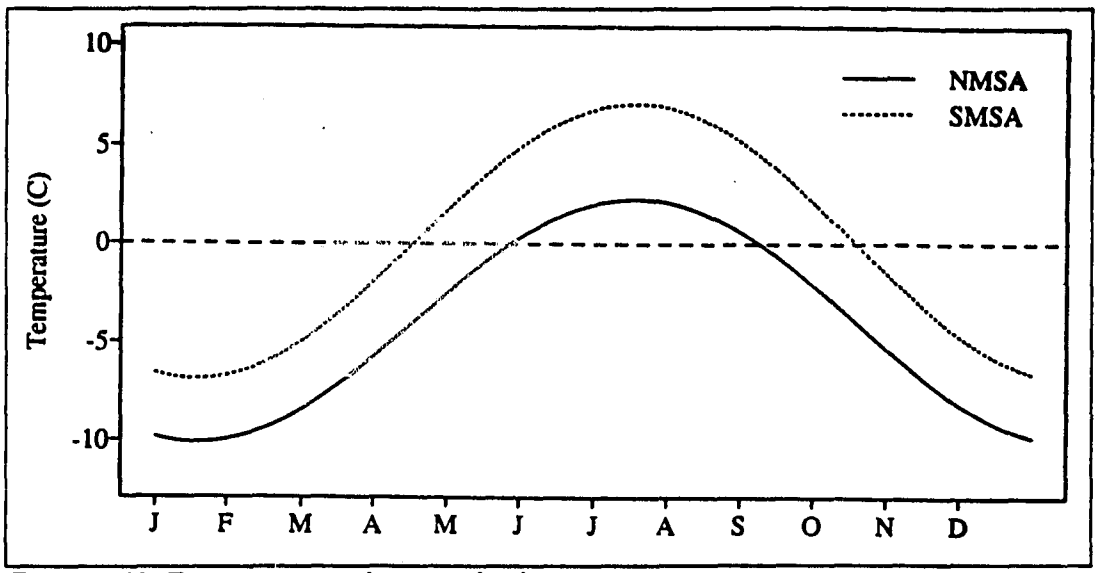

Figure 4.12: Temperature at damping depth.

Results and discussion.

Figure 4.13 shows the depth from the soil surface to the water table (the soil under the root zone is assumed saturated in this figure) as modeled for the two sites in the NMSA and the SMSA, based on the given input parameters. Unfortunately, no observations or other model results suitable for comparison were available at the time this thesis was written. However, the results do not seem realistic, - the sites are drier than expected in these areas, and in particular as compared to The National Atlas of Canada's [1974] mean values for runoff, which gives close to 100 mm runoff a year in the SMSA, and somewhere between 100 and 200 mm in the NMSA. The modeled runoff was 39 and 34 mm in the NMSA, and 2.8 and 0 mm in the SMSA, for Black Spruce and Fen respectively. The runoff at the Black Spruce sites was baseflow only, at the Fen it was surface runoff, and most of the runoff occurred during snow melt. As shown in Section 5.2, runoff in DHSVM is produced largely for saturated areas, which are dependent on lateral subsurface inflow. Lateral inflow cannot be represented in a 1-D equivalent of DHSVM, which might be a reason modeled runoff is so low.

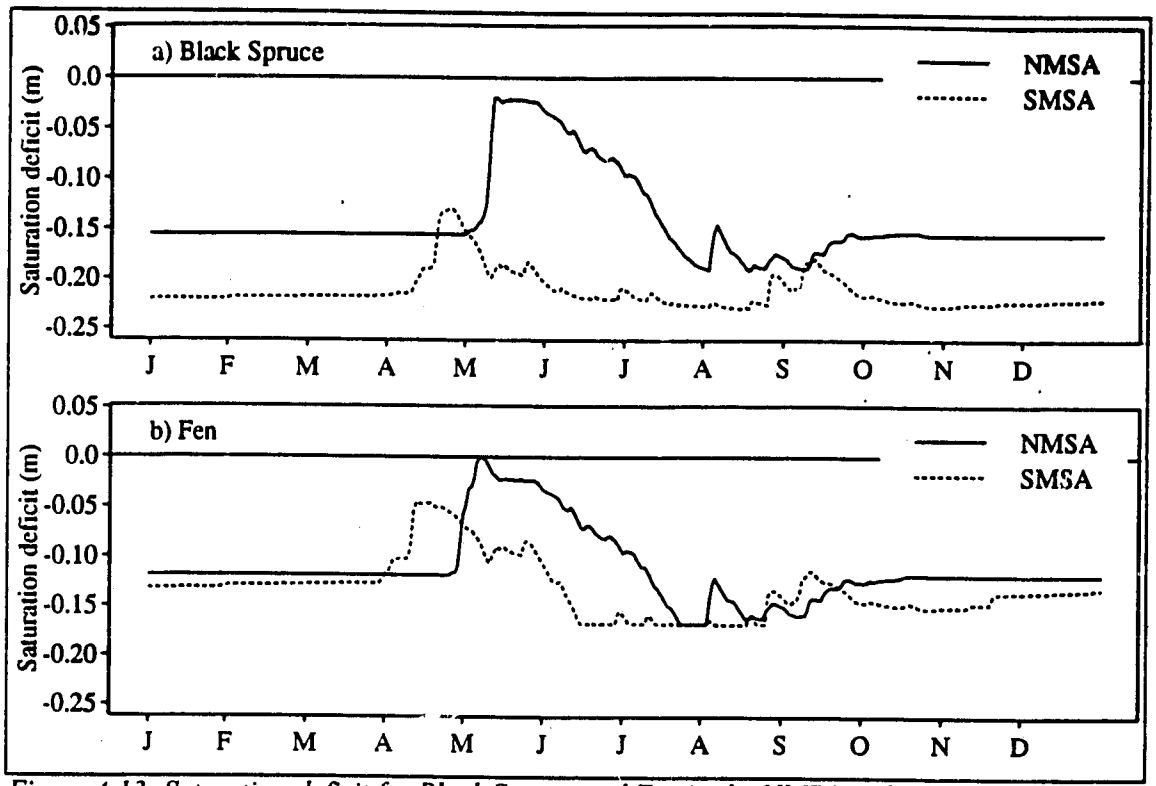

Figure 4.13: Saturation deficit for Black Spruce and Fen in the NMSA and the SMSA, after running DHSVM until equilibrium was reached in the root zones.

The baseflow in this analysis should represent net outflow. With no lateral inflow, the subsoils at NOBS and SOBS tended to dry out with the given lateral hydraulic conductivity. The lateral hydraulic conductivity was therefore decreased from 2.3 cm/hr to 0.5 cm/hr, which is within ranges given for sandy clay loam [Rawls et al., 1993]. The soil moisture increased somewhat after this change in the NMSA, and the site reached saturation for two days during snowmelt. Also, the soil underneath the root zones was saturated during the entire year. At SOBS, the subsoil still dried out, and the decreased hydraulic conductivity did not change neither soil moisture nor evapotranspiration.

Since the sites are dry, and the amount of surface runoff and baseflow is low, the modeled evapotranspiration (ET) is probably too high. The potential evaporation for grass sites at Thompson and Prince Abert as calculated by DHSVM, was about twice as high as the mean annual potential evapotranspiration reported at Thompson Airport and Prince Albert Airport, which might be one of the reasons the resulting ET seems to be high. DHSVM calculates

potential evaporation based on Penman-Monteith's equation (Eq. 3.3), by setting the canopy resistance equal to zero. In this equation, there are two parameters which depend heavily on the selected input values: Net radiation and aerodynamic resistance. Net radiation is calculated based on short- and longwave radiation, fraction of overstory cover, air temperature, extinction coefficients and albedo. Aerodynamic resistance is calculated from wind speed, roughness length, canopy attenuation coefficient and zero plane displacement height. Actual evaporation is estimated from potential evaporation, the amount of intercepted water (maximum 0.1 mm * LAI), and soil evaporation. Included in the formulation of transpiration are the canopy resistance, which depends on soil temperature, soil moisture, vapor pressure deficit, PAR and stomatal conductance. Some of these parameters were changed from the original values, both to investigate DHSVM's sensitivity to its input parameters, and in an attempt to obtain what is thought to be 'reasonable' results of soil moisture for the study sites in the NMSA and the SMSA. Table 4.4 describes the changes, and the resulting changes in soil moisture are shown in Figure 4.14. The lateral hydraulic conductivity was kept at 0.5 cm/hr for analyses 2 through 5; the other parameters were reset to their original values before the next analysis was done.

Table 4.4: Description of point modeling analyses.

1	Starting point, based on Table 4.4 and Table 4.5, lateral hydraulic conductivity of 0.5 cm/hr
2	Soil temperature in root zones decreased by 2 degrees
3	Reference height changed from 2 meters above the canopy to 29 meters above ground level.
4	Maximum stomatal conductance decreased from 13.5 m/hr to 5.4 m/hr for Black Spruce and from 22.5 m/hr to 7.2 m/hr for Fen
5	LAI decreased to 2/3 of Table 4.2 values.

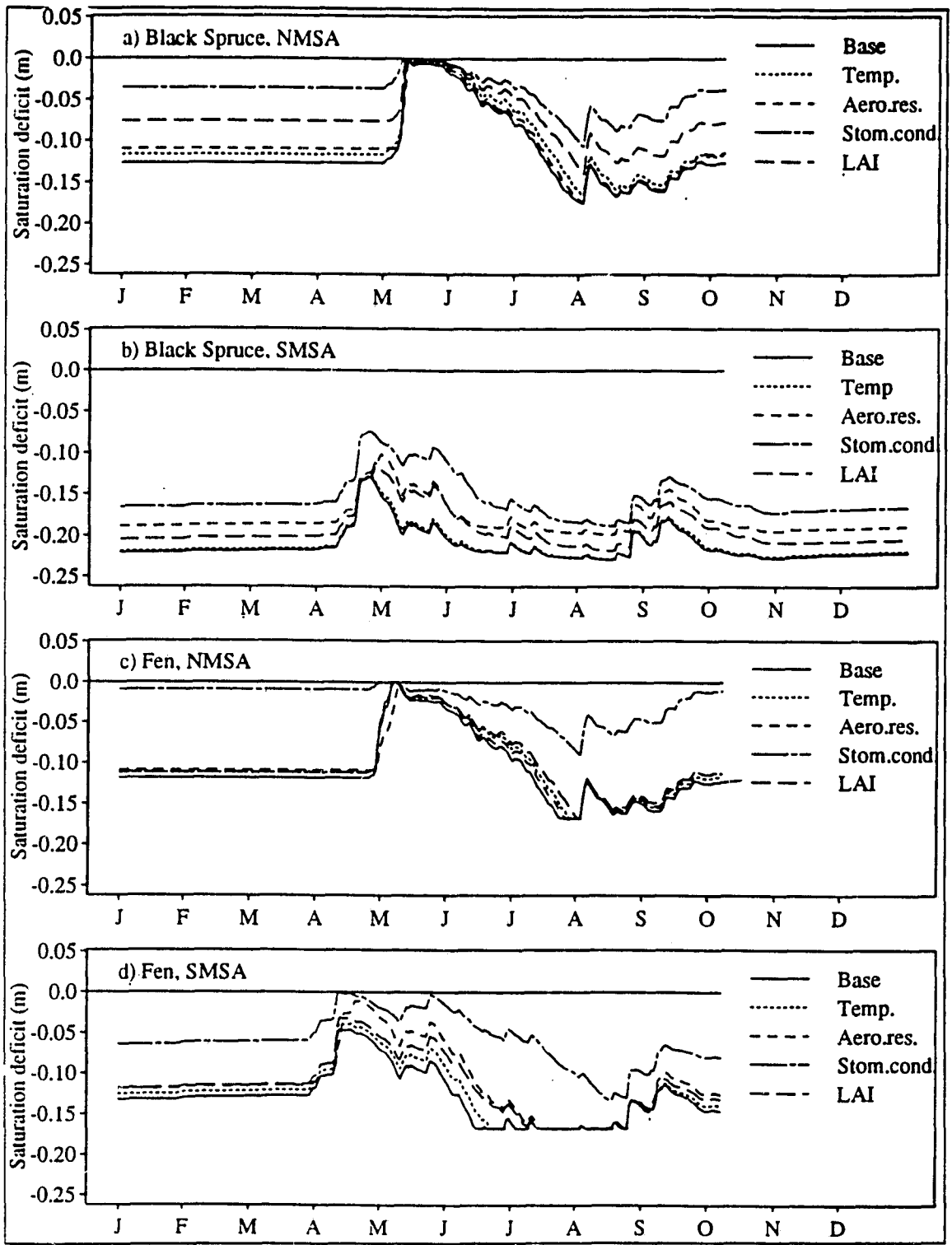

Figure 4.14. Sensitivity analyses of four sites to parameter changes indicated in Table 4.4. Analysis 1 = Base case, Analysis 2 = Soil temperature, Analysis 3 = Aerodynamic resistance, Analysis 4 = Stomatal conductance, and Analysis 5 = Leaf area index.

Prior to these analyses, the calculation of canopy resistance in DHSVM was changed from its original dependence on air temperature, to depend on soil temperature. The actual temperature in the root zones was estimated by a simple weighted average of the soil surface temperature and the temperature at damping depth. The actual soil temperature pattern may be different; for example, it is known that ice was found at a depth of 30 cm in the NOBS site in August 1994 [Dunham, personal communication], at which time the assumed temperature in the model at 1 m depth was 1°C. DHSVMs sensitivity to soil temperature was analyzed by decreasing the soil temperature in both root zones by 2°C. Transpiration did decrease; by 10 mm at NOBS but only by 1 mm at SOBS. In general, the decreased soil temperature did not influence resulting moisture content very much, see Figure 4.14. The reason for this can be explained by Figure 4.15, which illustrates the interactive effect of soil moisture and soil temperature on resulting canopy conductance, as assumed in DHSVM. The drier the soils are, the less influence decreases in soil temperature has, which explains the difference in response at NOBS and SOBS. The Fen sites had about the same soil moisture deficit as NOBS had. However, since the part of the soil column where the roots are located was drier at the Fen sites (all roots in the upper root zone layer), the influence of a 2°C decrease in soil temperature was lower at these sites than at NOBS.

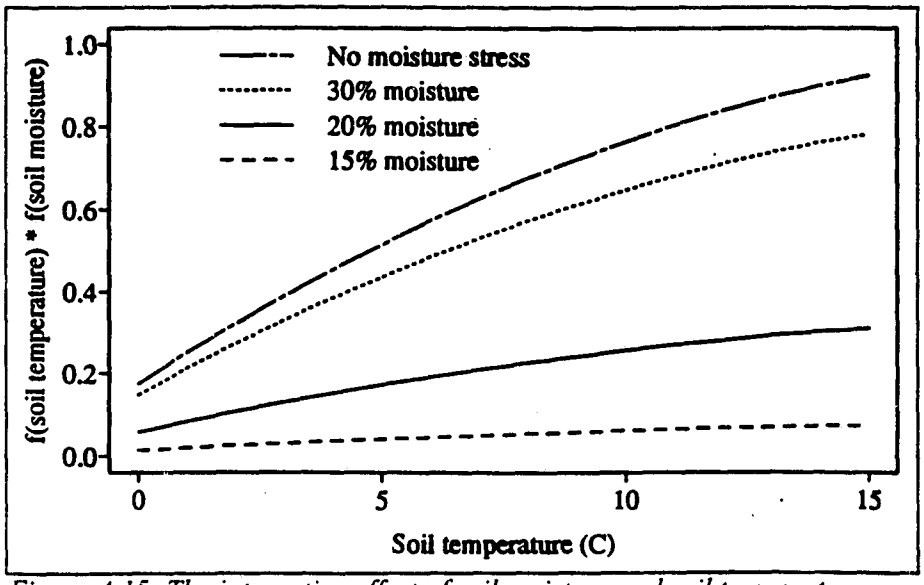

Figure 4.15: The interactive effect of soil moisture and soil temperature on canopy conductance (inverse of resistance).

Aerodynamic resistance strongly influences ET. In this study, wind speed was extrapolated logarithmically from the measured level at 2 meters above ground level to 2 m above the canopy. Which reference height to use has been widely discussed (see for example Zoumakis [1993]), and as a new approach the reference height was set to 29 m for both vegetation types: the height at which wind speed was measured at the NOBS site during the BOREAS project. Increasing aerodynamic resistance would decrease potential evaporation, but transpiration might increase (e.g. Section 4.1). In this study, the increased aerodynamic resistance resulted in decreased evaporation and increased transpiration in the growing season. The change in evaporation was mainly due to decreased evaporation of intercepted water. In the NMSA, the decreased resistance increased the snow cover (less sublimation, more condensation), and hence the snow cover disappeared later; the difference was two days at NFEN and ten days at NOBS. These ten days resulted in a total decrease in both evaporation and transpiration at NOBS. In the SMSA, where the snow pack originally was thinner, the delay in spring snow melt was two days at SFEN and four days at SOBS. Total ET in the SMSA decreased 2 mm at SOBS (transpiration increased from 251 mm to 262 mm) and increased 13 mm at SFEN (transpiration increased from 264 to 305 mm). The NOBS site was saturated for 7 subsequent days at the end of the snow season, and NFEN was saturated for two days; as in previous analyses. SOBS still did not reach saturation, neither did SFEN.

Maximum stomatal conductance, one of the parameters included in the formulation of canopy resistance (Eq. 3.6), influences transpiration directly. The values were changed within plausible ranges reported in the literature, and maximum stomatal conductance was decreased to 7.2 m/hr at the Fen sites (maximum stomatal conductance for deciduous shrub, reported by Mascart et al. [1991]), and to 5.4 m/hr at the Black Spruce sites, which is reported for conifers by Hunt et al. [1991]. The results showed that overstory transpiration decreased, as expected. Understory evapotranspiration and soil evaporation increased, though, because of increased soil moisture. At the SOBS site, for example, the overstory transpiration decreased by 8 percent, but understory evapotranspiration and soil evaporation increased somewhat, and the final ET only decreased by 1 percent. Looking at all sites, total ET decreased by up to 110 mm, or 30 percent (NFEN). For the reduced maximum stomatal conductance case, NFEN is almost completely saturated throughout the winter. In general the decreased stomatal conductance results in less evapotranspiration, and hence higher soil moisture.

LAI given in Table 4.4 was 5 for SOBS and 6 for SFEN, which for boreal species seems high compared to values suggested by Monteith [1975]. Monteith reports an LAI of 2-5 for coniferous forest, and only deciduous trees are given higher values. The Table 4.2 LAI in both the NMSA and the SMSA was multiplied by 2/3 to test its influences on resulting soil moisture. Decreasing LAI effected both evaporation and transpiration, and hence soil moisture (see Figure 4.14), but the effect was less than for the decreased stomatal conductance. At the Fen sites, a decrease in LAI did decrease the evapotranspiration from the vegetation, but decreased LAI increased the net radiation at the soil surface and hence soil evaporation increased. The total difference in ET is insignificant (358.6 mm at NFEN, as opposed to 358.3 mm in the analysis were aerodynamic resistance was increased). At the Black Spruce sites, the decreased overstory LAI resulted in decreased overstory evapotranspiration, increased understory evapotranspiration and soil evaporation, but the increase in soil evaporation was not as significant as at the Fen sites.

All changes improved the results somewhat, but alone they did not change the results to match the expected extent of saturation and runoff. The 'best' results were obtained by a composite of changes, and is shown in Figure 4.16. Stomatal conductance was set to 5.4 m/hr and 7.2 m/hr for Black Spruce and Fen, respectively, the reference height was kept at 29 m. The original assumption of soil temperature was retained. The net radiation was decreased by setting the albedo to 0.15 for Black Spruce, and 0.18 for Fen [Monteith, 1975], which decreases the potential evaporation. LAI at NOBS was kept at its original value, while it was set to 3.5 for SOBS (Table 4.2 LAI at SOBS is 5). Both Fen sites were given an LAI of 4. The SOBS site still did not reach saturation at any point, while the other sites were saturated for a period during snow melt, and were almost resaturated in the fall, following some rainstorms. Runoff, which mainly was caused by snow melt, was 165 mm (39 percent of precipitation) at NOBS, 160 mm (38%) at NFEN, 8 mm (2%) at SOBS, and 107 mm (28%) at SFEN. Long term averages given by The National Atlas of Canada [1974], indicate runoff ratios of 40% in the NMSA and 20% in the SMSA.

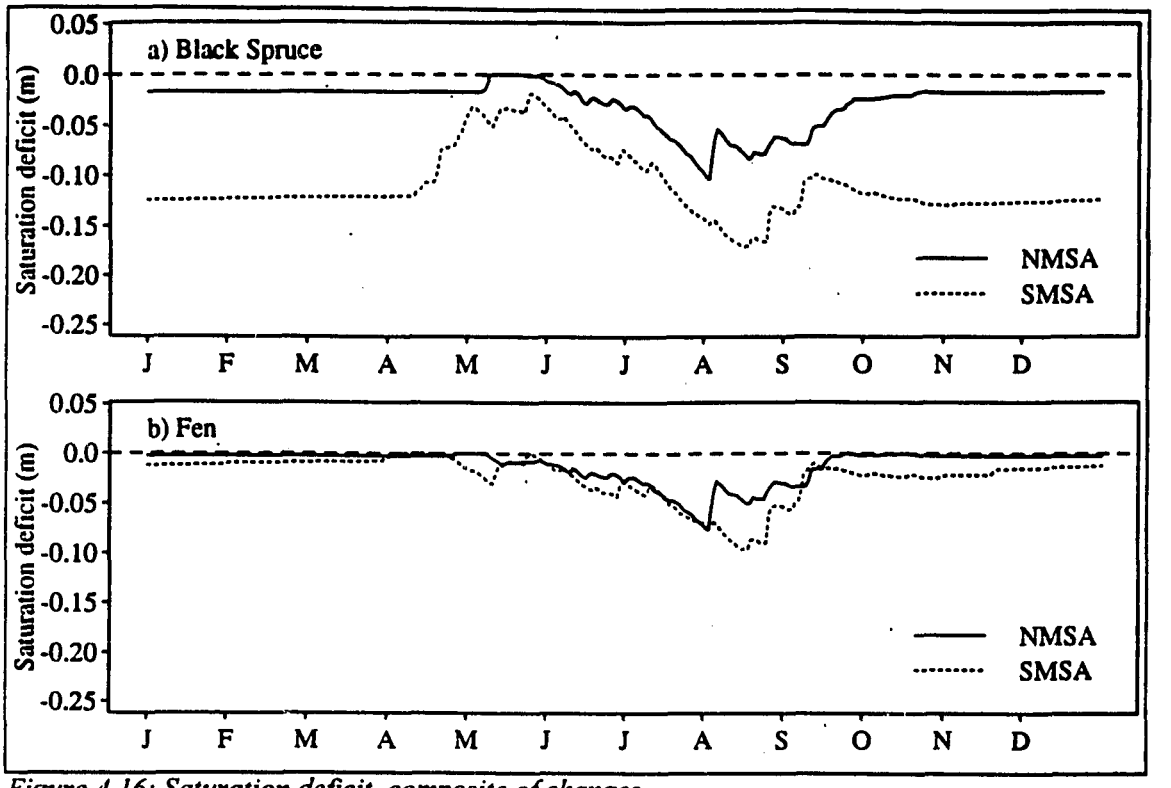

Figure 4.16: Saturation deficit, composite of changes.

The parameter that was changed the most, and which also changed the soil moisture the most, was maximum stomatal conductance. The values for maximum stomatal conductances used to obtain Figure 4.16 are in the lower range of what is reported in the literature, and it is possible that if other biophysical parameters (e.g nutrient limitation) had been incorporated in DHSVM, higher maximum stomatal conductances could have been used to obtain the same results. The sensitivity analyses also showed that soil temperature limitation influenced evapotranspiration in DHSVM more under wet conditions than under dry conditions, and a better estimate of temperatures in the soil column might have resulted in changed values of evapotranspiration.

The precipitation at Thompson Airport in 1989 was 77 percent of mean annual precipitation, while it was 96 percent of the mean at Prince Albert Airport. A simple scaling of the precipitation was done, to adjust the precipitation in 1989 to the long term mean annual precipitation. The effect on soil moisture was noticeable in both the NMSA and the SMSA

(Figure 4.17). SOBS was still dry, but reached saturation for two days in the spring. At NOBS and NFEN, the increased precipitation actually decreased the total evapotranspiration, since increased snow cover extended the snow season, and hence the active evapotranspiration period was shorter. If wind catch deficiencies of the rain gauges (especially during snowfall) were taken into account, e.g. Larson and Peck [1974], soil moisture would increase more. The rain gauges used at Thompson Airport and Prince Albert Airport are AES standard rain gauges [Tessmer, personal communication]. The gauges are unshielded, which almost certainly accounts for measurement deficiencies, especially for winter precipitation.

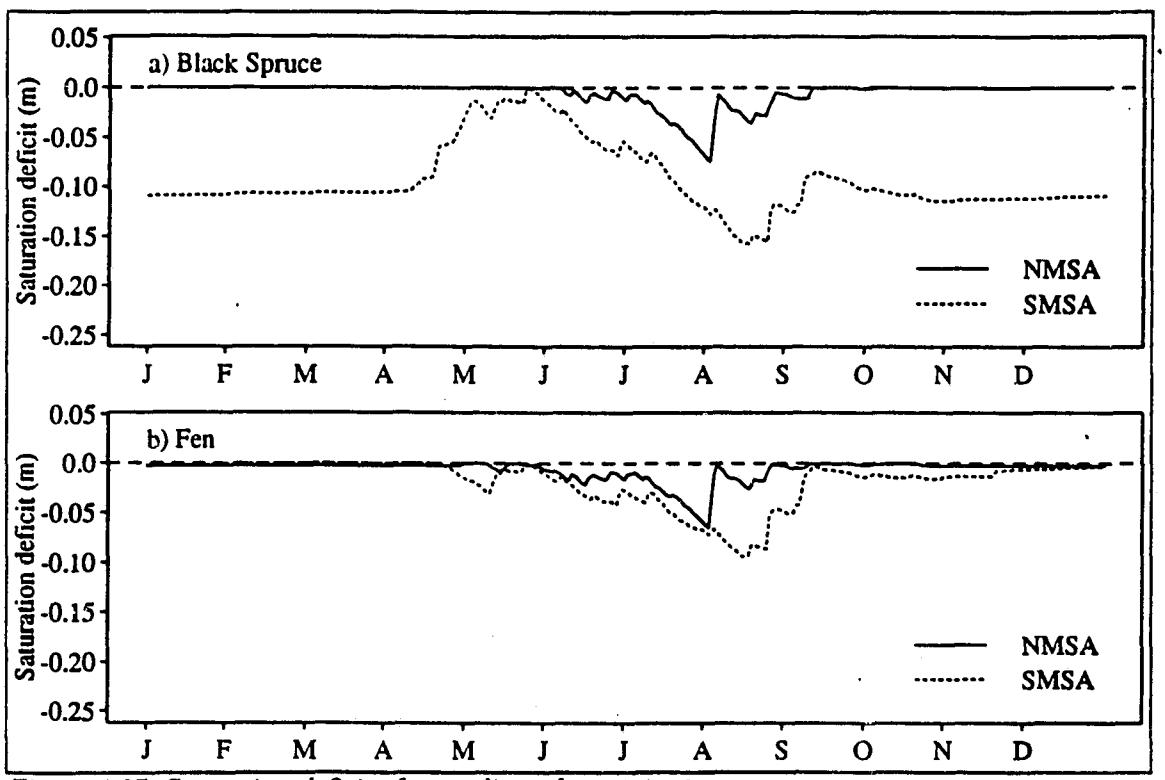

Figure 4.17: Saturation deficit after scaling of precipitation.

Fen areas are normally located in depressions, which would cause supply of water from lateral inflow, in addition to precipitation. In this analysis, the Fen was saturated in the fall, due to some heavy rainstorms, and stayed more or less saturated during the snow season. During the mid summer, when evapotranspiration was high, the Fen became drier. If lateral inflow had been accounted for in the point version of DHSVM, the Fen would have been saturated longer into the summer.

Comparing the differences in moisture and heat fluxes between the two vegetation types and the different climates, one can see several contrasts in Figures 4.16 through 4.20. As already mentioned, the south is generally drier than the north, both because precipitation is lower and net radiation is higher. In the north, a larger part of the annual precipitation falls as snow (Figure 4.18), and the north experiences less evapotranspiration (Figure 4.19), mainly because the snow free period is shorter and net radiation is lower. The runoff (surface runoff or percolation) is higher in the north. For both sites, most of the runoff is concentrated in the spring.

In the NMSA, net radiation during the snow season typically was -70 W/m^2 at the Fen site, and -35 W/m^2 at the Black Spruce site. This is less than Male and Granger [1981, cf Hendrie and Price, 1978] reported at snow surface for a leafless deciduous forest site (33 W/m^2) and for an open area (10 W/m^2) in Ontario (45°N), but the ratio between open and forested areas is similar. According to Male and Granger [1981], the high albedo of snow causes the radiation balance to be governed by the longwave fluxes, and since the forest cover acts to reduce the incoming shortwave radiation and increase the longwave radiation, the net radiation in the snow season is typically higher within forests than in open areas. Incoming shortwave radiation was, of course, lower in the middle of the winter than in the spring. However, air temperature fluctuated between -35°C and -5°C during most of the snow season, and since long wave radiation governs the radiation balance over the winter, any increasing or decreasing trend in net radiation over the snow season was hard to detect. During the entire year, net radiation was negative for 206 days at NFEN, and for 166 days at SFEN.

In the DHSVM analyses, the incoming longwave radiation at the snow surface was 5 to 10 times higher than the incoming shortwave radiation in March/April, and 20% higher at NOBS than at NFEN. In the middle of the winter, when shortwave radiation was lower, the ratio could be up to 100. The ratios were similar in the southern area, but because of the southern location, the net radiation was less negative, and hence sensible heat flux less positive. Figure 4.20 shows latent and sensible heat at the snow surface in the snow season, and for the vegetation when there is no snow on ground. The figure shows that the sensible heat flux (into the snow pack) was higher in the open Fen area than inside a Black Spruce forest. (Positive sensible heat indicates that the snow pack is colder than the surrounding air.) DHSVM calculates sensible

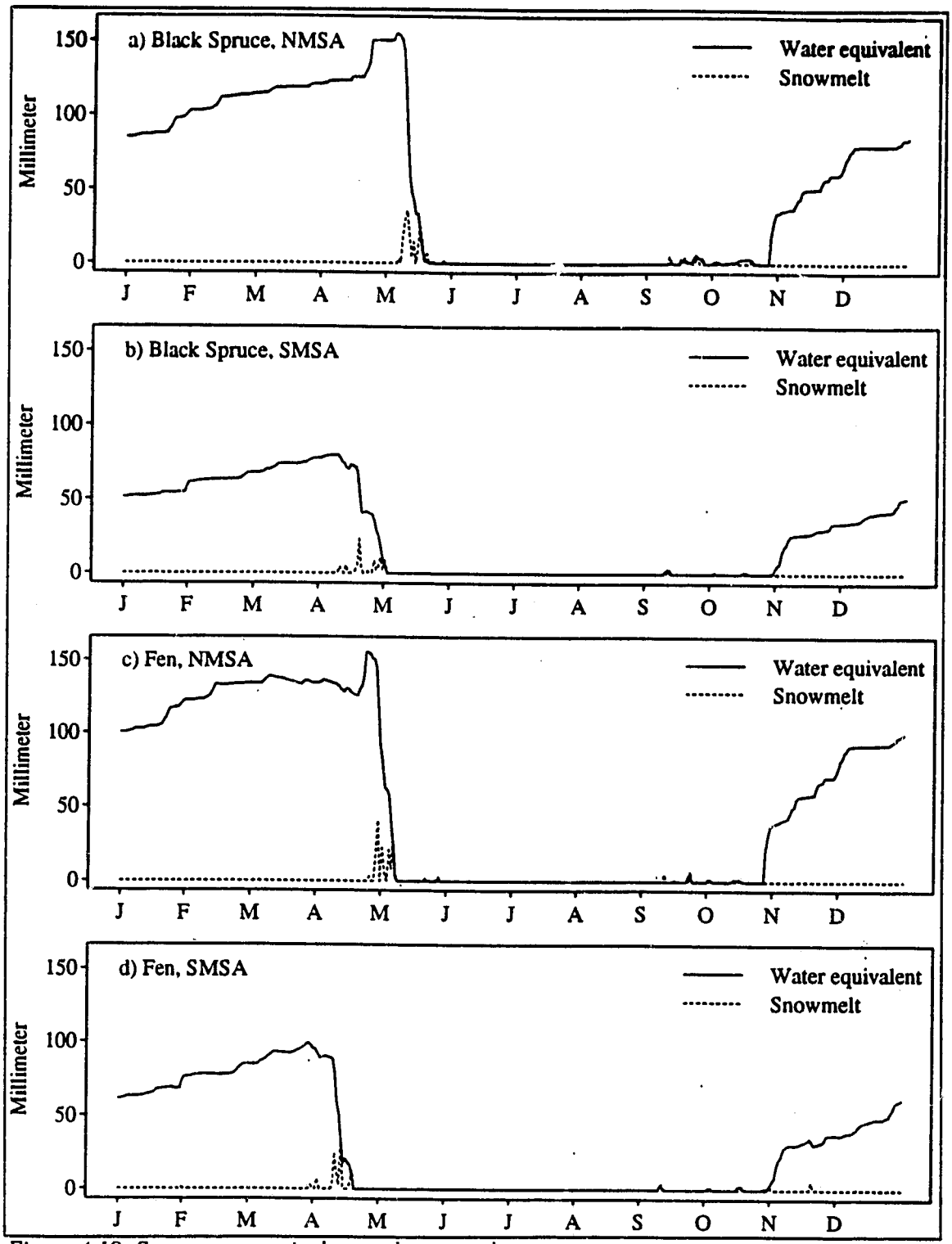

Figure 4.18: Snow water equivalent and snow melt.

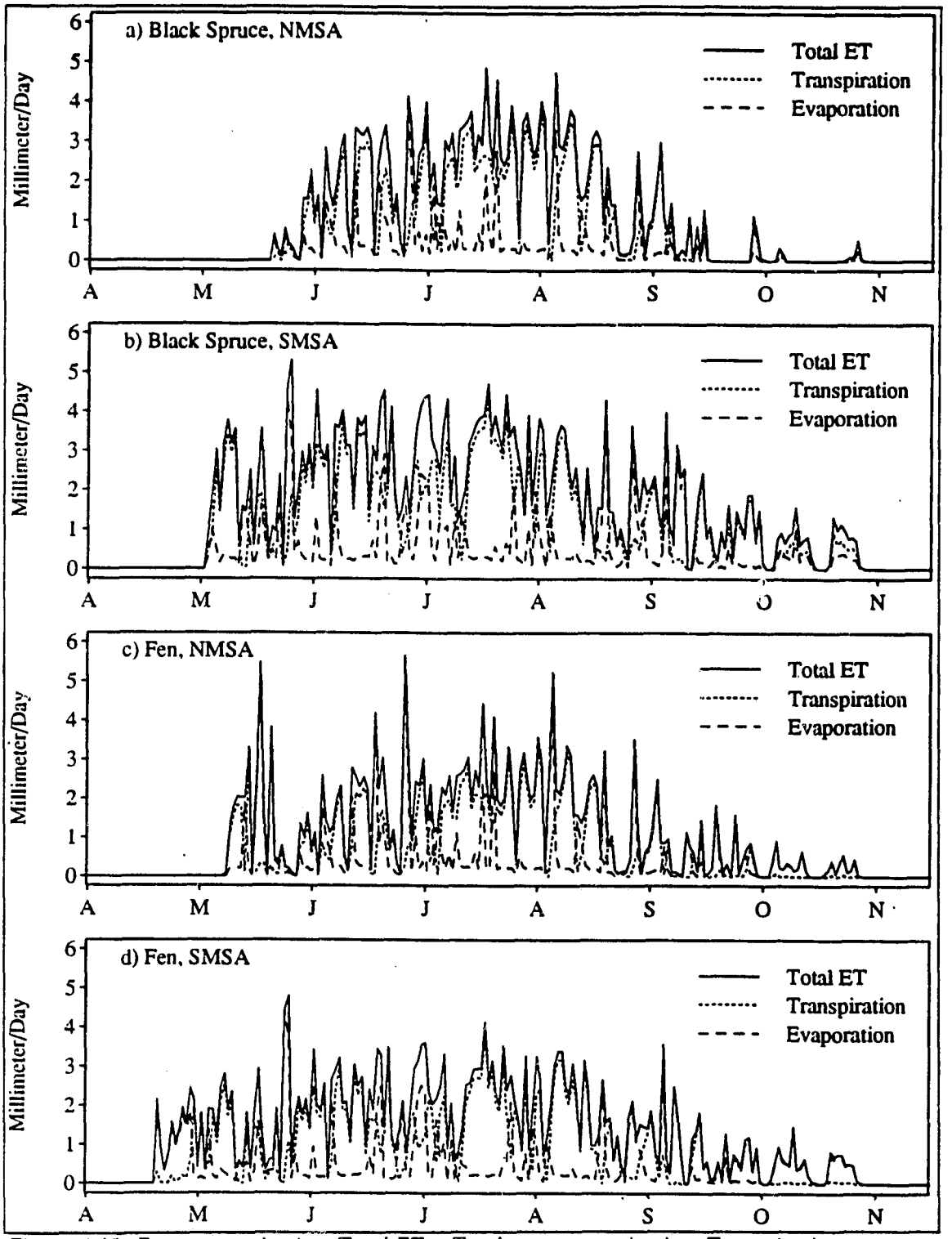

Figure 4.19: Evapotranspiration. Total ET = Total evapotranspiration, Transpiration = Transpiration from overstory and understory, Evaporation = Soil evaporation and evaporation of intercepted water.

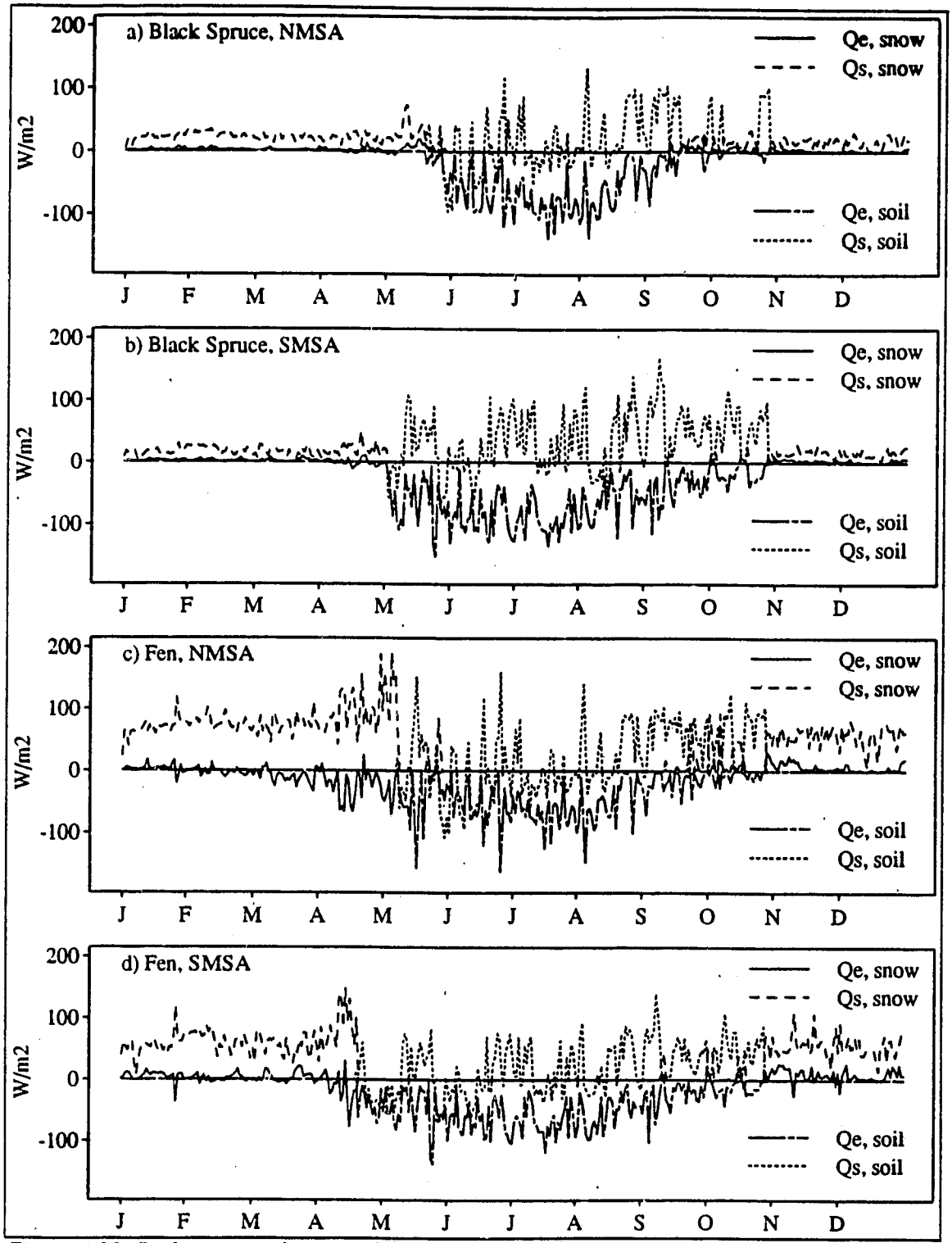

Figure 4.20: Daily average latent and sensible heat. Q_e = Latent heat, Q_s = Sensible heat.

heat based on an energy balance approach, and since the latent heat flux is low in periods when snow covers the ground, sensible heat becomes the main component which has to equalize outgoing net radiation in the energy budget, which explains why sensible heat flux was lower at the Fen sites than at the Black Spruce sites.

Because there is no overstory, and hence no snow interception, the model predicted that the Fen sites had the largest amount of snow. Since sensible heat flux was higher at the Fen sites than at the Black Spruce sites, one would think that the snow was coldest at the Fen sites, and thus melted later. However, the aerodynamic resistance is less in the open area than in the forest, which resulted in a generally colder snow temperature at the Black Spruce sites than at the Fen sites, and therefore the Fen sites became free of snow first, even though the net radiation was lower. The fact that the air temperature might be different within a forest canopy than in an open area, is not taken into account in DHSVM.

Incoming shortwave radiation at northern latitudes varies substantially over the year (see Figure 2.1), and is, assuming clear-sky conditions, highest in the middle of June. In these analyses, net radiation (total incoming radiation - $\varepsilon\sigma T^4$, where T is the surface temperature, and emissivity, ε, in DHSVM is assumed equal to unity) is higher in May/June than later on in the season, which results in periods with negative sensible heat (flux upwards from the vegetation) in the early summer, and positive sensible heat (flux into the vegetation) in the late summer and fall. Latent heat is highest in the spring and mid summer, and decreases when soil moisture becomes limiting in the late summer and fall. It is, on average, higher in the SMSA, and also higher at the Black Spruce sites than at the Fen sites, because of higher total LAI at the Black Spruce sites.

Conclusion.

These results show that the timing of energy and moisture supply are the most important determinants of latent heat flux. This is especially noticeable in the north, where moisture supply in the form of snowmelt is highest in the spring, but because the soils reach field capacity the water percolates through the soil column or runs off as surface water and is thus

lost by the vegetation. Later in the summer, the sites in the north dry out, because of limited water supply.

Radiation and the aerodynamic resistance control the sensible heat transfer and snow temperature. Even though the net radiation is lower in the open area than in the forest, the snow temperature is lowest within the forest, because of the high aerodynamic resistance under the canopy. Consequently, the snow in the open area becomes isothermal earlier in the spring than the snow under the canopy does, and therefore becomes free of snow first.

DHSVM is quite sensitive to many of its input parameters, but calibration within physically reasonable ranges is expected to give reasonable results when the more detailed summer 1994 observation data become available. While several different combinations of parameters might lead to similar results for total ET and runoff, the partitioning of ET into evaporation and transpiration, and runoff into surface runoff and baseflow should help in the parameter identification process.

4.3 MOSS ANALYSIS.

Background.

Stand structure and function in the boreal forest are largely controlled by the moss-organic layer [Bonan and Shugart, 1989]. The presence of a moss layer contributes to organic matter accumulation, decreases soil temperatures, increases soil moisture, and reduces nutrient availability. Mosses thrive and form a continuous cover where conditions are both moist and shady. In cold, wet Black Spruce stands, up to 80-90 percent of the above-ground biomass may be contained in the moss layer. Moss establishment and productivity are apparently promoted by the low temperature, high water content, and poor nutrient status of Black Spruce soils [Bonan and Shugart, 1989].

Approach.

A surface layer, consisting of moss and peat, was added to the point version of DHSVM, to analyze the role of moss in the hydrologic cycle The purpose was to be able to change the depth

of the root zones and the distribution of overstory roots in the different layers of the soil column, while maintaining the root fraction in the lowest root zone (10 percent). Two different approaches were taken:

1. Add a moss layer, and assume all overstory roots are beneath this layer.
2. Change parts of the upper soil layer from mineral soil to peat, and distribute the roots evenly in these upper two layers; keep 10 percent of the roots in the lowest root zone.

For both approaches, moss layers (porosity: 80 percent) of 20 cm were specified (see Table 4.5). In the base case, both root zone layers were assumed to consist of sandy clay loam (porosity: 40 percent). The total root zone depth was 50 cm, meaning for approach 1 the total soil depth was 70 cm. The understory was assumed to consist of moss only, while the overstory height was 10 m, making the site characteristics similar to those of the OBS site in the NMSA. For both approaches, soil evaporation was allowed to extract water only from the upper soil layer. The vegetation and soil characteristics were as in the final run for NOBS in Section 4.2.

Table 4.5: Description of soil layers and fraction of roots in the different layers.

	Moss layer		Root zone 1		Root zone 2	
	Depth	Overstory root fraction	Depth	Overstory root fraction	Depth	Overstory root fraction
Base	0	0	0.25	0.9	0.25	0.1
Approach 1	0.20	0	0.25	0.9	0.25	0.1
Approach 2	0.20	0.72	0.05	0.18	0.25	0.1

The moss analysis was run at hourly time steps for the first two weeks of September 1994, which includes some of the period during which moss field work was done (see Appendix 1). Wind speed and air temperature for this period were taken from the measurements at the OBS tower, and solar radiation, relative humidity and precipitation were taken from the OJP site in the NMSA. Longwave radiation data were not available, but were estimated from net radiation and air temperature measured at OBS. During these two weeks, soil moisture was measured at

OBS every other day by Dr. Richard Cuenca and William Price (Bioresource Engineering Department, Oregon State University), and these measurements were used to estimate initial soil moisture conditions in the root zones: 30 percent in root zone 1 and 40 percent in root zone 2 (i.e. root zone 2 was saturated). Soil moisture of the moss layer was estimated from field observations, which gave a moisture content of 20 percent.

Results and discussion.

Figure 4.21 shows modeled latent and sensible heat, for the base case and Approach 1 and 2, compared to observed values. Some values were missing in the observed record; these were given a value of zero in the figure. The figure shows that the modeled latent heat in general appears to be too high for all cases, and is highest during the precipitation events on September 4 and 5. During this period, the predicted evapotranspiration (ET) was caused mainly by evaporation of intercepted water; 28.6 percent of the rainfall intercepted and evaporated, which is almost identical to the field observation of 28.1 percent interception. However, the modeled intercepted water evaporated during the same time step as it was intercepted, which does not agree with field experience. As a consequence of high latent heat flux, the predicted sensible heat flux was too low. However, Approach 2, - overstory roots in the humus layer, gave the results that were closer to the observed values. This was mainly caused by decreased overstory transpiration, because a greater fraction of the roots were in the moss layer, which was dryer than the underlying mineral soil. It should be kept in mind that the analysis was run for two weeks only. When it was run until equilibrium, with 1989 data, the evapotranspiration was highest in Approach 2, because of higher moisture content in the porous moss layer than in the mineral soil, and the fact that the majority of the roots were located in this wetter layer in Approach 2.

Figure 4.22 shows the ratio of understory and soil ET to total ET. Compared to field work results (Appendix 1), the predicted ratio was a lot more stable, and it also appears that the predicted ratio, on average, was higher than observed. Whether this is a result of incorrect input parameters or deficiencies in the model structure, is hard to say. It could be that the aerodynamic resistance under the canopy was too low (which results in increased transpiration, see Section 4.1). On the other hand, increased aerodynamic resistance would increase the

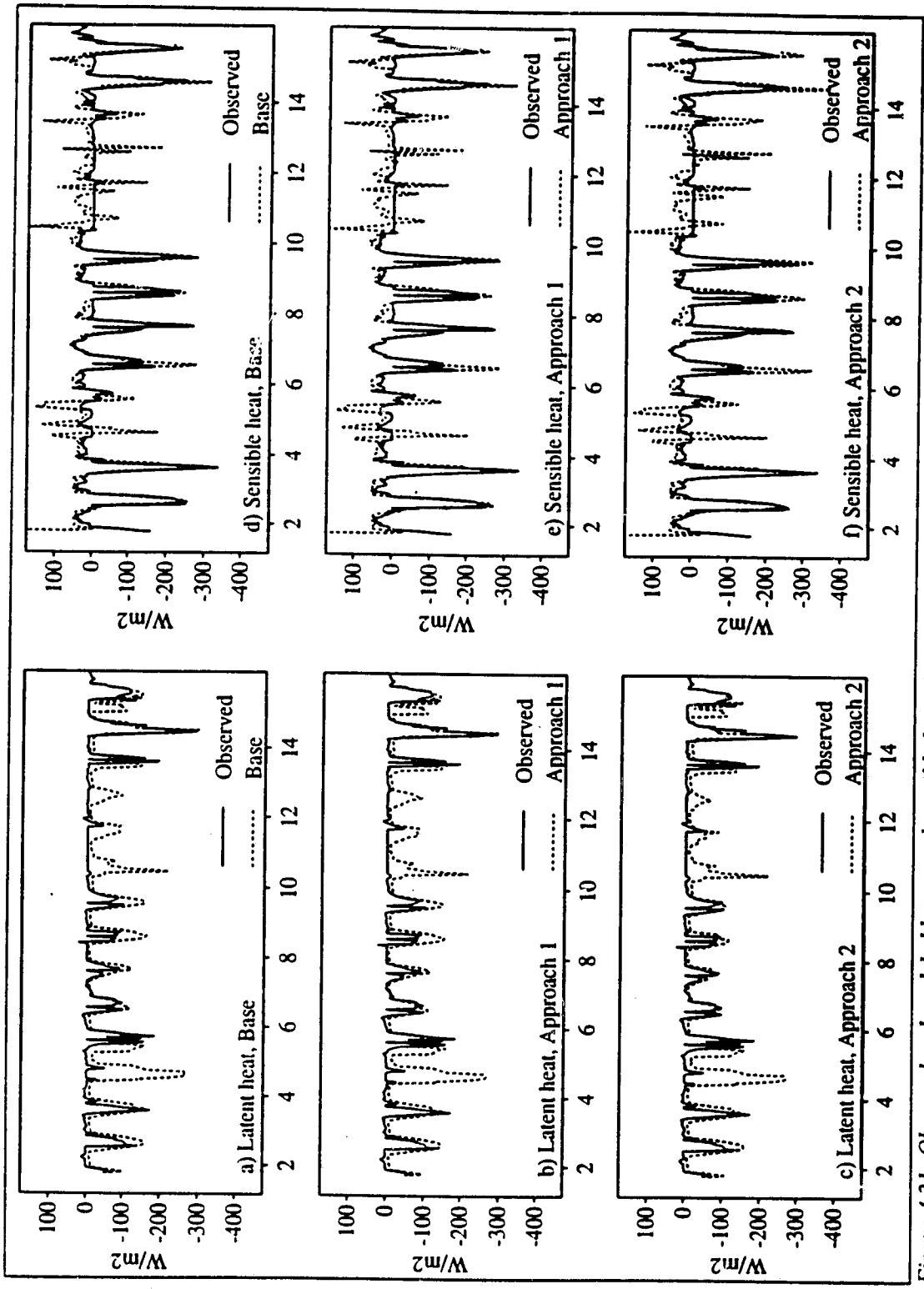

Figure 4.21: Observed and modeled latent and sensible heat, September 2 through 15, shown at hourly time steps.

evaporation of intercepted water, which would make the model predictions during precipitation events even worse. Another possibility is that the assumed leaf area index for the moss (2.0) was too high, or that stomatal resistance for the moss was too low. The high latent heat flux could also be a result of the assumed soil temperatures (measured soil temperatures were not available). With a soil moisture content of 20 percent, changes in soil temperatures would influence the resulting transpiration somewhat, both for overstory and understory.

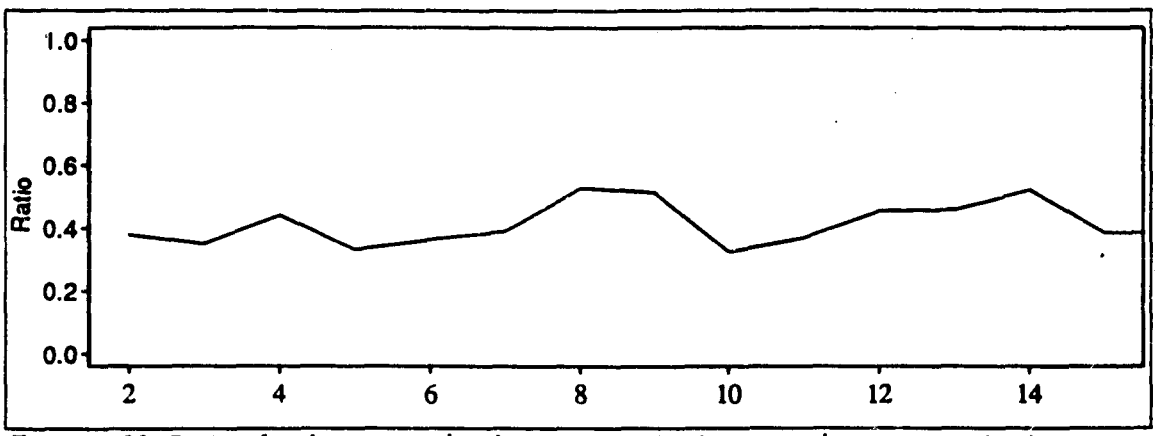

Figure 4.22: Ratio of understory and soil evapotranspiration to total evapotranspiration, September 2 through 15.

The predicted sensible heat flux showed some fluctuations that were not reported in the observed record of sensible heat fluxes, e.g. on September 4 and 5. At this time, some smaller rainstorms occurred, which, because of cloud cover, resulted in periods with low net radiation (35 W/m^2 at noon on September 4, for example); while it could be a lot higher just a few hours later (450 W/m^2 at 3 pm). As already mentioned, the predicted latent heat flux seems to be too high during these rainy periods, and the predicted sensible heat flux started fluctuating in order to maintain the energy balance.

Conclusion.

The modified version of DHSVM used in this analysis showed that the predicted heat fluxes were closer to observed heat fluxes when overstory roots were assumed to occur in the moss layer, than when no moss layer was assumed, or when the roots were assumed to occur under the moss layer. The model had some difficulties predicting heat fluxes that were similar to

observed heat fluxes, though; the predicted latent heat flux was too high compared to measured values. Another deficiency was that the ratio of ET from understory and soil to total ET appeared to be too high, compared to field observations. However, the sensitivity analysis showed that the moss layer has a significant influence on evapotranspiration, as do the location of roots in the soil column. It also shows that it is not only the presence of moss that has to be taken into account, but also the distribution of roots in the soil column.

CHAPTER 5: SPATIAL ANALYSES.

5.1 BACKGROUND.

A preliminary run of the fully spatially distributed version of DHSVM was made for the SMSA. This preliminary run was intended to provide insight about differences in heat and moisture fluxes of different vegetation types. A second purpose was to investigate the effect of spatial resolution of precipitation on resulting heat flux predictions. Since DHSVM has not previously been used in low relief areas with a continental climate, it was also of interest to identify parts of the model that will need to be modified to improve performance in boreal regions. The period of interest for this study was the beginning of May to mid August 1994, which includes two of the three BOREAS Intensive Field Campaigns (IFCs), and is the period during which precipitation radar data were available at the time of this study.

5.2 APPROACH.

Data.

Meteorological data.

The model was run at a daily time step for one year, to obtain initial values for soil moisture and saturation deficit. For the first part of the initialization run (May through December 14, 1993), meteorological data from 1989 measured at Prince Albert Airport were used because more local or recent data were not available. From December 15, 1993, meteorological data at 15 minute resolution were available from the SRC-station at OJP, and these data were aggregated up to 24 hour time steps. For April 1994, precipitation data were not available at OJP, and the precipitation measured at the SRC-station at OA was taken as a substitute.

The resulting values for soil moisture and saturation deficit from the initialization run were used as input to the final simulation, which was run with 3 hour time steps. Temperature, wind speed, relative humidity and longwave radiation were obtained from OJP. Shortwave radiation was calculated by use of IPW and measured incident solar radiation at OJP (see Section 3.3). Longwave radiation data were missing from June 29 through July 26, and from July 15 through

July 20 all values were missing at OJP. During this period, the meteorological station at OA was not functioning as well, and meteorological data from the AES-station at Nipawin, about 80 km southeast of OJP, were used. Precipitation data for the period of interest were obtained from the precipitation radar, which was located south of the SMSA (see Figure 3.3). The precipitation data, originally at 10 minute resolution, were aggregated to 3 hour time steps and prepared for use in DHSVM by Reiner Schnur (Department of Civil Engineering, University of Washington). The radar is known to overestimate precipitation [Krauss et al., 1994], and by comparing the amount of precipitation given from the radar image to the amount measured by rain gauges, the values were multiplied by 2/3. Figure 5.1 illustrates the average amount of precipitation at the SMSA, and the temperature measured at OJP for the period of interest. Total precipitation was 380.2 mm, which means that during these three and a half months, the area received 95 percent of mean annual precipitation. For comparison, the fraction of annual precipitation for the same period in 1989 was 41 percent.

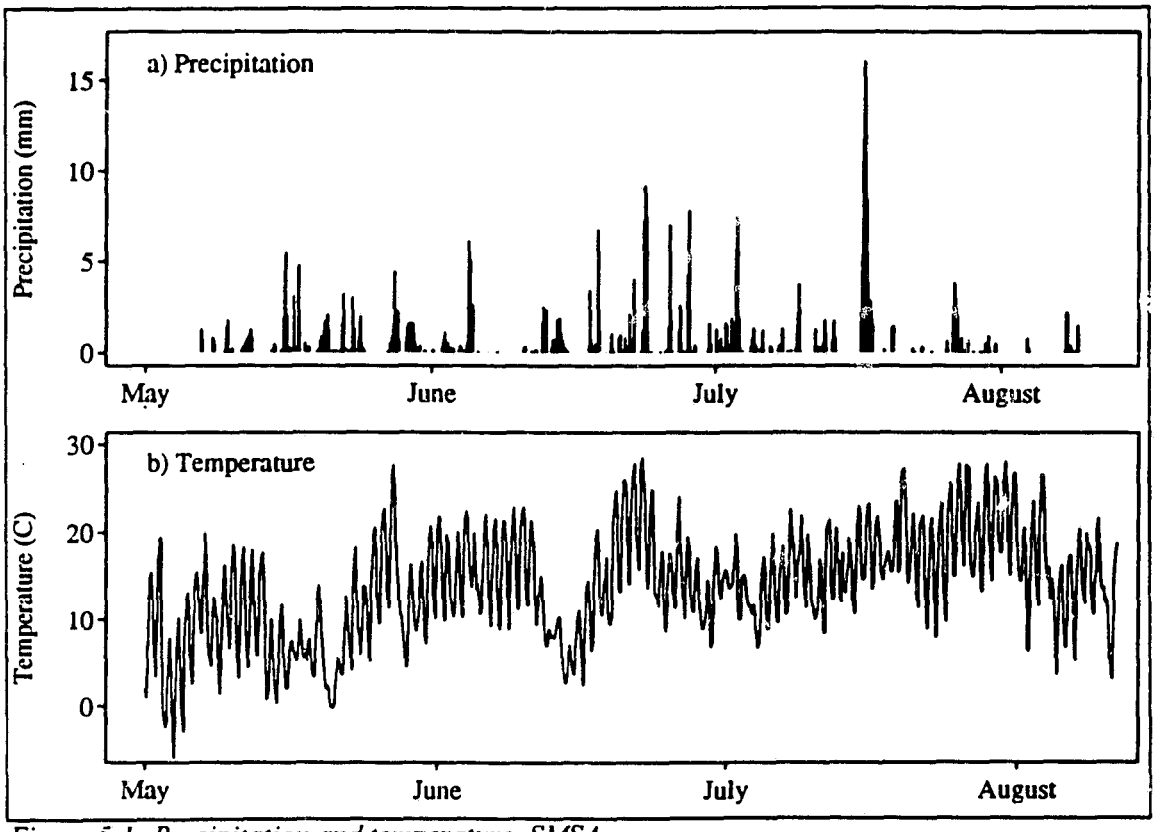

Figure 5.1: Precipitation and temperature. SMSA.

Vegetation and soil parameters.

Information about, and illustrations of, vegetation and soil cover in the SMSA are given in Section 3.3. The same canopy height, understory height, leaf area index and stomatal conductance used in the final point modeling run (see Section 4.2) were used for Conifer wet (Old Black Spruce (OBS)) and Fen. Some values for Conifer Dry (Old Jack Pine (OJP)) and Deciduous (Aspen) were taken from the modeling comparison group (see Section 4.2), but the deciduous trees were taken to be 18.7 m (instead of the given 20 m), to make sure all the vegetation was at least 2 m below the wind speed measurement height at OJP (20.7 m). The three regeneration vegetation types were assumed to be a mix of deciduous trees and conifers, with more conifers in the older group, hence Regeneration (older) is somewhat similar to Young Jack Pine (YJP).

Table 5.1: Vegetation parameters.

	Conif. Wet	Conif. Dry	Mixed	Decid.	Reg. Young	Reg. Med.	Reg. Older	Fen
Height, overstory (m)	12.0	13.0	15.0	18.7	3.0	4.0	5.0	-
Height, understory (m)	0.2	0.1	0.3	1.0	0.1	0.1	0.1	1.0
LAI, overstory (projected)	3.5	2.5	4.0	4.5	2.0	2.1	2.2	-
LAI, understory (projected)	2.0	1.0	2.0	4.0	1.0	1.0	1.0	4.0
Maximum stomatal conductance (m/hr)	5.4	5.4	7.5	9.0	12.0	12.0	12.0	7.2
Fraction of overstory cover	0.5	0.5	0.5	0.5	0.3	0.35	0.4	-
Depth, humus layer (m)	0.20	0.04	0.10	0.02	0.04	0.04	0.04	0.20
Depth, root zone 1 (m)	0.05	0.21	0.15	0.24	0.21	0.21	0.21	0.05
Depth, root zone 2 (m)	0.25	0.75	0.75	0.75	0.25	0.25	0.25	0.25
Fraction of overstory roots in humus layer	0.72	0.06	0.4	0.01	0.16	0.1	0.05	-
Fraction of overstory roots in root zone 1	0.18	0.74	0.4	0.48	0.74	0.8	0.85	-
Canopy attenuation coefficient	2	2	2	2	2	2	2	-
Extinction coefficient	0.5	0.5	0.5	0.5	0.5	0.5	0.5	0.5

Parameters for porosity, bubbling pressure and pore size distribution (Table 5.2) were taken from Clapp and Hornberger [1978], while estimates of effective porosity and saturated hydraulic conductivity were taken from U.S. Department of Agriculture's recommended values given by Rawls et al. [1993]. The available water values (porosity - wilting point) were taken from the digital soil maps (Table 3.4.)

Table 5.2: Soil parameters.

	Humus/ Marsh	Loam	Fine sandy loam	Sandy loam	Loamy sand	Sand
Porosity	0.5/0.8	0.45	0.44	0.44	0.41	0.40
Field capacity	0.3/0.4	0.25	0.24	0.24	0.21	0.20
Wilting point	0.13	0.10	0.14	0.14	0.16	0.15
Bubbling pressure	0.12	0.48	0.25	0.22	0.09	0.12
Pore size distribution	0.19	0.19	0.20	0.20	0.23	0.25
Saturated hyd. cond. (m/hr)	0.072	0.013	0.022	0.022	0.06	0.24
Lateral hyd. cond. (m/hr)	0.01	0.013	0.022	0.022	0.06	0.24

Soil temperatures at the OJP site were available at depths of 2, 16 and 32 cm from May 23 through the summer, and these temperatures were used in the calculation of canopy resistance (see Section 3.2). The temperature in the soil column was assumed to vary linearly between the measured values, and the temperature at the average root zone depth was taken as the actual temperature in that root zone. If the average root zone depth was over 32 cm, the given temperature at 32 cm was used. From May 1 to May 22 the soil temperature was assumed to vary as described in Section 4.2. The modeled soil surface temperature was used to calculate sensible heat flux and ground heat flux.

The soil files (Table 3.4), gave information about depth of humus layer, soil type in surface mineral soil layer and 'main' layer. The vegetation image originally had a higher resolution than the soil image, and since vegetation type and depth of humus layer are thought to be related, the depth of the humus layer was made dependent on vegetation type rather than soil type.

Method.

Areas of Conifer wet (OBS), Conifer dry (OJP), Deciduous (Aspen), Regeneration-older (YJP) and Fen were located in the vegetation image. The digital vegetation and soil maps did not necessarily match the known conditions on the ground, which can be caused by the original spatial resolution, the classification scheme, the reprojection or the resampling of the images. If the vegetation and soil type in the digital images were consistent with the actual vegetation and soil type at the location of the BOREAS Tower Flux (TF) sites, moisture and heat fluxes were aggregated and averaged over these areas. Otherwise, an area where both the vegetation type and the soil type were homogeneous was identified. OBS and OJP were the only sites which appeared with homogeneous characteristics around the TF sites in both the soil- and vegetation images. The Old Aspen site in BOREAS was located outside the SMSA, and the selected area of aspen was located about 9 km south of OJP. YJP in this study was located about 1 km east of the actual YJP site, in order to find an area with homogeneous soils. The BOREAS Fen site was located in an area which in the soil image had sandy soils, which is clearly an error. Therefore, the selected Fen area was about 10 km northeast of the Fen TF site, where the soil image reported "Marsh". Table 5.3 gives the location and some descriptive data of the selected areas, and Figure 5.2 illustrates the approximate location of the TF sites and the selected vegetation areas.

Table 5.3: Description and location of vegetation areas in the SMSA (UTM, NAD 27, zone 13).

	Soil class	Pixels	Location	TF-location	Description
OBS	Sandy loam	39	NW: 5982000N, 491900E SE: 5981200N, 492500E	5981904N, 492000E	Gently sloping eastwards
OJP	Loamy sand/ Sand	28	NW: 5974200N, 520000E SE: 5973600N, 520700E	5974015N, 520314E	Gently sloping westwards
Aspen	Sand	15	NW: 5967500N, 520300E SE: 5966900N, 520700E	5942688N, 420874E	Sloping eastwards
YJP	Loamy sand/ Sand	16	NW: 5970200N, 523800E SE: 5969600N, 524400E	5969705N, 523201E	Gently sloping westwards
Fen	"Marsh"	30	NW: 5963200N, 517400E SE: 5962600N, 517900E	5961204N, 525101E	Gently sloping southwards

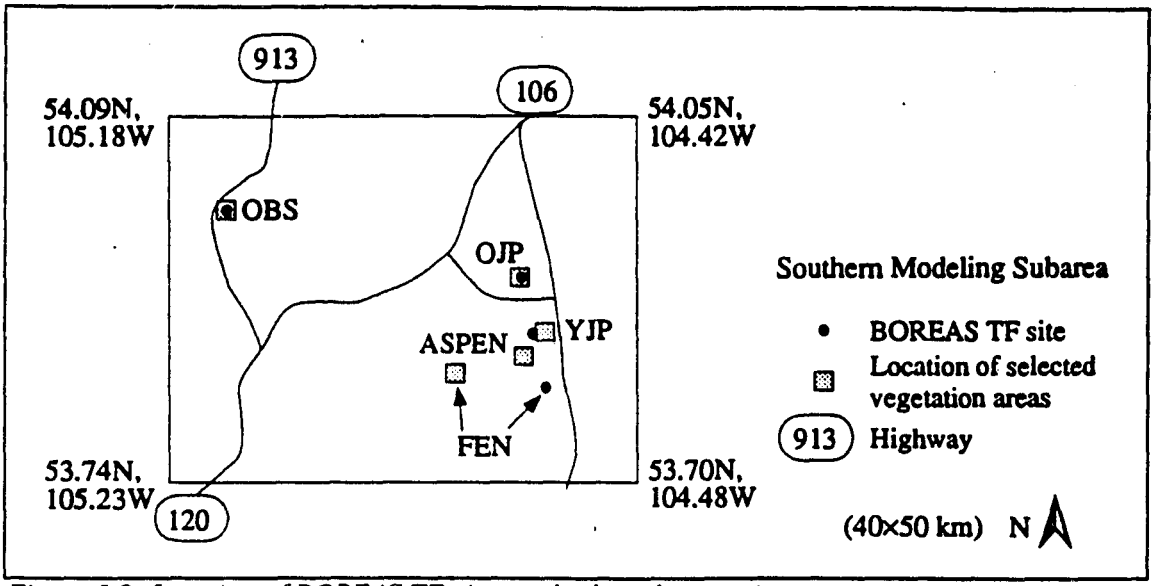

Figure 5.2: Location of BOREAS TF-sites and selected vegetation areas.

5.2 RESULTS AND DISCUSSION.

Comparison to measured values.

Available data for validation of the spatially distributed simulation were somewhat limited at the time this thesis was written. The limited data that were available are compared to the model predictions in the remainder of this section. In the future, a large amount of ground data and remotely sensed data for the BOREAS areas that were collected in 1994 and is currently being processed will be available (e.g. heat and moisture fluxes at the TF sites), and it is anticipated that these data will be used to reduce some of the major model deficiencies reported here.

Snow depth in initialization period.

The last part of the initialization period (December 15, 1993 to April 30, 1994) was done with meteorological data from the SRC-station at OJP. Snow depth was recorded at this site, and Figure 5.3 shows the measured snow depth and the modeled snow water equivalent at OJP. Most of the snow at OJP was gone by April 11, while the model predicts all snow to be gone by April 25. The modeled snow water equivalent is the average of the 28 pixels around the TF-site

at OJP, and it can be seen from Figure 5.3 that the modeled onset of snow melt is a little after the actual (about a week).

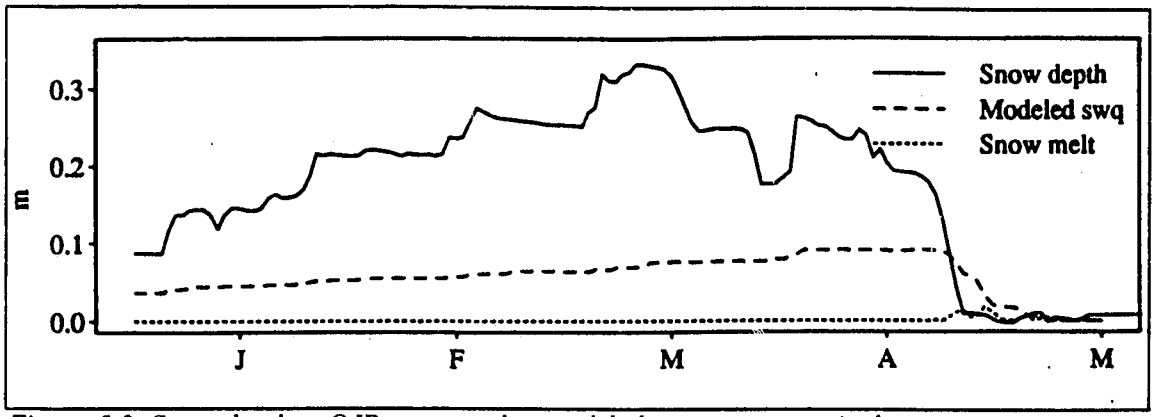

Figure 5.3: Snow depth at OJP compared to modeled snow water equivalent.

Modeled streamflow, compared to observed streamflow of the White Gull Watershed.

Figure 5.4 shows the modeled surface runoff and groundwater flow, compared to streamflow measured at the outlet of the White Gull Watershed, of which most is located within the SMSA. The White Gull Watershed is about 574 km^2 [Neff, personal communication], while the DEM of the SMSA, which was used in this simulation, is 2008 km^2. Mean measured streamflow was 5.6 m^3/s, or 87.4 mm of water, while the model predicted a mean streamflow of 22.0 m^3/s, which is equivalent to 97.5 mm of water. Hence, the modeled runoff was 12 percent higher than observed. In contrast, the extent of saturated areas was less than expected; on average 6 percent of the area was saturated, but the fraction ranged from close to zero, in between rainstorms, to 80 percent during a heavy rainstorm in the middle of July. (The "expected" soil moisture pattern is based on personal and BOREAS investigators field experiences during the summer 1994, when the area, on average, was very wet in the spring, but dried out significantly through the summer. Fen and OBS were wet most of the summer, while Aspen, OJP and YJP were drier.)

The reason for the low percentage of saturated areas might be explained as follows: The root zones in DHSVM can become saturated because of precipitation, snow melt or exfiltration of water from the underlying soil. When the surface layer becomes saturated, the excess water goes to surface runoff, and is no further interaction with the forest floor occurs. Consequently,

the surface layer can be saturated at one time step, but if no precipitation occurs, soil evaporation and/or evapotranspiration from the vegetation will cause the soil moisture to be depleted in the next time step, unless the underlying soil supplies the root zones with water. In practice, it follows that if no precipitation occurs, only areas with higher lateral inflow than outflow can be saturated, i.e. depression areas. If the surface flow had been allowed to interact with the forest floor on its way out of the area, i.e. could have infiltrated to the soil again, one might have seen a larger fraction of saturated areas.

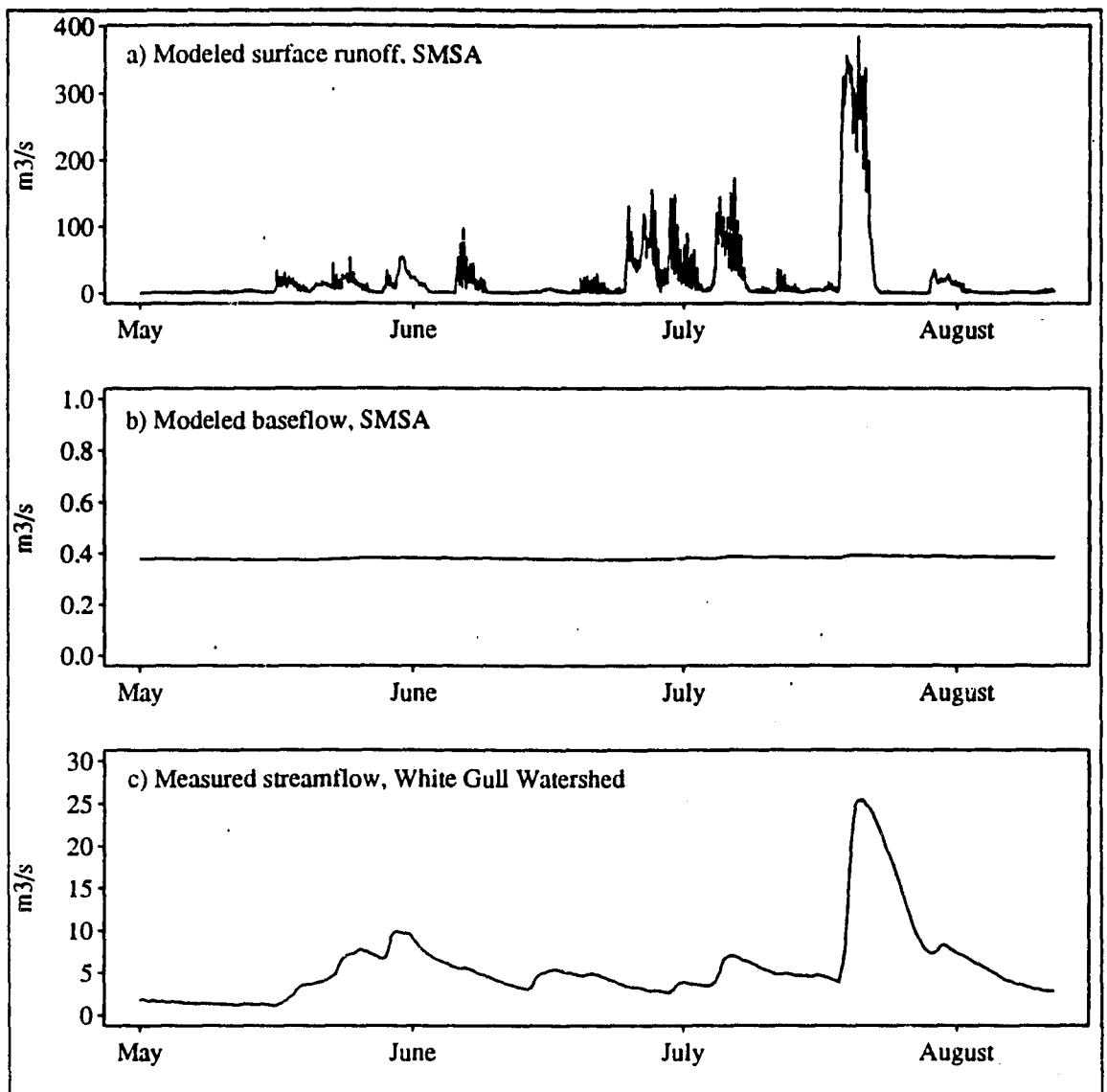

Figure 5.4: Modeled surface runoff and baseflow for the SMSA, and measured streamflow for the White Gull Watershed.

Figure 5.4 shows that the model predicted the timing of some of the peaks about right, but missed others. Some of the discrepancies can be caused by differences in spatial precipitation or errors in the radar image. The modeled peak in the beginning of June, for example, is caused by a heavy rainstorm reported in the radar image, which the rain gauges in the area reported as only minor. The modeled surface recession curve drops much more quickly than the measured streamflow recession. Predicted peak flow was relatively much higher for the SMSA than observed for the White Gull Watershed, and baseflow out of the area was much too small compared to observed baseflow. Modeled baseflow hardly responded to precipitation, even to the heavy rainstorm in the middle of July.

The lateral hydraulic conductivity (K_s) governs the amount of baseflow, but the level was stable both with a K_s of 0.1 m/hr and a K_s of 10 m/hr. However, surface runoff, soil moisture and saturation deficit were quite sensitive to K_s. The reason that the surface runoff, but not the baseflow, was sensitive to K_s can be traced to the topography, and the fact that in this study the modeled area was not a watershed. The DHSVM routing scheme is based on surface slopes taken from the DEM, and the computed travel time represents the time it would take for the surface runoff to reach the edges of the SMSA. The location with the highest number of pixels draining to it, as predicted by the routing scheme, was in the middle of the SMSA, and hence the edges of the SMSA did not represent the natural outlet of the baseflow in DHSVM. If the model simulations had been based on a watershed, as is conventional hydrologic modeling, one would probably have seen more variable, and maybe higher, baseflow. In addition, when the groundwater moved from an area with "steep" slopes to an area that was almost flat, the flow velocity decreased and further drainage was slow. Hence, water exfiltrated into the root zones, where it either was taken up by roots or, if the root zones became saturated, it ended up as surface runoff.

Latent and sensible heat at OJP.

Measured latent and sensible heat fluxes at the OJP-site were available from May 23 through the summer. Figure 5.5 shows the modeled and observed latent and sensible heat at this site. The modeled heat fluxes represent the average of 28 pixels including the location of the tower at OJP. The modeled latent heat was consistently higher than the observed latent heat, which

either indicates that the area was modeled as too wet, or that the vegetation and/or soil in the DHSVM was allowed to evapotranspire more than it actually did. Definite conclusions are hard to make, but it does appear that the discrepancies in latent heat predictions were higher during precipitation events than in the dry-down periods, which would be consistent with the results of the moss analysis (Section 4.3). When the modeled latent heat is higher than observed, one would expect the modeled sensible heat to be lower than observed, since sensible heat is computed based on values of latent heat, among other variables. However, in this analysis the modeled sensible heat was often lower than observed sensible heat during day time, while it was higher at night.

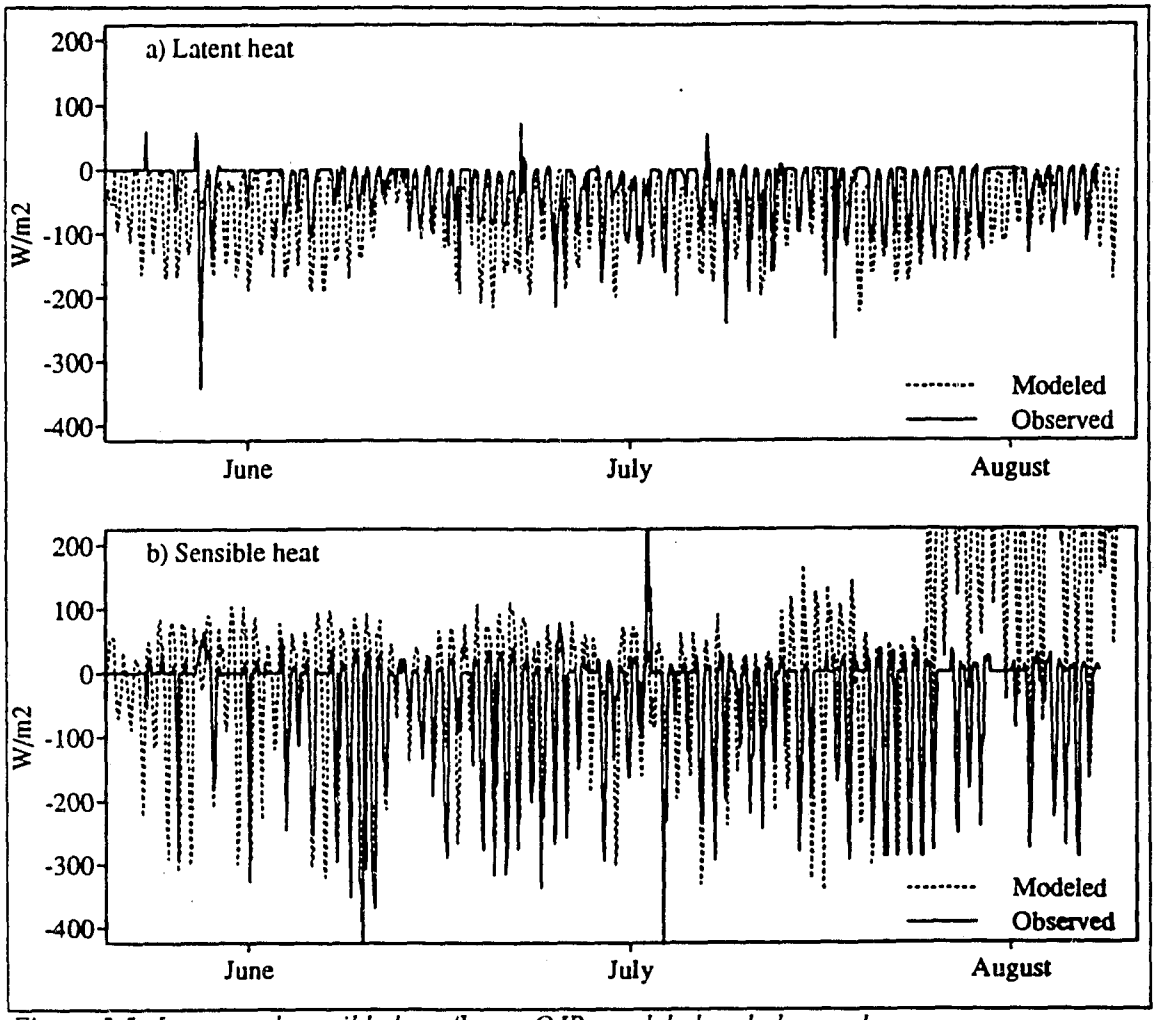

Figure 5.5: Latent and sensible heat flux at OJP, modeled and observed.

Since the measured heat storage and soil heat flux at OJP represent something slightly different from what DHSVM calculates (measured ground heat flux to 1 cm and canopy heat storage as opposed to ground heat flux to 1 m and soil heat storage), it might not be correct to compare these values, but, for both variables, the measured values were higher than the model predicted. Measured ground heat flux, for example, typically reached a peak value of 80 W/m^2, while calculated ground heat flux at the most was around 25 W/m^2. The version of DHSVM used in this study did not use an atmospheric stability correction, which probably would have decreased the sensible heat flux at night (colder vegetation temperature than air temperature results in stable conditions). The unexpected increase in modeled sensible heat in the end of the summer can be explained by a reported, sudden decrease in observed longwave radiation, - before July 29 typical longwave radiation was 300 W/m^2; after this date it dropped to 50 W/m^2, which may be an instrument error.

Heat fluxes and moisture in different vegetation areas.

Figure 5.6 illustrates the latent and sensible heat fluxes for the different vegetation types, while Figure 5.7 shows total daily evapotranspiration, and Figure 5.8 shows saturation deficit for the same areas. The latent heat fluxes reflect each vegetation type's leaf area index (LAI) and soil moisture at the site. Aspen had the highest total LAI (overstory + understory), but the site was fairly dry; hence the vegetation was under moisture stress, which explains why the latent heat flux at Aspen was lower than at OBS, for example. The OBS site was wet (Figure 5.8a), and with an LAI of 3.5 for overstory and 2.0 for understory, the total evapotranspiration was high, which resulted in high latent heat flux. Hence, mid-day sensible heat was lower at this site than at most other sites.

All sites had a fairly high (50 - 100 W/m^2) incoming sensible heat flux at night, which indicates that the vegetation was colder than the surrounding air. The incoming sensible heat was lower at night at the Fen site than at the other sites, and less negative during the day. The Fen site was saturated, or nearly saturated, most of the summer, and since the heat capacity of water (in DHSVM assumed to be 4.19 $Jg^{-1}K^{-1}$) is twice as high as the heat capacity of soil (DHSVM uses 2.0 $Jg^{-1}K^{-1}$, which is typical for fairly dry sand), more energy was stored in the wet soils at the Fen site during the day. Heat was not released from the soil until past midnight, which resulted

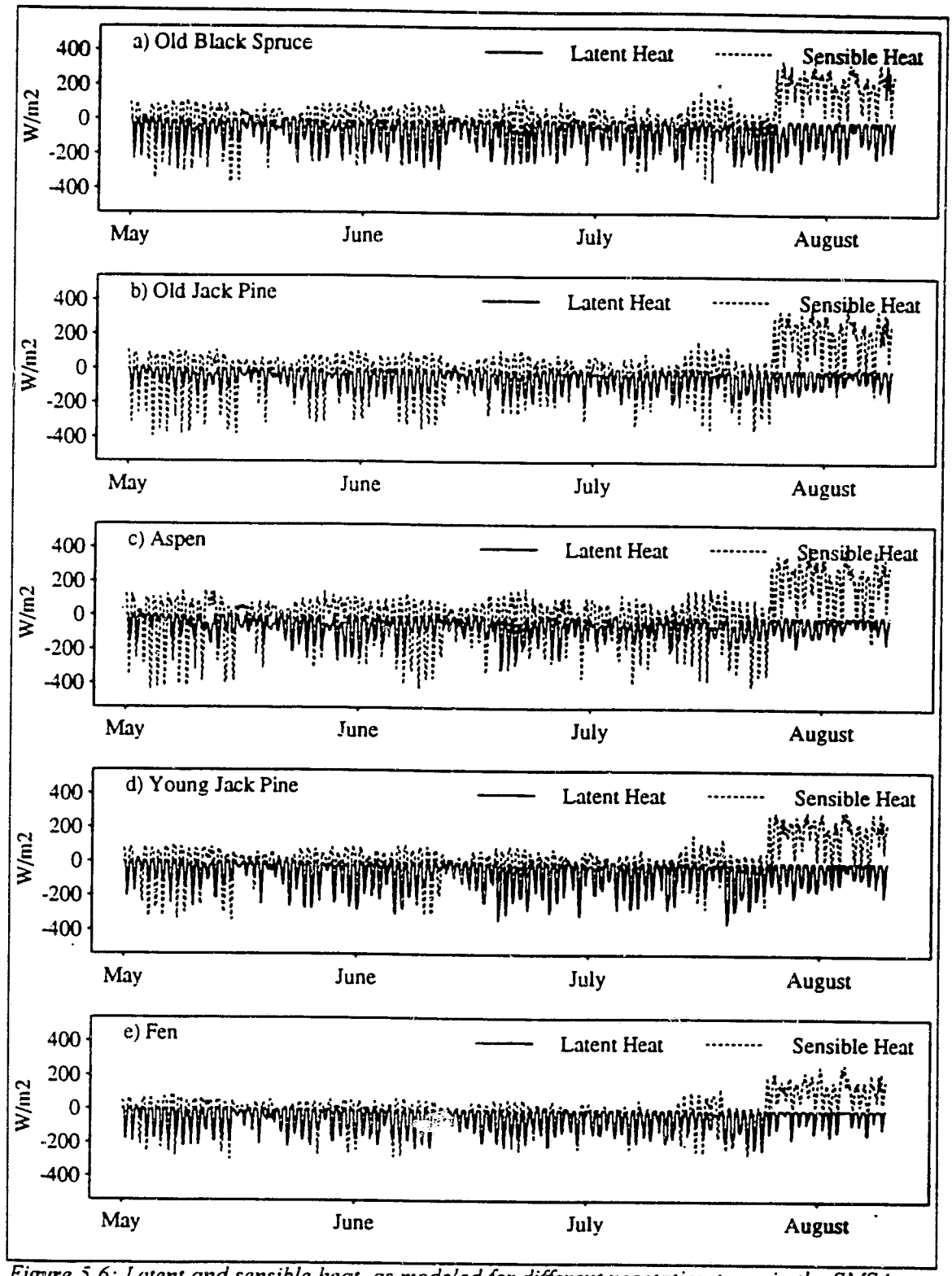

Figure 5.6: Latent and sensible heat, as modeled for different vegetation types in the SMSA.

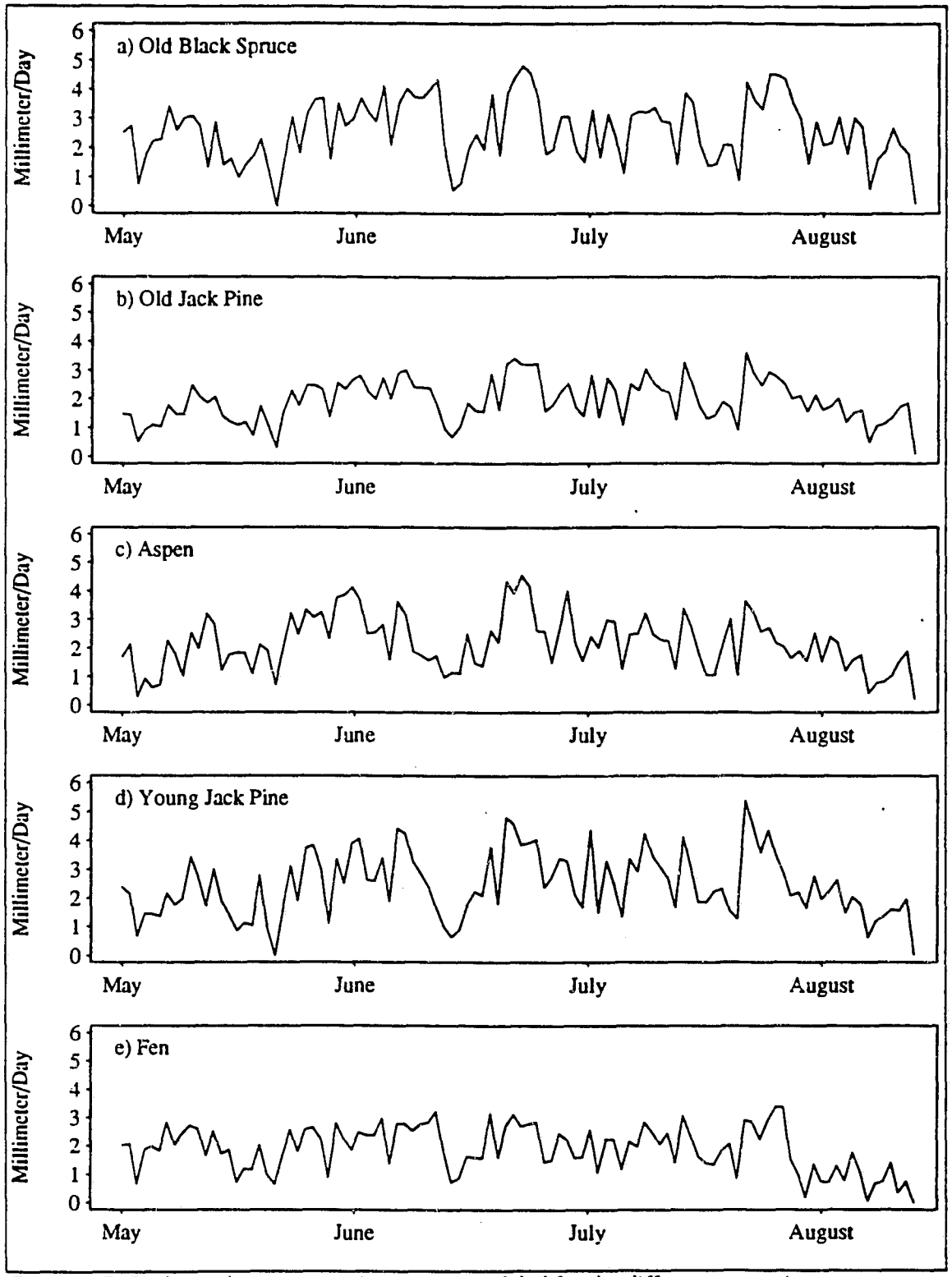

Figure 5.7: Daily total evapotranspiration, as modeled for the different vegetation areas.

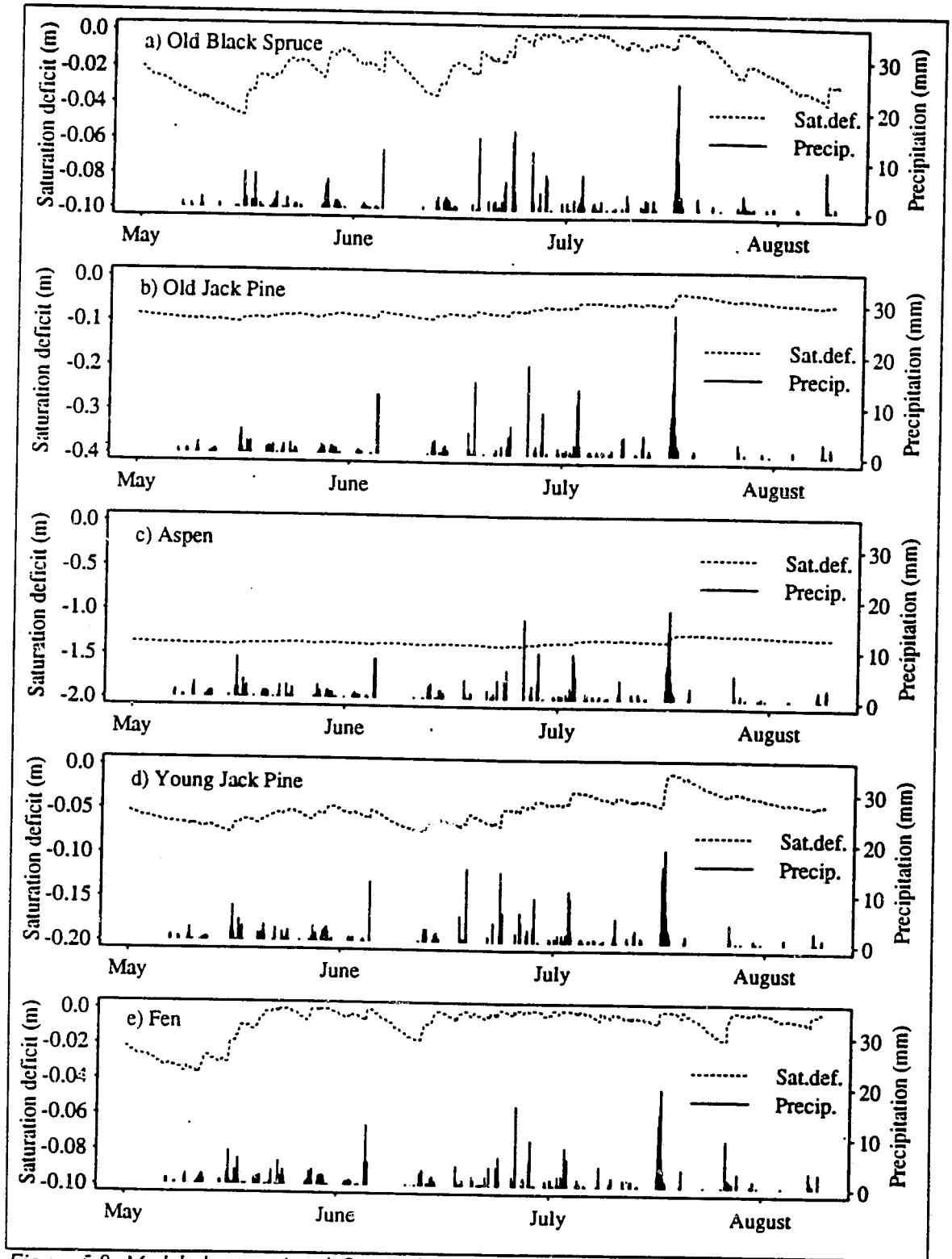

Figure 5.8: Modeled saturation deficit at the different sites. Precipitation amounts are given as bars for 3 hour totals.

in the relatively lower sensible heat flux at Fen at night. Aspen was the driest site, and heat storage was the least here; hence Aspen had the highest sensible heat flux at night. The soil heat capacity used in DHSVM is typical for mineral soils. Wet organic material has slightly higher heat capacity [Monteith and Unsworth, 1990], which would increase the heat storage somewhat (assuming the same surface temperature), but relatively more at dry sites than at wet sites.

The differences in sensible heat fluxes during the day were also caused by differences in latent heat fluxes, i.e. evapotranspiration (ET). Total evapotranspiration over the summer ranged from 193 mm (49 percent of precipitation) at the Fen site to 270 mm (69 percent of precipitation) at the OBS site. YJP actually had the next highest evapotranspiration amount (255 mm), which might seem surprising, given the lower LAI (2.2 as opposed to Aspen's 4.5, for example). Higher soil moisture, larger fraction of roots in the warmer, upper parts of the soil column, and higher stomatal conductance are all variables that contributed to this result, but the most important factor was probably the difference in seasonal precipitation between the two sites, - 381.8 mm at YJP as opposed to 340.5 mm at Aspen.

The Fen, which is located in an area with "very poor" drainage (Table 3.4), was saturated, or near saturation, during the entire summer. The Aspen site was on a hillslope, and the soils consisted of sand, which resulted in a dry site. OBS was fairly wet, in spite of its high latent heat flux, which was caused by its location with quite low hydraulic conductivity. Both Pine sites had sandy soils, but the area was fairly flat, and hence drainage was slow. All sites responded quickly to precipitation, and soil moisture at OJP and YJP actually increased during this wet summer. Hence, OBS, Fen and Aspen had a soil moisture pattern as expected, while the increase in moisture content at OJP and YJP was unexpected. The reason for this unexpected increase in soil moisture, is unknown, but this was a very wet summer. The predicted evapotranspiration was higher than observed (Figure 5.3), which should result in lower soil moisture. With a higher hydraulic conductivity, the soils were drier at the end of the spin up period, but the soil moisture over the summer increased relatively more. Decreasing the hydraulic conductivity would have increased the soil moisture over the entire season, which does not seem plausible. Also, the hydraulic conductivity used for the Pine areas (0.24 m/hr), is in the lower range of what is expected for sand.

Despite the fact that the extent of saturated areas was lower than expected, the SMSA, on average, was fairly wet. As stated in section 4.2, transpiration in DHSVM is more sensitive to soil temperatures under wet conditions than under dry conditions (Figure 4.15). Hence, the prediction of latent heat fluxes might be improved with a more accurate estimate of soil temperatures, - in this study a simple linear relationship between measured soil temperatures was assumed. In addition, the soil temperatures measured at OJP were assumed to be valid for the entire SMSA, which might not be true. For example, in the end of July, 1994, the soil temperature at 32 cm at OJP was around 12°C, while it was around 8°C at 20 cm depth at OBS during the same period. The moss and peat at OBS contributes to decreased soil temperatures compared to OJP, which has sandy soils.

Comparing the saturation deficit for the Black Spruce and the Fen sites resulting from the point analyses and the spatial analyses, it can be seen that the spatial analyses resulted in wetter conditions at the two sites. A reason for this might be lateral inflow, but the more likely reason is that the wet summer of 1994 results in higher soil moisture. The precipitation was 380 mm during the period of study in 1994, while it was only 153 mm during the same period in 1989.

Spatial variation of precipitation, and its influence on heat fluxes.

Precipitation, especially under convective conditions, is known to have high spatial variability. Conventionally, measurements are made at points using rain gauges. One of the most common methods of estimating areal precipitation from gauge observations is the Thiessen method, which assigns any location in the area of interest, the rainfall at the closest gauge. Radar measurements of rainfall provide the spatial distribution of precipitation, which is an important advantage compared to point observations. In this section, a simple resampling of the radar images was performed to assess the implications of using precipitation gauge data in lieu of the radar precipitation products.

The previous analyses in this section were done with precipitation information obtained from radar measurements. In this section, the effect of spatial resolution of precipitation on surface heat fluxes will be investigated. DHSVM was run for the same period and with the same initial conditions as reported earlier in this chapter, but with a precipitation field based on Thiessen

polygons of the radar estimates at the location of the precipitation gauges. That is, Thiessen-polygons for the SMSA were formed by using the value from the radar images corresponding to the locations of precipitation gauges in, or close to, the SMSA (Figure 3.3). The area was hence divided as shown in Figure 5.9.

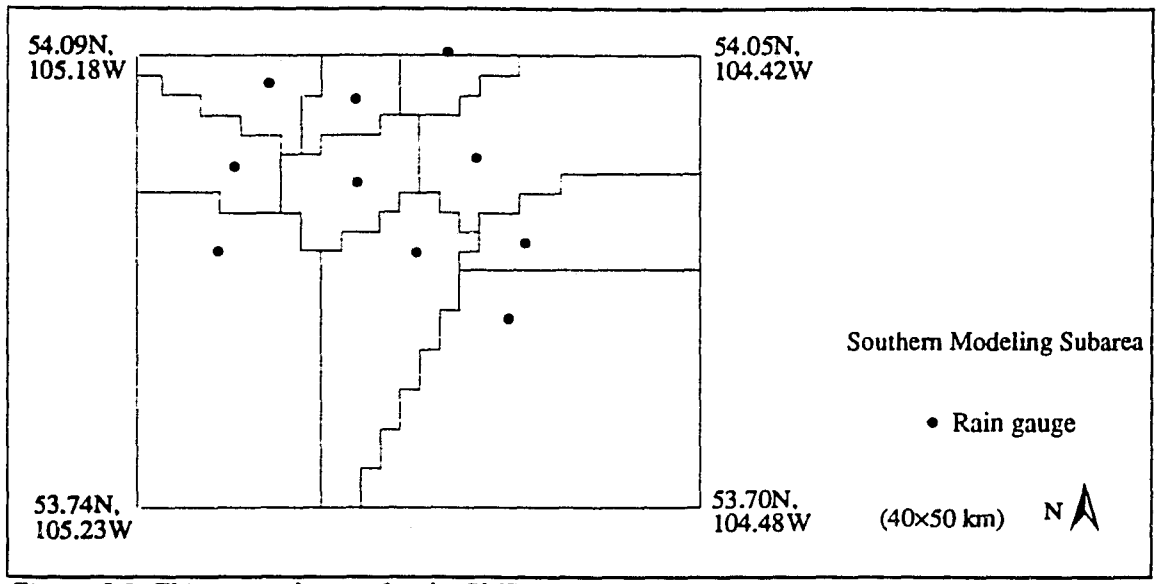

Figure 5.9: Thiessen polygons for the SMSA.

The total differences in seasonal precipitation, evapotranspiration and runoff resulting from the two methods were 380 vs. 387 mm of precipitation, 269 vs. 271 mm evapotranspiration and 97.5 mm vs. 102 mm runoff, for the radar images and the Thiessen polygons, respectively. This indicates that aggregated values of water balance components were quite similar. However, time series of spatially averaged latent and sensible heat, for example, show that even if the total differences were small, substantial differences occurred for shorter periods, as shown in Figure 5.10 for the OBS site. The figure shows that the difference in heat fluxes, caused by different precipitation patterns, could be over 50 W/m^2, which is quite substantial considering the absolute mid day heat flux on average was around 200 W/m^2. The deviations coincide with different amounts of precipitation. Higher amounts of precipitation are followed by higher latent heat fluxes from the vegetation (primarily due to direct evaporation of canopy interception), which results in lower sensible heat flux.

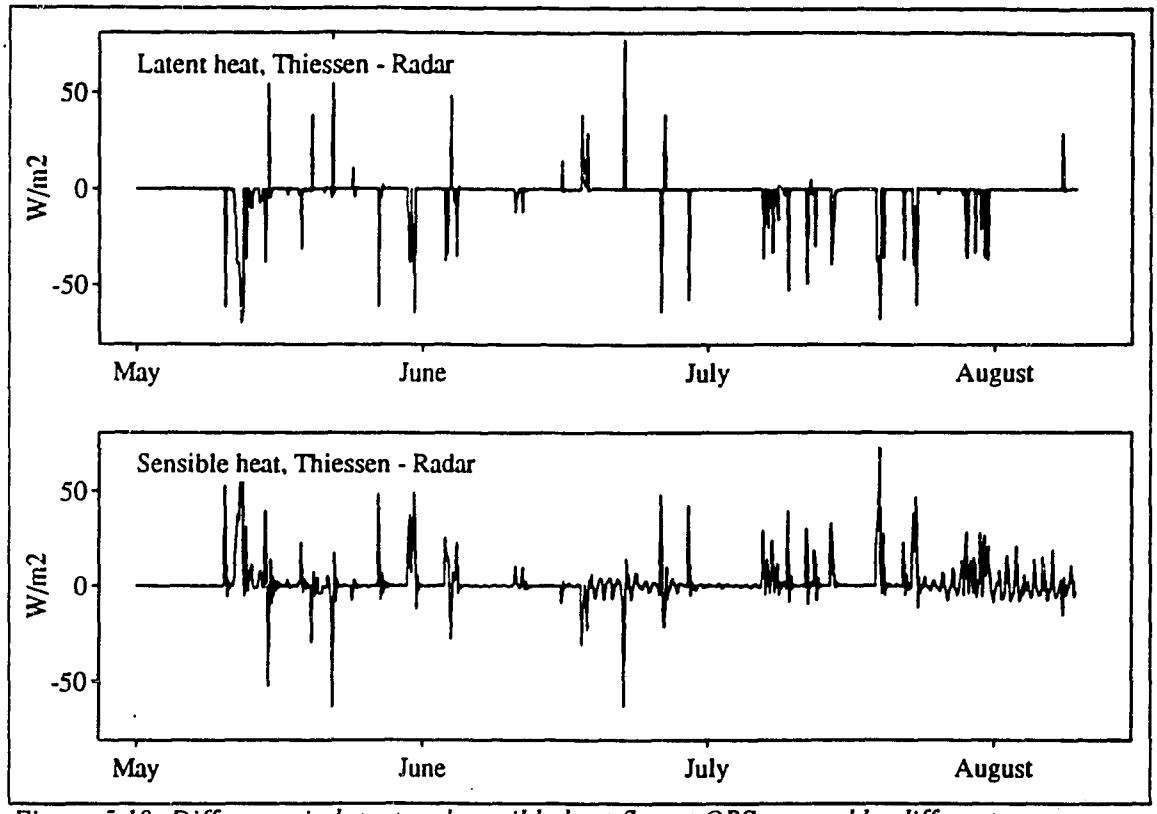

Figure 5.10: Difference in latent and sensible heat flux at OBS, caused by different precipitation fields.

More importantly, significant spatial differences in the latent and sensible heat fluxes occurred. Figure 5.11 shows an example of the spatial distribution of latent heat flux by use of the radar image and the Thiessen image. The images represent a time step when a rain storm occurred (June 6), and the latent heat flux from the vegetation is higher in areas with rainfall than areas without rainfall.

In Figure 5.11, it is not only the precipitation field that is apparent, but also vegetation type interacts strongly with wet and dry areas. The lakes, which in DHSVM always evaporate at potential rate, have lower latent heat flux than many vegetated areas have. The vegetation type's differences in leaf area index can also clearly be seen, - the higher LAI, the higher latent heat flux during this rainstorm.

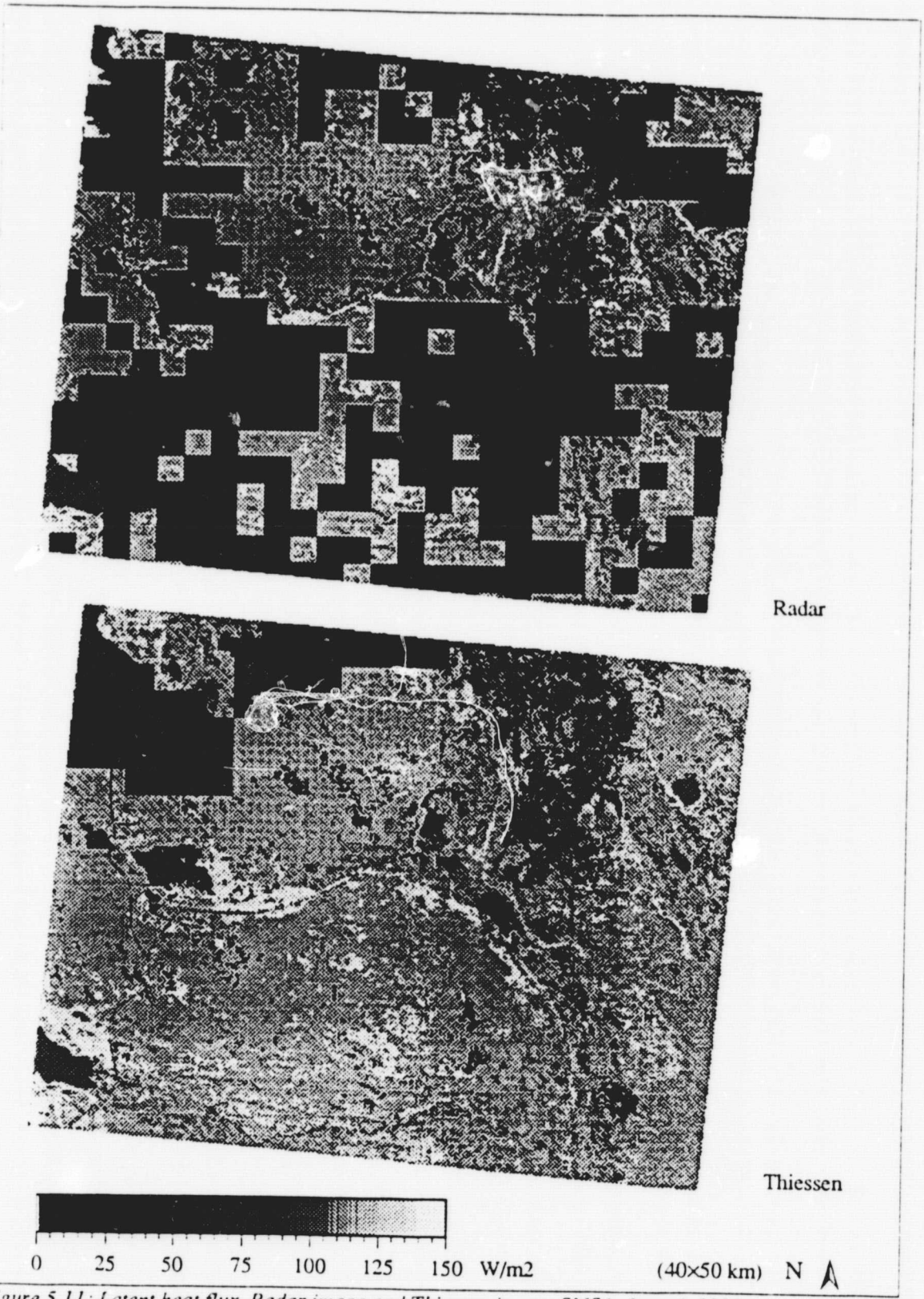

Figure 5.11: Latent heat flux. Radar image and Thiessen image. SMSA, June 6, 1994.

5.3 CONCLUSION.

DHSVM was successfully implemented, and predicted the amount of runoff for the SMSA about right on a seasonal basis. However, the predicted shape of the hydrograph had great errors for many storm events. The model predicted the timing of the peaks about right, but peak flow was higher than observed, while baseflow was much lower. Old Black Spruce, Aspen and Fen soil moisture trends were as expected, while the soil moisture at Old Jack Pine and Young Jack Pine increased during the summer, contrary to expectation. The modeled latent heat flux at Old Jack Pine was higher than observed, which might be related to the wet soil conditions or too high evaporation following precipitation events. It was also seen that vegetation type and location, in addition to the precipitation field, had a great influence on surface heat fluxes.

CHAPTER 6: CONCLUSIONS.

6.1 SUMMARY.

Preliminary hydrologic modeling of boreal ecosystems under different climatic conditions was performed, using a modified version of the distributed hydrology-soil-vegetation model (DHSVM) of Wigmosta et al. [1994]. The model was applied to two locations in the northern and southern extreme of the Canadian boreal forest; near Thompson, Manitoba, and just north of Prince Albert, Saskatchewan. The study focused on energy and moisture fluxes for different types of vegetation, contrasts between the two areas, and on spatial variability in moisture and heat fluxes within the southern area during summer 1994.

An initial analysis was made of DHSVM's formulation of aerodynamic resistances. Some of the assumptions were found to be unrealistic, in particular the way understory resistance with overstory cover was calculated, and the assumption of linear dependence of wind speed on fraction of overstory cover. The formulation was therefore changed in two ways: 1) The exponential part of the wind profile was specified to merge into the lower logarithmic wind profile above the understory, as opposed to within the understory as specified by Wigmosta et al. [1994], and 2) The assumption of linear dependence of wind on fraction of overstory cover was removed; instead the canopy attenuation coefficient and roughness characteristics should be used to account for forest density.

The role of moss in the hydrologic cycle was investigated through both field observations and modeling. Observations showed that a significant amount of the precipitation that reaches the forest floor is lost through evapotranspiration from the moss. Through sensitivity analyses, the moss was found to be an important component in the hydrologic cycle, and the root distribution in the moss and mineral soil influences the resulting heat fluxes noticeably. The simple modification to DHSVM, which incorporated a moss layer, performed fairly well, but the predicted latent heat fluxes were too high compared to measured values.

Through point and spatially distributed modeling, relations between water use and vegetation were studied; within a limited area, and between two locations in the boreal region. Both vegetation type and climate were found to have significantly effect on moisture and heat fluxes,

along with the spatial resolution of precipitation. There was a tendency for predicted evapotranspiration to be unrealistic. In DHSVM, soil moisture is the main limitation for evapotranspiration, while observations show that evaporative fraction is fairly low even when soil moisture is high. Whether soil temperature or other biophysical parameters (e.g. nutrient limitation) should limit transpiration, or the predicted evaporation is too high, remains to be resolved.

6.2 CONCLUSIONS.

The main conclusions of the research are:

1) The aerodynamic resistance is sensitive to roughness characteristics and the assumed shape of the wind profile. The previous DHSVM assumption of the shape of the vertical wind profile within forests was found to give unrealistic aerodynamic resistances for understory, compared to the aerodynamic resistance in open areas. The inconsistency of lower aerodynamic resistance under the forest canopy than in open areas was eliminated by assuming that the lower logarithmic wind profile within forests matches the exponential wind profile above the understory, and not within the understory as originally assumed. The lower logarithmic wind profile is the dominant term in calculations of resistances under the canopy, and including this term in the formulation of understory resistance in DHSVM caused this variable to increase substantially. The removal of the assumption of linear dependence of wind on fraction of overstory cover, in favor of using the canopy attenuation coefficient and roughness characteristics to account for forest density, caused the overstory resistance to decrease. These two modifications resulted in increased understory resistance. Increased resistance resulted in decreased evaporation, but transpiration increased.

2) Field work and model sensitivity analyses using a simple modification of DHSVM that incorporated a moss layer showed that moss is an important factor in the hydrologic cycle. A significant amount of the spatial variable throughfall is lost through evapotranspiration from the moss. The resulting latent and sensible heat fluxes are sensitive to the presence or absence of a moss carpet, and also to the root distribution in the soil column. The modified version of DHSVM had some difficulties predicting the amount and relative contribution of latent heat

flux from understory, soil and overstory, which might be caused by incorrect input parameters or deficiencies in the model structure.

3) DHSVM can be calibrated to give reasonable results for runoff and evapotranspiration, but it is quite sensitive to some of the input parameters that were tested, e.g. leaf area index, hydraulic conductivity, stomatal conductance and aerodynamic resistance. Based on the results from the point modeling, it appears that the vegetation in the southern extreme of the boreal region is more limited by water than is the vegetation in the northern extreme. The modeling results also suggest that the timing of energy and moisture supply is important in predicting the vegetation response to climate. The modeled evapotranspiration, in the point analyses, was not sensitive to soil temperature. This was especially apparent in the dry, southern area, while soil temperature became a relatively more important factor under wet conditions.

4) The modified version of the distributed version of DHSVM used in this study, had some difficulties predicting runoff. Surface runoff was higher than observed total runoff, and the recession curve in the hydrograph was more or less absent. On the other hand, the fraction of saturated areas was less than expected. It was speculated that these results might be caused by the fact that surface flow should have been allowed to interact with the soil, i.e. reinfiltrate, if flowing over unsaturated areas on its way to the outlet.

5) The predicted net radiation in the winter season was less negative in the forest than in open areas, which resulted in higher sensible heat flux (to the snow pack) in open areas. The snow temperature was nevertheless coldest in the forest, because of the high aerodynamic resistance under the forest canopy. Consequently, the snow in the open area became isothermal earlier in the spring than the snow under the canopy did, and therefore became free of snow first, even though the snow cover was thickest in open areas.

6) The predicted latent heat fluxes in general were too high compared to measured values, both in the moss analysis and in the spatially distributed analysis. Several factors might have contributed to this result, but it is not known which one was most important. Is soil temperature limitation not dominant enough in the model assumptions, are some of the input parameters (e.g. LAI) incorrect, should some other model assumptions be modified, or would the latent

heat flux decrease if DHSVM incorporated other biophysical limitations, e.g. nutrient limitation, in the formulation of transpiration?

7) The modeling results give some ideas about what might happen if climate warming occurs. Higher temperatures would result in less snowfall and a shorter snow season, which would increase the active season for evapotranspiration. In addition, the soil temperatures would increase. Assuming the present amount of precipitation, this would probably result in higher annual evapotranspiration, and hence less runoff, especially in the northern extreme of the boreal forest. However, there are still many questions to be answered, and analyses to be done before a full dynamic modeling of coupled hydrology-soil-vegetation with the purpose of predicting vegetation response to climate change can be successful.

6.3 RECOMMENDATIONS FOR FURTHER RESEARCH.

1) DHSVM uses a composite of exponential and logarithmic equations to represent the vertical wind profile within and above the canopy. Whether the suggested formulation for calculating aerodynamic resistance is physically correct or not, is unknown. Some insight might be gained by comparing the aerodynamic resistances calculated by DHSVM to estimates from other SVATS schemes (soil-vegetation-atmosphere transfer scheme). For instance, comparison with the scheme used by SiB [Sellers et al., 1986] which has a similar assumption of wind profiles within the canopy, would be useful. What is really needed, though, are comparisons to field observations, some of which will become available as the 1994 BOREAS observation data are processed.

2) The rain gauges at Thompson Airport and Prince Albert Airport are unshielded, which almost certainly accounts for measurement deficiencies. The SRC-stations at OJP both in the NMSA and SMSA have shielded rain gauges in forest clearings. A comparison of measured precipitation at these gauges to what is measured at the unshielded gauges would give information about the magnitude of catchment errors in the unshielded gauges, which could be used to obtain more correct precipitation data.

3) Theoretical analyses (Section 4.3) and field work (Appendix 1) showed that moss, and the distribution of roots in the organic soil and the mineral soil, can have a significant influence on evaporation and transpiration. The field work only lasted for one month, and in addition an unfortunate thunderstorm resulted in loss of microclimate and surface flux data for about half the period. More data would be helpful in developing a physically realistic moss submodel, for example measurements of understory latent and sensible heat, stomatal conductance of both overstory and understory, distribution of overstory roots in the soil column and more accurate soil characteristics.

4) The soils in the boreal region can be frozen well into the summer. The original version of DHSVM does not account for frozen soils, and flow of water in the saturated zone occurs unobstructed even if the soil temperature is below the freezing point. In this study, no baseflow was allowed when the temperature at damping depth dropped below 0°C, and this scheme of modeling water movement in cold periods can be improved. The way infiltration and percolation of water is calculated under these circumstances should be considered changed as well. In addition, it would be helpful to get improved estimates of soil temperatures and a better understanding of how this parameter interacts with other parameters, e.g. soil moisture in limitation of water uptake by roots in the boreal forests.

5) The SMSA is fairly flat, with an elevation range of only 224 m over an area of 2000 km^2. As a consequence, the digital elevation model has large areas with the same elevation, and this results in slow subsurface flow. The catchments delineated from the DEM did not correspond to the observed catchment boundaries, which might be caused by the fact that the scheme which is used to determine drainage areas has to make a decision of where the water flows, when, according to the elevations given in the DEM, it could flow in several directions. The direction in which the water flows can be crucial in the calculations of energy and moisture fluxes for smaller areas, and it would be useful to get the flow directions about right in DHSVM. One solution might be to impose the streams in the DEM, and force the water to follow these paths.

6) The spatially distributed modeling showed that subsurface flow out of DHSVM was extremely insensitive to precipitation, even following heavy rainstorms. Consequently, the recession curve in the hydrograph, which is quite evident in streamflow measurements, was essentially absent. This might result in part because the modeled area was not a watershed, or

due to resolution problems in the DEM, but it is more likely evidence of a structural deficiency in the model. Should the response of the surface runoff be slower, or should the baseflow respond more to precipitation? DHSVM at present models surface and subsurface flow in the saturated zone under the root zones. In areas that are as wet as the SMSA was in the summer 1994, it might be necessary consider lateral flow in the saturated part of the root zones. In flat, forested areas, the pattern of the surface flow should also be considered. How much of the water emerging at the surface actually drains off directly, how much is stored in surface depressions, and how much of it reinfiltrates into the soil? In this study, DHSVM predicts that most of the discharge occurred as surface runoff; the observed hydrograph suggest that the subsurface component is much larger than in the model.

LIST OF REFERENCES

AES Environment Canada: *Modelling the global climate system*, Minister of supply and services, Canada, 1994.

Arkley, R.J.: Climates of some great soil groups of the western United States, *Soil Science*, 103 (1967) 389-400.

Arola, A.: *Effects of subgrid scale spatial variability on mesoscale snow modeling*. M.S.C.E Thesis, University of Washington, Seattle, 81 p, 1993.

Billings, W.D., Luken, J.O., Mortensen, D.A., Peterson, K.M.: Arctic tundra: a source or sink for atmospheric carbon dioxide in a changing environment?, *Oecologia*, 53 (1982) 7-11.

Billings, W.D., Luken, J.O., Mortensen, D.A., Peterson, K.M.: Increasing atmospheric carbon dioxide: possible effects on arctic tundra. *Oecologia*, 58 (1983) 286-289.

Black, R.A., Bliss, L.C.: Reproductive ecology of Picea Mariana (Mill.) BSP at tree line near Inuvik, Northwestern Territories, Canada, *Ecological Monographs*, 50 (1980) 331-354.

Bonan, G.B., Shugart, H.H.: Environmental factors and ecological processes in boreal forests, *Annual Review of Ecology and Systematics*, 20 (1989) 1-28.

Bonan, G.B., Pollard, D., Thompson, S.L.: Effects of boreal forest vegetation on global climate, *Nature*, 359 (1992) 716-718.

Bonan, G.B., Sirois, L.: Air temperature, tree growth and the northern and southern range limits to Picea mariana, *Journal of Vegetation Science*, 3 (1992) 495-506.

BOREAS Experiment Plan, version 3.0, NASA/Goddard Space Flight Center, Greenbelt, 1994.

BOREAS Science Team: Early results from the Boreal Ecosystem-Atmosphere Study (BOREAS), *Bulletin of American Meteorological Society*, 1995 (in press).

Brown, R.T.P., Mikola, P.: The influence of fruticose soil lichens upon the mycorr nizae and seedling growth of forest trees, *Acta Forestalia Fennica*, 141 (1974) 1-22.

Bruin, H.A.R. de, Moore, C.J.: Zero plane displacement and roughness length for tall vegetation derived from a simple mass conservation hypothesis, *Boundary-Layer Meteorology*, 31 (1985) 39-49.

Bryson, R.A.: Air masses, streamlines, and the boreal forest, *Geographical Bulletin*, 8 (1966) 228-269.

Busby, J.R., Bliss, L.C., Hamilton, C.D.: Microclimate control of growth rates and habitats of the boreal forest mosses, Tomenthypnum nitens and Hylocomium splendens, *Ecological Monographs*, 48 (1978) 95-110.

Businger, J.A.: Aerodynamics of vegetated surfaces. In D. A. de Vries and N. H. Afgan (eds): *"Heat and mass transfer in the biosphere"*, Wiley, New York, 1975.

Calder, I.R., Wright, I.R.: Gamma ray attenuation studies of interception from Sitka spruce: some evidence for an additional transport mechanism, *Water Resources Research*, 22 (1986) 409-417.

Campbell, G.S.: *An introduction to environmental biophysics*, Springer-Verlag, New York, 159 p, 1977.

Chabot, B.F., Hicks, D.J.: The ecology of leaf life spans, *Annual Review of Ecology and Systematics*, 13 (1982) 229-259.

Clapp, R.B., Hornberger, G.M.: Empirical equations for some soil hydraulic properties, *Water Resources Research*, 14 (1978) 601-604.

Coughlan, J.: NASA Ames Research Center, Moffett Field, personal communication, 1994.

Cox, C.B., Moore, P.D.: *Biogeography: an ecological and evolutionary approach*, 5th ed., Blackwell Scientific Publications, Boston, 326 p, 1993.

Critchfield, H.: *General climatology*, 4th ed., Prentice-Hall, Englewood Cliffs, 453 p, 1983.

Crum, H.: *Mosses of the Great Lakes Forest*, University Herbarium, University of Michigan, Ann Arbor, 404 p, 1976.

D'Arrigo, R., Jacoby, G.C., Fung, I.Y.: Boreal forests and atmosphere-biosphere exchange of carbon dioxide, *Nature*, 329 (1987) 321-323.

Davis, M.B.: Quaternary history and the stability of forest communities. In D.C West, H.H Shugart, and D.B. Botkin (eds.): *"Forest succession: concepts and application"*, Springer-Verlag, New York, 517 p, 1981.

Dickinson, R.E., Henderson-Sellers, A., Kennedy, P.J., Wilson, M.F.: Biosphere-atmosphere transfer scheme (BATS) for the NCAR Community Climate Model, *Tech. Note NCAR/TN-275+STR*, Natl. Cent. for Atm. Res., Boulder, Colorado, 1986.

Dickinson, R.E., Henderson-Sellers, A., Rosenzweig, C., Sellers, P.J.: Evapotranspiration models with canopy resistance for use in climate models, A review, *Agricultural and Forest Meteorology*, 54 (1991) 373-388.

Dolgin, I.M.: *Ecology and conservation, 1*, Unesco, Paris, pp 41-61, 1970.

Dooge, J.C.I.: Hydrologic models and climate change, *Journal of Geophysical Research*, 97 (1992) 2677-2688.

Dubayah, R., Dozier, J., Davis, F.W.: Topographic distribution of clear-sky radiation over the Konza prairie, Kansa, *Water Resources Research*, 20 (1990) 679-690.

Dunham, K.: Department of Geography, University of Toronto, personal communication, 1994.

Eley, J.: Canada Atmospheric Environment Service, Saskatoon, personal communication, 1994.

Emanuel, W.R., Shugart, H.H., Stevenson, M.P.: Climate change and the broad-scale distribution of terrestrial ecosystem complexes, *Climatic Change*, 7 (1985) 29-43.

French, H.M., Slaymaker, O.: Canada's cold land mass. In H.M. French, O. Slaymaker (eds.):*Canada's cold environments*, McGill-Queen's University Press, Montreal, 340 p, 1993a.

French, H.M., Slaymaker, O.: The changing cold environments. In H.M. French, O. Slaymaker (eds.): *Canada's cold environments*, McGill-Queen's University Press, Montreal, 340 p, 1993b.

Frew, J.E.: *The image processing workbench*, Ph.D. thesis, Dept. of Geography, University of California, Santa Barbara, 306 p, 1990.

Gates, D.M.: *Climate change and its biological consequences*, Sinaues Associates, Sunderland, 280 p, 1993.

George, M.F., Burke, M.J., Pellett, H.M., Johnson, A.G.: Low temperature exotherms and woody plant distribution, *HortScience*, 9 (1974) 519-522.

Grace, J.: *Plant-atmosphere relationships*, Chapman and Hall, New York, 92 p, 1983.

Graetz, R.D.: The nature and significance of the feedback of changes in terrestrial vegetation on global atmospheric and climatic change, *Climatic Change*, 18 (1991) 147-173

Hare, F.K.: Climate and zonal divisions of the boreal forest formation in eastern Canada, *Geographical Review*, 40 (1950) 615-635.

Hare, F.K., Ritchie, J.C.: The boreal bioclimates, *Geographical Review*, 62 (1972) 333-365.

Hay, J.E.: Aspects of heat and moisture balance in Canada. Ph.D. thesis, University of London, 1969.

Heitor, A., Biga, A.J., Rosa, R.: Thermal radiation components of the energy balance at the ground, *Agricultural and Forest Meteorology*, 54 (1991) 29-48.

Hendrie, L.K., Price, A.G.: Energy balance and snowmelt in a leafless deciduous forest. In *Proceeding of the Perch Lake Study Symposium/Workshop*, AECL-6404, At. Energ. of Can. Ltd., Chalk River, Ont., 1978.

Hopkins, D.M.: Some characteristics of the climate in forest and tundra regions in Alaska, *Arctic*, 12 (1959) 215-220.

Houghton, J.T., Jenkins, G.J., Ephraums, J.J. (eds.): *Climate change: the IPCC scientific assessment*, Cambridge University Press, Cmabridge, 364 p, 1990.

Hunt, E.R. Jr., Running, S.W., Federer, C.A.: Extrapolating plant water flow resistances and capicitances to regional scales, *Agricultural and Forest Meteorology*, 54 (1991) 169-195.

Idso, S.B.: *Carbon dioxide and global change: earth in transition*, IBR Press, Tempe, 292 p, 1989.

Jones, H.G.: *Plants and microclimate: a quantitative approach to environmental plant physiology*, 2nd ed., Cambridge University Press, Cambridge, 428 p, 1992.

Jäger, J.: *Developing policies for responding to climatic change*, World Meteorological Organization : United Nations Environment Programme, Geneva, 53 p, 1988.

Kauppi, P., Posch, M.: Sensitivity of boreal forest to possible climatic warming, *Climatic Change*, 7 (1985) 45-54.

King, G.A., Neilson, R.P.: The transient response of vegetation to climate change: a potential source of CO_2 to the atmosphere, *Water, Air and Soil Pollution*, 64 (1992) 365-383.

Krauss, T., Eley, J., Soulis, E.D., Kuowen, N., Nijssen, B., Schnur, R., Lettenmaier, D.P.: Evaluation of radar precipitation measurements during the 1994 BOREAS Field Campaigns, *EOS*, 75 (44) (1994) 298.

Larsen, J.A.: *The boreal ecosystem*, Academic Press, New York, 500 p, 1980.

Larsen, L.W., Peck, E.L.: Accuracy of precipitation measurements for hydrologic modeling, *Water Resources Research*, 10 (1974) 857-863.

Lindroth, A.: Aerodynamic and canopy resistance of short-rotation forest in relation to leaf area index and climate, *Boundary-Layer Meteorology*, 66 (1993) 265-279.

Linsley, R.K., Kohler, M.A., Paulhus, J.L.H.: *Hydrology for engineers*, 3rd ed., Mc Graw-Hill, 508 p, 1982.

Longley, K., Jacobsen, D., Marks, D.: *Supplement to the image processing workbench (IPW)*, U.S. Environ. Protect. Agency, Corvallis, Oregon, 1992.

Maidment, D.R., Olivera, J.F., Calver, A., Eatherall, A., Fraczek, W.: A unit hydrograph derived from a spatially distributed velocity field, *Hydrologic Processes*, 1995 (in press).

Male, D.H., Granger, R.J (1981): Snow surface energy exchange, *Water Resources Research*, 17 (1981) 6009-6027.

Manabe, S., Stouffer, R.J.: Sensitivity of a global climate model to an increase of CO_2 concentration in the atmosphere, *Journal of Geophysical Research*, 85 (1980) 5529-5554.

Mascart, P., Taconet, O., Pinty, J.P., Mehrez, M.B.: Canopy resistance formulation and its effect in mesoscale models: a HAPEX perspective, *Agricultural and Forest Meteorology*, 54 (1991) 319-351.

Meentemeyer, V.: Macroclimate and lignin control of decomposition rates, *Ecology*, 59 (1978)465-472.

Monin, A.S., Yaglom, A.M.: *Statistical fluid mechanics: mechanics of turbulence, Vol. I*, MIT Press, Cambridge, 1971.

Monk, C.D.: An ecological significance of evergreenness, *Ecology*, 47 (1966) 504-505.

Monserud, R.A., Tchebakova, N.M., Leemans, R.: Global vegetation changes predicted by the modified Budyko model, *Climatic Change*, 25 (1993) 59-83.

Monteith, J.L.: *Principles of environmental physics*, American Elsevier Pub. Co., New York, 241 p, 1973.

Monteith, J.L.: *Vegetation and the atmosphere, vol I and II*, Academic Press, New York, 1975-1976.

Monteith, J.L., Unsworth, M.H.: *Principles of environmental physics*, 2nd ed., Edward Arnold, New York, 291 p, 1990.

The National Atlas of Canada, 4th ed., The Macmillan Company of Canada, Ottawa, 254 p, 1974.

Neilson, R.P., Marks, D.: A global perspective of regional vegetation and hydrologic sensitivities from climatic change, *Journal of Vegetation Science*, 5 (1994) 715-730.

Neff, T: Department of Civil Engineering, University of Waterloo, Waterloo, personal comminication, 1995.

Oechel, W.C., Lawrence, W.T.: Taiga. In B.F. Chabot, H.A. Mooney (eds.): *Physiological ecology of North American plant communities*, Chapman and Hall, New York, 351 p, 1985.

Örlander, G., Gemmel, P., Hunt, J.: *Site preparation: a Swedish overview*, Forestry Canada, Victoria, 62 p, 1990.

Orvig, S: Climates of the polar regions, vol 14. In H.E. Landsberg (ed.): *World survey of climatology*, Elsevier Publishing, New York, 1970.

Pastor, J., Post, W.M.: Response of northern forests to CO_2-induced climate change, *Nature*, 334 (1988) 55-58.

Prentice, K.C.: Bioclimatic distribution of vegetation for General Circulation Model studies, *Journal of Geophysical Research*, 95 (1990) 11811-11830.

Prentice, K.C., Fung, I.Y.: Bioclimate simulations test the sensitivity of terrestrial C storage to perturbed climates, *Nature*, 346 (1990) 48-51.

Pruitt, W.O. Jr.: *Boreal ecology*, Edward Arnold, London, 73 p, 1978.

Rawls W.J., Ahuja, L.R., Brakensiek, D.L., Shirmohammadi, A.: Infiltration and soil water movement. In D.R. Maidment (ed.): *Handbook of hydrology*, McGraw Hill, New York, 1350 p, 1993.

Rizzo, B., Wiken, E.: Assessing the sensitivity of Canada's ecosystems to climatic change, *Climatic Change*, 21 (1992) 37-55.

Rogers, H.H., Thomas, J.F., Bingham, G.E.: Response of agronomic and forest species to elevated atmospheric carbon dioxide, *Science*, 220 (1983) 428-429.

Rouse, W.R.: Northern climates. In H.M. French, O. Slaymaker, (eds.): *Canada's cold environments*, McGill-Queen's University Press, 1993.

Rowe, J.S.: *Forest regions of Canada*, Information Canada, Ottawa, 172 p, 1977.

Rowntree, P.R.: Review of General Circulation Models as a basis for predicting the effects of vegetation change on climate. In E.R.C. Reynolds and F.B. Thompson: *Forests, climate and hydrology: regional impacts*, United Nations University, Tokyo, 217 p, 1988.

Sakai, A., Weiser, C.J.: Freezing resistance of trees in North America with reference to tree regions, *Ecology*, 54 (1973) 118-126.

Sargent, N.E.: Redistribution of the Canadian boreal forest under a warmed climate, *Climatological Bulletin*, 22 (3) (1988) 23-34.

Sellers, P.J., Shuttleworth, J.W., Dorman, J.L., Dalcher, A., Roberts, J.M.: Calibrating the Simple Biosphere model (SiB) for Amazonian tropical forest using field and remote sensing data, *Journal of Applied Meteorology*, 28 (1989) 727-759.

Shaw, R.H., Pereira, A.R.: Aerodynamic roughness of a plant community: a numerical experiment, *Agricultural Meteorology*, 26 (1982) 51-65.

Shuttleworth, W.J.: Evaporation. In D.R. Maidment (ed.): *Handbook in hydrology*, McGraw Hill, New York, 1350 p, 1993.

Shuttleworth, W.J., Wallace, J.S.: Evaporation from sparse crops - an energy combination theory, *Quarterly Journal of the Royal Meteorological Society*, 111 (1985) 839-855.

Sirois, L.: The transition between boreal forest and tundra. In H.H. Shugart, R. Leemans and G.B. Bonan (eds.): *A systems analysis of the global boreal forest*, Cambridge University Press, Cambridge, 565 p, 1992.

Skre, O.: The regional distribution of vascular plants in Scandinavia with requirements for high summer temperatures, *Norwegian Journal of Botany*, 26 (1979) 295-318.

Skre, O., Oechel, W.C.: Moss functioning in different taiga ecosystems in interior Alaska, *Oecologia* 48 (1981) 50-59.

Smith, T.M., Shugart, H.H., Bonan, G.B, Smith, J.B.: Modeling the potential response of vegetation to global climate change, *Advances in Ecological Research*, 22 (1991) 93-116.

Stathers, R.J., Spittlehouse, D.L.: *Forest soil temperature manual*, Canada/BC Economic & Regional Development Agrrement, 47 p, 1990.

Stephenson, N.L.: Climate control of vegetation distribution: the role of the water balance, *The American Naturalist*, 135 (1990) 649-670.

Strong, W.L., La Roi, G.H.: Rooting depths and successional development of selected boreal forest communities, *Canadian Journal of Forest Research*, 13 (1983) 577-588.

Tessmer, D.: Canada Atmospheric Environment Service, Saskatoon, personal communication, 1994.

Tivy, J.: *Biogeography: a study of plants in the ecosphere*, 3rd ed., J. Miley, New York, 452 p, 1993.

Tryon, P.R., Chapin, F.S.III: Temperature control over root growth and root biomass in taiga forest trees, *Canadian Journal of Forest Research*, 13 (1983) 827-833.

Vertessy, R.A., Hatton, T.J., O'Shaughnessy, P.J., Jayasuriya, M.D.A.: Predicting water yield from a mountain ash forest catchment using a terrain analysis based catchment model, *Water Resources Research*, 150 (1993) 665-700.

Viereck, L.A.: *Forest ecology of the Alaska taiga*, Proc. Circumpolar Conf. North Ecol., Ottawa, 1975.

Vowinckel, T., Oechel, W.C., Boll, W.G.: The effect of climate on the photosynthesis of Picea Mariana at the subarctic tree line. 1. Field measurements, *Canadian Journal of Botany*, 53 (1975) 604-620.

Walter, H.: *Vegetation of the earth and ecological systems of the geobiosphere*, 2nd ed., Springer-Verlag, New York, 274 p, 1979.

Watts, W.A: The late quaternary vegetation history of the southeastern United States. *AnnualReview of Ecology and Systematics*, 11 (1980) 387-409.

Weetman, G.: The relationship between feathermoss growth and the nutrition of black spruce. In: *Proceedings of the Third International Peat Conference*, 1968.

Wigley, T.M.L., Raper, S.C.B.: Thermal expansion of sea water associated with global warming, *Nature*, 330 (1987) 127-131.

Wigmosta, M., Vail, L.W., Lettenmaier, D.P.: A distributed hydrology-vegetation model for complex terrain, *Water Resources Research*, 30 (1994) 1665-1679.

Woodward, F.I.: *Climate and plant distribution*, Cambridge University Press, Cambridge, 174 p, 1987.

Wyman, R.L. (ed.): *Global climate change and life on earth*, Routledge, Chapman and Hall, New York, 282 p, 1991.

Zoumakis, N.M.: Estimating the zero-plane displacement and roughness length for tall vegetation and forest canopies using semi-empirical wind profiles, *Journal of Applied Meteorology*, 32 (1993) 574-579.

Zoumakis, N.M.: Determination of the mean wind speed and momentum diffusivity profiles above tall vegetation and forest canopies using a mass conservation assumption, *Journal of Applied Meteorology*, 33 (1994) 295-303.

Page intentionally left blank

APPENDIX 1: MOSS, FIELD WORK.

Background.

Where mosses cover the ground, they are thought to exert important controls on soil moisture and evapotranspiration from the forest canopy, especially for species such as Black Spruce which has much of its root structure in the moss. The purpose of the field work reported in this appendix was to collect preliminary data about water retention in moss. The work was carried out during August and September, 1994, at the OBS site in the NMSA (NOBS), where the understory is dominated by moss.

Pleurozium Schreberi.

The moss in the NOBS site is a common feather moss called Pleurozium Schreberi - Scherbers moss (Figure A1). Pleurozium Schreberi is a rather robust plant that grows in loose, light-green or yellowish mats. The branched stems grow straight from the base. The plants are 7-16 cm high with 20-43 mm long setae. Pleurozium Schreberi has no paraphyllia, and the stomata are small. It grows on humus, mineral soil and other substrata in dry, open woods and also in bogs or coniferous swamps. [Crum, 1976]. It is not able to translocate significant amounts of water from the soil, and is therefore dependent on water absorbed by leaves [Skre and Oechel, 1981]. In North America, Pleurozium Schreberi occurs mainly in boreal and subarctic regions [Busby et al., 1978].

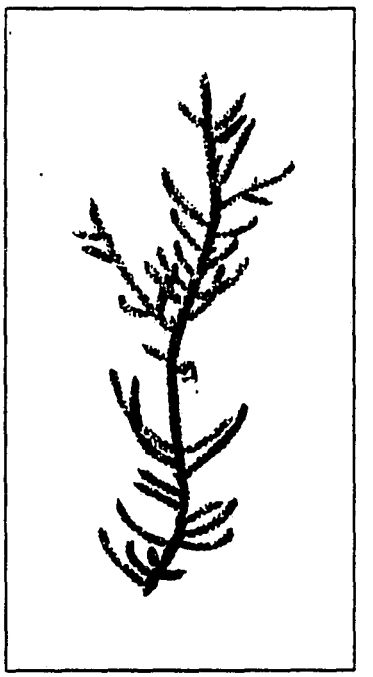

Figure A1: Pleurozium Schreberi.
Source: Crum [1976]

Method.

Two plots were selected, and 6 samples in three different thicknesses were cut at each plot by Kira Dunham of the Department of Geography, University of Toronto. The samples were about 20×20 cm wide. The L-samples, consisting of the living part of the moss, were about 10 cm thick, the LF-samples (living and fabric layers) were about 15 cm thick, and the LFH-samples (living, fabric and humic layers) were 25-29 cm thick. For each thickness, drainage was prevented from one of the samples at each plot by keeping the sample in a plastic bag. Because the LF and LFH-samples were tall and unstable, bottomless plastic bags were put around these samples to prevent loss of material. All the samples had a tray underneath them. Figure A2 illustrates the different samples.

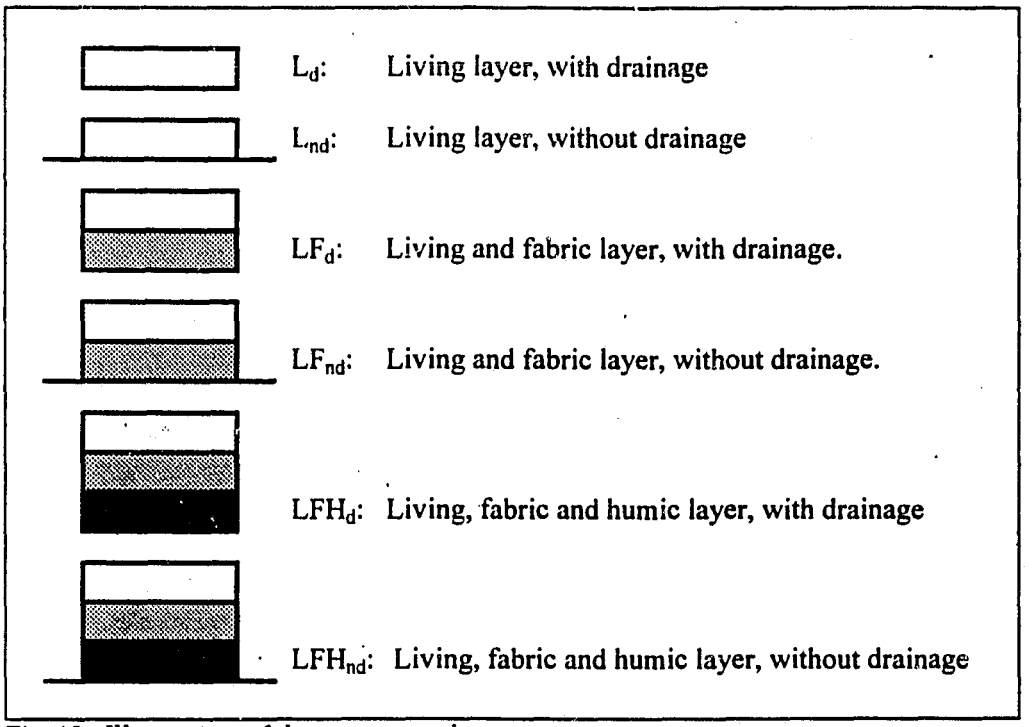

Fig A2: Illustration of the moss-samples.

To measure throughfall, garbage pails of diameter 49.5 cm were set out near the plots (5 locations each consisting of 3 garbage pails). Precipitation was measured in three pails in an open area close to the plots as well. Figure A3 shows the location of the plots, throughfall- and

precipitation pails. A tipping bucket precipitation gauge was located at the NOBS site, but unfortunately it did not function during the observation period.

The moss samples were weighed at 4 pm (local time) every day, from August 15 to September 15, 1994. In case of rainfall, the samples were weighed when it stopped raining, at which time the amount of water in the throughfall- and precipitation pails was measured as well. Richard Fernandes (Department of Geography, University of Toronto) did the field work from September 7 to September 15.

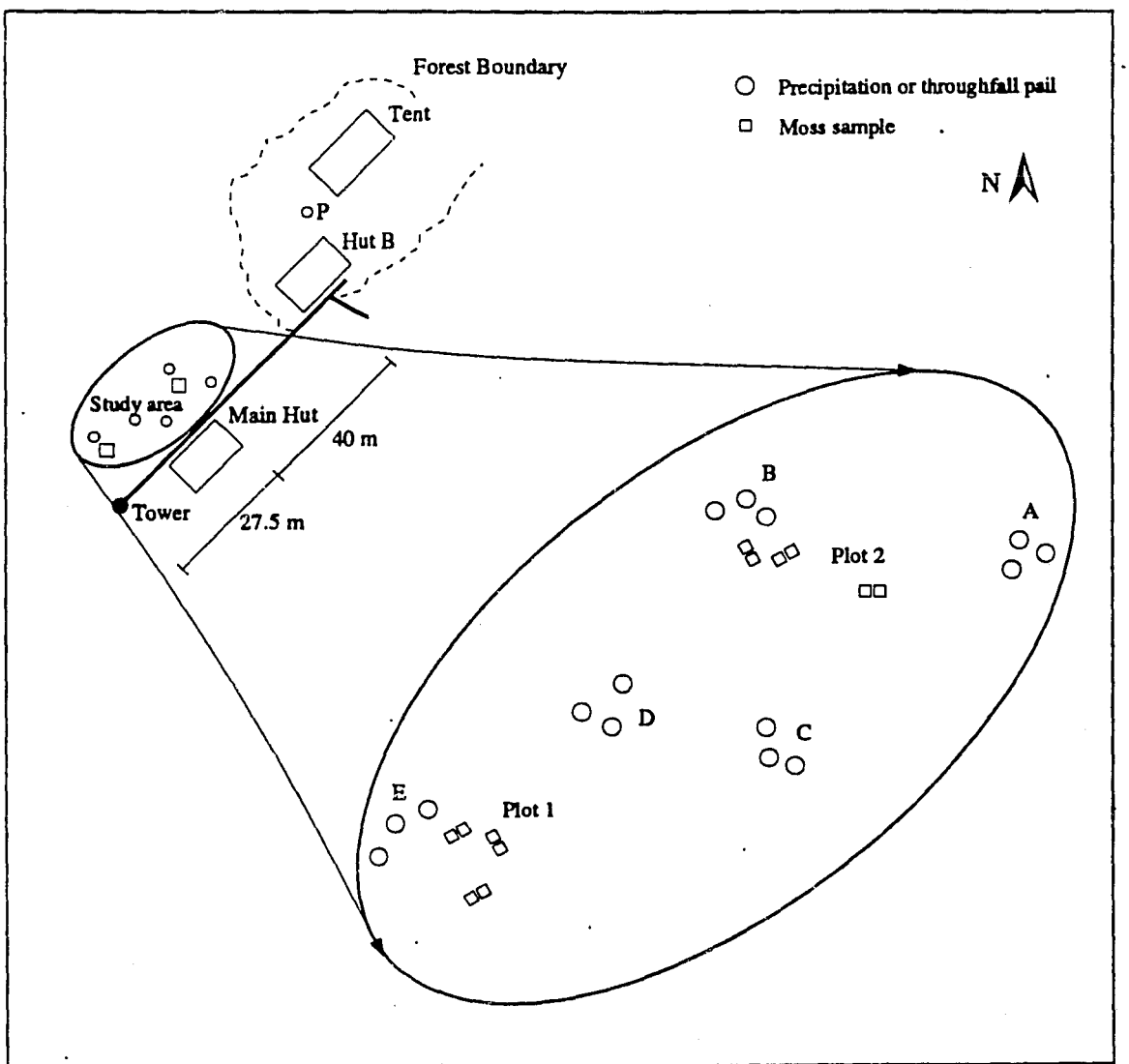

Figure A3: Location of the plots, throughfall- and precipitation pails.

Results and discussion.

Figure A4 shows how the weights of the moss changed, together with the amount of precipitation measured in the open area. Figure A5 shows moss weights relative to initial weight of the samples. The exact values of moss weights, throughfall and precipitation can be found in Tables A1-A4. The numbers represent net weights, i.e. the weight of tray and bag was subtracted from the measured weights.

During the period of observation, there were five significant rainfall events, at approximately one week intervals. Generally, the three different strata (L, LF, LFH) show the same pattern in the dry-down periods, - the samples with drainage lose some more water than those without drainage. The difference in weight loss is larger the thicker the sample (LFH>LF>L). Relative to water uptake during the rainstorms, the L_{nd}-samples on average lost 85% of the amount of water the L_d samples lost, the LF_{nd}-samples lost 56% of what the LF_d-samples did, and the LFH_{nd}-samples lost 42% of what the LFH_d-samples lost, meaning that if the period of observation is representative, the moss would lose about half the amount of water absorbed through evapotranspiration, and half of it would be lost through drainage. The final difference in weight is also influenced by the variable amount of throughfall that reached each sample. The average ratio of throughfall to precipitation in the clearing during the field observation period was 76.4%, but varied from 0% to 141.2%, which indicates that the amount of precipitation that reached the ground had high spatial variability.

The weight loss experienced by the samples without drainage has to be caused by evaporation and transpiration. Because of prevention of drainage, the samples were wetter than they would have been in their natural environment. Assuming this difference is small, one can compare the weight loss of these samples to the latent heat calculated from measurements at the flux tower. Latent heat data from the Old Black Spruce site were obtained from the NOBS BOREAS tower captain Dr. Steve Wofsy, Department of Earth and Planetary Science, Harvard University, in time steps of approximately half an hour. The flux tower unfortunately was hit by lightning on August 15, and did not function during the first two weeks of the observation period. Figure A6 compares evapotranspiration from the moss-samples with no drainage to the evapotranspiration measured at the flux tower (calculated from latent heat flux), from the time the tower started operating again after the thunderstorm (September 1), and through September 13. The values

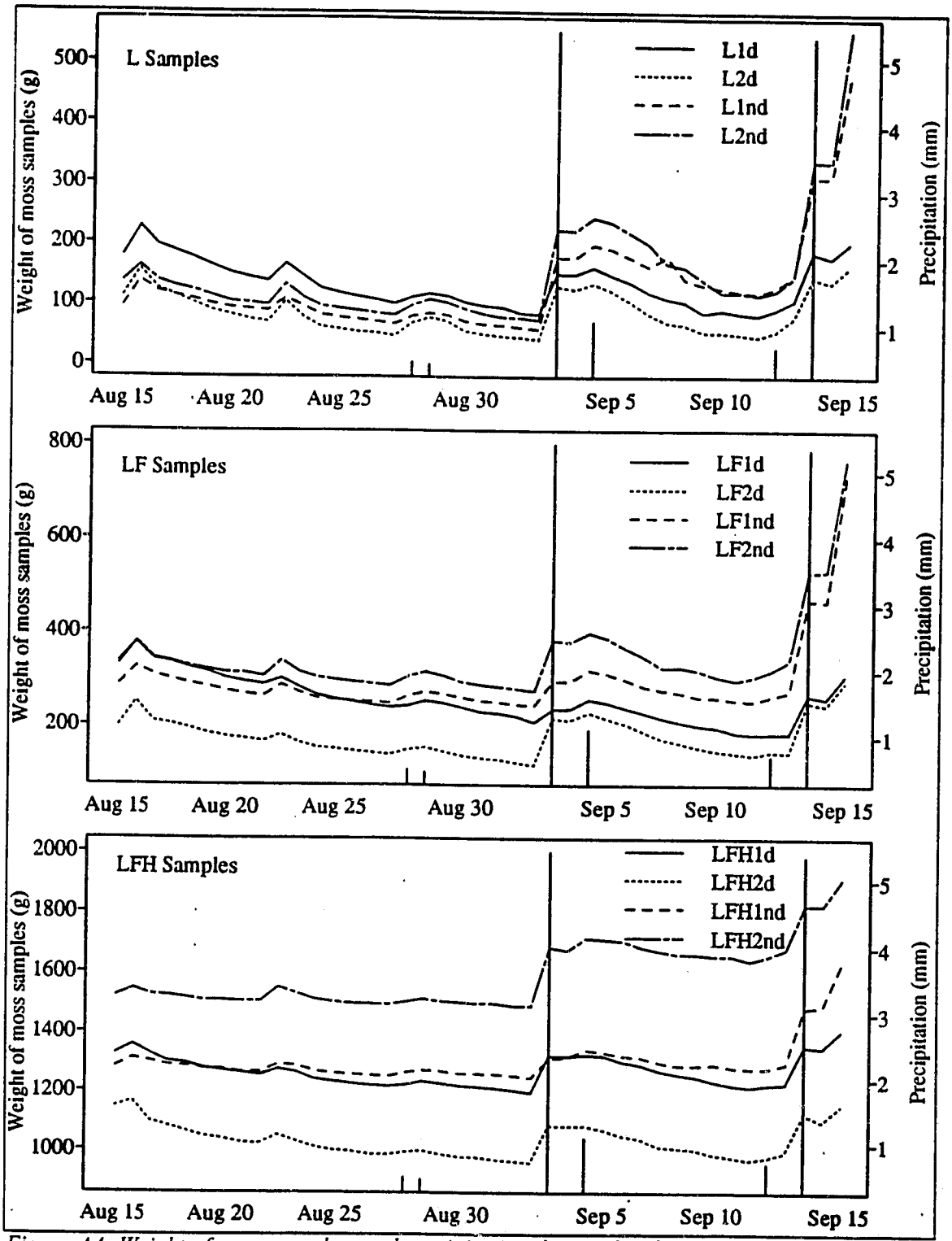

Figure A4: Weight of moss samples, and precipitation during the observation period. The legend refers to the thickness of the moss sample (see Figure A2), and plot location (Figure A3). Precipitation amounts are given as bars for storm totals.

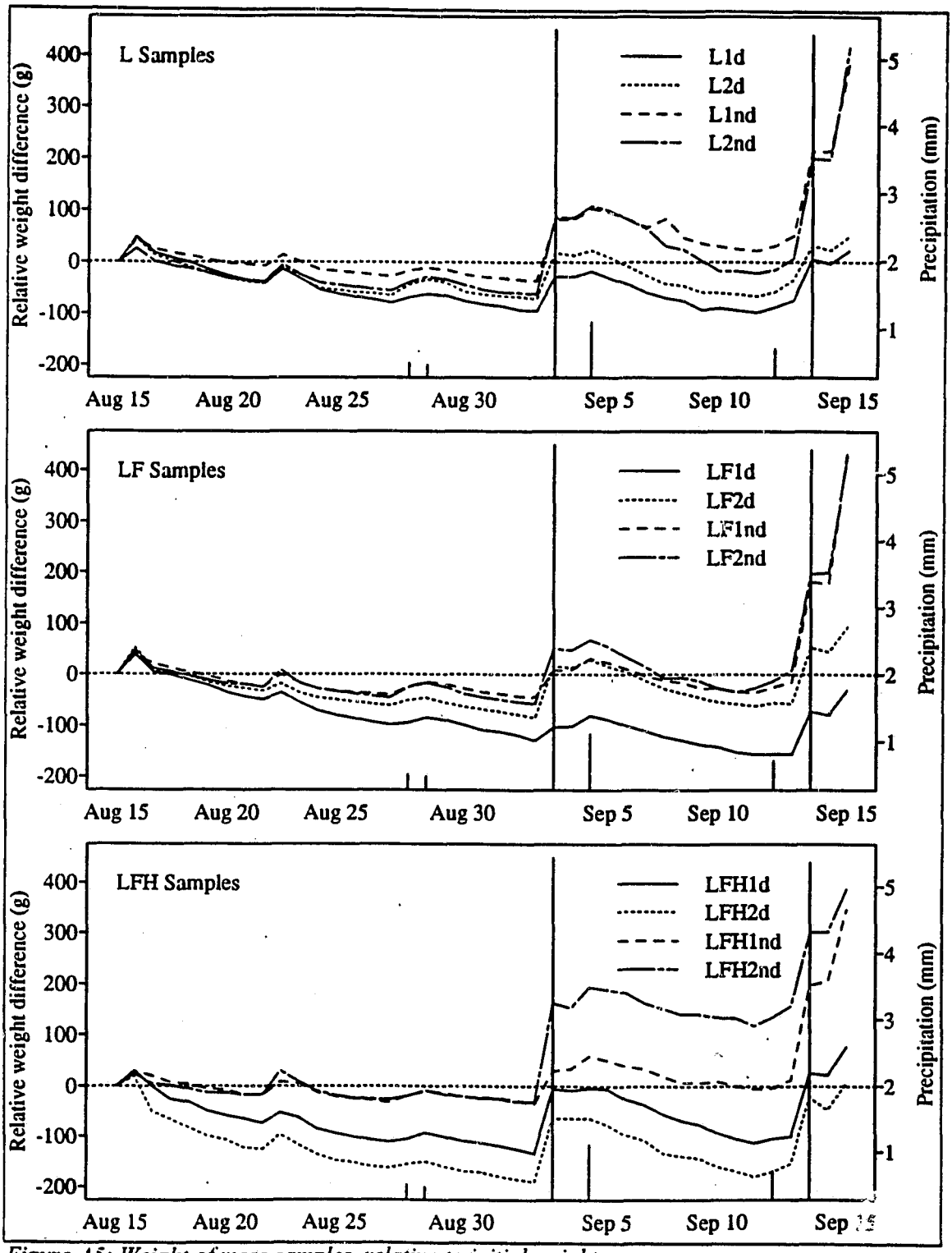

Figure A5: Weight of moss samples, relative to initial weight.

given for each time step are accumulated losses from previous measurement. The moss measurements were all taken around 4 pm (local time), except 4b, which was taken between two showers of rain on September 4 (6.15 pm), and 5a, which was taken at 9.30 am on September 5 (after the rainstorm ended). The measurements at 4 pm on September 4 were taken at the end of a rainstorm, and the negative value means the samples increased in weight because of the rainfall. The moisture flux presented for the tower for this time step is positive in spite of the rainfall, and is caused by missing values in the tower record. The loss of water through evapotranspiration from the moss samples is quite stable during the dry-down period, but has a small negative trend.

Figure A7 shows the ratio of latent heat from the moss to latent heat measured at the tower, and shows that the ratio ranges from close to zero up to 0.7. Figure A7 does not include the time steps when it was raining. From the results given in Figure 4.7, one cannot conclude whether the ratio increases or decreases as time since the previous rainstorm passes by. The fraction of evaporation that occurred from the moss increased after the rainstorm on September 4 and 5, but as Figure A7 shows, it does not seem to decrease in the dry-down period. The rainstorms during this period were small (maximum 5 mm precipitation), and a heavier rainstorm might have indicated more clearly whether the fraction of evapotranspiration from the moss carpet would increase or decrease after a rainstorms, and also in the dry-down periods.

It should also be mentioned that the tower flux measurements are preliminary, and that missing values exist. Mostly, the gaps in measurements are less than two hours, but on September 10 6 hours of data (10 am to 4 pm local time) are missing, and on September 11 18 hours of data (4 pm, September 10 to 10 am, September 11) are missing. When the gaps extended 3 hours, the values in figure A6 and A7 represent the average of the available measurements, otherwise the missing values were given the previous time step's value.

Conclusion.

The field work showed that where moss dominates the ground, a significant amount of the precipitation that reaches the forest floor is lost through evapotranspiration from the moss. Hence, the moss is an important component in the hydrologic cycle in the boreal region, where

moss is the dominant ground cover. This information led to an incorporation of a third root zone in DHSVM; a humus layer in addition to the two existing root zones. It has also been shown that the spatial variability of throughfall is high. More research is needed to determine the relative importance of evapotranspiration from moss, compared to overstory evapotranspiration and drainage, and to determine how best to incorporate moss hydrologic properties in models such as DHSVM.

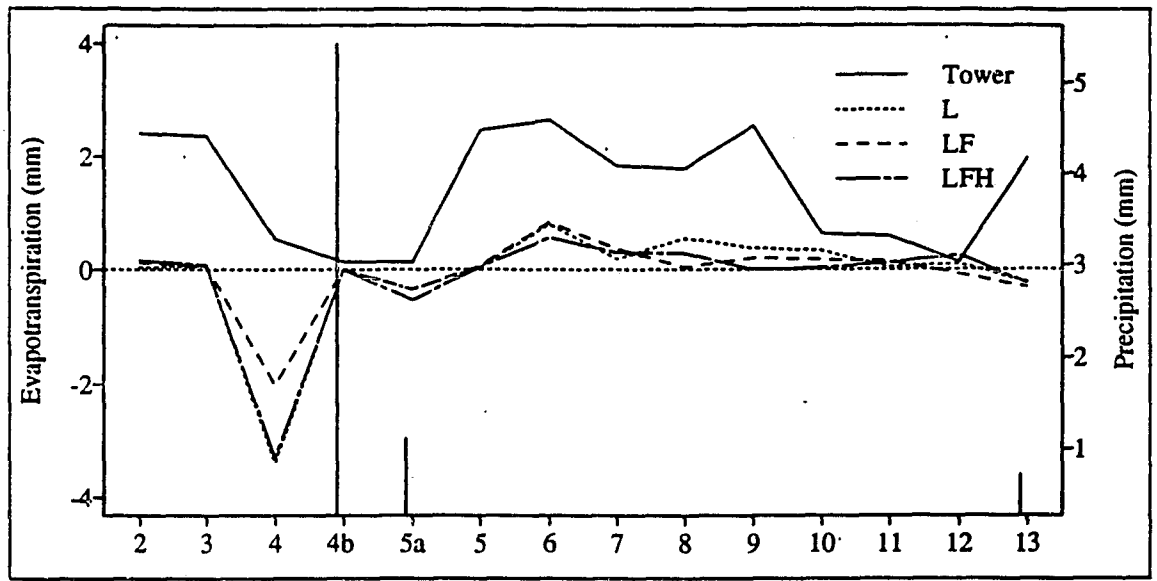

Figure A6: Evapotranspiration as measured at NOBS tower (calculated from latent heat flux) and equivalent evapotranspiration from moss, from September 2 through 13. The bars illustrate the precipitation measured in the open area. The x-axis represents the date and time of the measurements, which for 4b is September 4 at 6.15 pm, and 5a is at 9.30 am on September 5. All other measurements were taken around 4 pm.

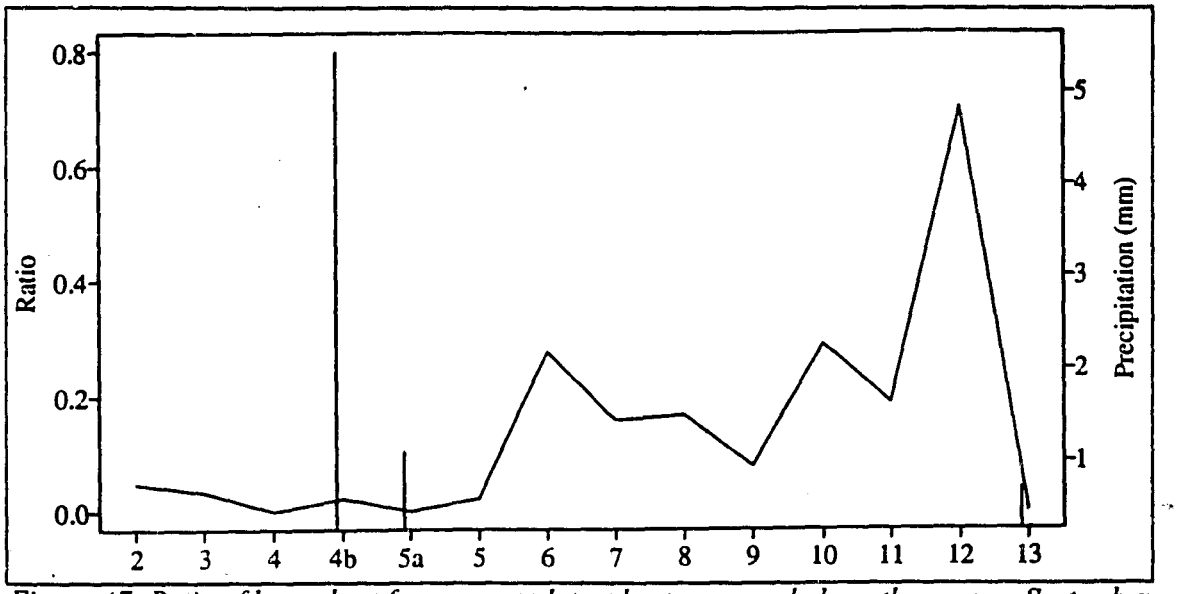

Figure A7: Ratio of latent heat from moss to latent heat measured above the canopy, September 2 through 13.

Table A1: Moss weights, plot 1 (grams).

Date	Time	L1d	L1nd	LF1d	LF1nd	LFH1d	LFH1nd
8-15	16.00	178.18	95.03	336.98	287.10	1328.19	1282.61
8-15	19.30	226.18	138.03	377.98	325.10	1358.19	1312.61
8-16	16.00	196.18	120.03	341.98	309.10	1328.19	1302.61
8-17	16.00	186.18	113.03	335.98	299.10	1302.19	1290.61
8-18	16.00	176.18	107.03	324.98	291.10	1296.19	1286.61
8-19	16.00	163.18	99.03	315.98	284.10	1279.19	1277.61
8-20	16.00	151.18	93.03	301.98	274.10	1270.19	1275.61
8-21	16.00	143.18	91.03	293.98	268.10	1264.19	1265.61
8-22	16.00	137.18	88.03	287.98	263.10	1255.19	1265.61
8-22	22.00	165.18	109.03	301.98	287.10	1276.19	1291.61
8-23	16.00	145.18	95.03	281.98	271.10	1266.19	1287.61
8-24	16.00	125.18	81.03	265.98	259.10	1244.19	1270.61
8-25	16.00	117.18	77.03	256.98	255.10	1234.19	1262.61
8-26	16.00	111.18	74.03	250.98	252.10	1227.19	1258.61
8-27	16.00	106.18	70.03	243.98	250.10	1221.19	1254.61
8-28	16.00	100.18	67.03	238.98	248.10	1217.19	1249.61
8-29	16.00	111.18	80.03	242.98	263.10	1223.19	1264.61
8-29	10.00	117.18	85.03	252.98	273.10	1235.19	1272.61
8-29	13.35	113.18	81.03	247.98	268.10	1227.19	1269.61
8-30	16.00	103.18	71.03	238.98	260.10	1219.19	1260.61
8-31	16.00	97.18	66.03	228.98	253.10	1215.19	1260.61
9-1	16.00	94.18	64.03	225.98	250.10	1210.19	1259.61
9-2	16.00	85.18	61.03	218.98	245.10	1203.19	1253.61
9-3	16.00	83.18	58.03	207.98	243.10	1195.19	1246.61
9-4	16.30	150.18	178.03	234.98	295.10	1323.19	1312.61
9-4	18.15	149.18	177.03	235.98	296.10	1320.19	1316.61
9-5	9.30	161.18	198.03	256.98	319.10	1325.19	1342.61
9-5	16.00	147.18	191.03	248.98	311.10	1323.19	1334.61
9-6	12.30	135.18	177.03	236.98	298.10	1302.19	1322.61
9-6	16.30	119.18	162.03	226.98	284.10	1291.19	1316.61
9-7	16.00	109.18	179.03	215.98	276.10	1273.19	1302.61
9-8	16.08	103.18	141.03	207.98	271.10	1260.19	1289.61
9-9	16.00	85.18	131.03	199.98	261.10	1252.19	1289.61
9-10	16.00	89.18	125.03	194.98	260.10	1235.19	1292.61
9-11	16.00	84.18	120.03	184.98	254.10	1223.19	1283.61
9-12	16.00	80.18	117.03	180.98	252.10	1215.19	1277.61
9-13	16.08	91.18	127.03	181.98	263.10	1224.19	1279.61
9-13	16.00	105.18	147.03	181.98	273.10	1228.19	1295.61
9-14	12.30	184.18	308.03	264.98	469.10	1354.19	1481.61
9-14	16.00	175.18	309.03	257.98	465.10	1350.19	1489.61
9-15	12.15	200.18	481.03	306.98	731.10	1406.19	1629.61
Net dry weight		47.19	34.30	111.81	130.45	312.05	408.67

Table A2: Moss weights, plot 2 (grams).

Date	Time	L2	L2nd	LF2	LF2nd	LFH2	LFH2nd
8-15	16.00	111.40	136.02	198.37	331.26	1146.51	1521.21
8-15	19.30	156.40	162.02	251.37	379.26	1166.51	1546.21
8-16	16.00	124.40	138.02	208.37	344.26	1096.51	1526.21
8-17	16.00	113.40	129.02	203.37	336.26	1081.51	1523.21
8-18	16.00	101.40	123.02	194.37	328.26	1064.51	1516.21
8-19	16.00	89.40	113.02	183.37	320.26	1047.51	1508.21
8-20	16.00	81.40	104.02	175.37	313.26	1039.51	1508.21
8-21	16.00	73.40	101.02	171.37	312.26	1024.51	1504.21
8-22	16.00	69.40	98.02	166.37	306.26	1021.51	1505.21
8-22	22.00	103.40	132.02	180.37	339.26	1050.51	1551.21
8-23	16.00	77.40	110.02	162.37	314.26	1029.51	1530.21
8-24	16.00	61.40	96.02	153.37	303.26	1011.51	1512.21
8-25	16.00	57.40	92.02	149.37	298.26	999.51	1503.21
8-26	16.00	53.40	88.02	145.37	294.26	995.51	1498.21
8-27	16.00	51.40	84.02	140.37	289.26	986.51	1495.21
8-28	16.00	47.40	81.02	137.37	286.26	983.51	1494.21
8-29	16.00	68.40	98.02	148.37	306.26	992.51	1502.21
8-29	10.00	78.40	108.02	153.37	315.26	997.51	1513.21
8-29	13.35	71.40	102.02	144.37	307.26	986.51	1505.21
8-30	16.00	54.40	92.02	135.37	294.26	977.51	1501.21
8-31	16.00	49.40	83.02	130.37	287.26	975.51	1497.21
9-1	16.00	46.40	78.02	126.37	283.26	967.51	1497.21
9-2	16.00	44.40	77.02	120.37	278.26	961.51	1489.21
9-3	16.00	41.40	74.02	114.37	274.26	956.51	1489.21
9-4	16.30	129.40	223.02	215.37	382.26	1083.51	1684.21
9-4	18.15	124.40	221.02	212.37	379.26	1082.51	1675.21
9-5	9.30	134.40	244.02	228.37	399.26	1083.51	1716.21
9-5	16.00	121.40	235.02	215.37	386.26	1070.51	1711.21
9-6	12.30	103.40	217.02	203.37	365.26	1049.51	1705.21
9-6	16.30	84.40	200.02	186.37	347.26	1038.51	1684.21
9-7	16.00	69.40	167.02	171.37	324.26	1013.51	1673.21
9-8	16.08	65.40	160.02	162.37	325.26	1007.51	1662.21
9-9	16.00	53.40	139.02	153.37	318.26	1003.51	1662.21
9-10	16.00	52.40	118.02	145.37	304.26	986.51	1656.21
9-11	16.00	49.40	119.02	140.37	297.26	977.51	1655.21
9-12	16.00	45.40	114.02	136.37	305.26	966.51	1640.21
9-13	16.08	54.40	122.02	144.37	319.26	976.51	1657.21
9-13	16.00	77.40	144.02	141.37	340.26	993.51	1679.21
9-14	12.30	143.40	336.02	251.37	528.26	1125.51	1823.21
9-14	16.00	134.40	334.02	243.37	531.26	1099.51	1824.21
9-15	12.15	161.40	552.02	292.37	765.26	1152.51	1909.21
Net dry weight		35.73	44.15	69.48	97.33	309.57	433.94

Table A3: Precipitation (mm).

Date	Time (local)	P1	P2	P3
8-23	8.00	NA	NA	NA
8-29	10.40	0.51	0.48	0.51
8-29	14.00	0.47	0.44	0.49
9-4	18.40	5.39	5.48	5.44
9-5	10.00	1.00	1.16	1.18
9-13	13.19	0.70	0.70	0.74
9-14	13.30	5.20	5.20	5.68

Table A4: Throughfall (mm).

Date	Time (local)	A1	A2	A3	B1	B2	B3	C1	C2	C3	D1	D2	D3	E1	E2	E3
8-23	8.00	0.64	0.39	0.49	0.13	0.16	0.21	0.36	0.60	0.63	0.85	0.58	1.03	0.94	1.08	0.31
8-29	10.40	0.03	0.10	0.26	0.12	0.00	0.00	0.12	0.01	0.29	0.37	0.38	0.14	0.13	0.08	0.02
8-29	14.00	0.04	0.12	0.23	0.16	0.00	0.10	0.08	0.16	0.18	0.34	0.29	0.23	0.16	0.16	0.15
9-4	18.40	1.53	2.42	2.82	3.40	2.60	2.66	5.20	5.00	3.80	7.68	4.49	6.56	4.09	2.76	6.66
9-5	10.00	0.66	0.58	0.58	0.78	0.46	0.64	0.56	0.27	0.49	0.86	0.57	0.82	0.62	0.68	0.50
9-13	13.19	0.61	0.45	0.58	0.34	0.43	0.13	0.83	0.94	0.48	0.45	0.75	0.49	0.74	0.58	0.21
9-14	13.30	5.06	5.20	4.30	3.30	3.25	3.35	6.34	7.48	3.78	3.83	5.01	7.20	4.25	4.49	5.68

APPENDIX 2: NOTATION.

The following list defines symbols used in this thesis. Subscript *i* stands for *o* (overstory), *u* (understory), *g* (ground surface) or *s* (snow).

c_n: Canopy attenuation coefficient
c_p: Specific heat of air
d_{0i}: Zero plane displacement height
dt: Time step
e: Vapor pressure
e_s: Saturation vapor pressure
ET: Evapotranspiration
E_i: Evaporation from intercepted water
E_p: Potential evaporation
f_{bs}: Canopy resistance correction factor, soil temperature. Black spruce
f_{jp}: Canopy resistance correction factor, soil temperature. Jack pine
h_i: Height
k: von Karman's constant
Q_e: Latent heat flux
Q_s: Sensible heat flux
r_{ai}: Aerodynamic resistance
r_c: Canopy resistance
r_{exp}: Aerodynamic resistance, exponential part of wind profile
r_{log}: Aerodynamic resistance, logarithmic profile near the ground surface
r_{over_i}: Aerodynamic resistance, upper logarithmic profile
r_s: Stomatal resistance
R_n: Net radiation
T_a: Temperature, air
T_s: Temperature, soil surface
u: Wind speed
z: Height above ground level
z_{0i}: Roughness length
z_m: Height at which the wind profile is assumed to go from exponential to logarithmic
z_x: Reference height

Δ: Slope of the saturated vapor pressure-temperature curve
γ: Psychrometic constant
λ_v: Latent heat of evaporation
θ: Soil moisture
ρ_a: Density of moist air
ρ_p: Snowpack density